Experimental and Theoretical Characterization on the Sublimation (Evaporation) Kinetics of Fine Aerosol Particles (Droplets)

Vom Fachbereich Maschinenbau und Verfahrenstechnik

der Technischen Universität Kaiserslautern

zur Erlangung des akademischen Grades

Doktor-Ingenieur (Dr.-Ing.)

genehmigte Dissertation

von

Ms. Sc. Haomin Ding

aus Beijing/China

Kaiserslautern 2008

D386

Dekan:	Prof. Dr.-Ing. S. Ripperger
Vorsitzender der Promotionskommission:	Prof. Dr. rer. nat. R. Ulber
Berichterstatter:	Prof. Dr.-Ing. S. Ripperger
	Prof. Dr.-Ing. B. Sachweh
	Prof. Dr. J-F. Chen
Tag der mündlichen Prüfung:	18. Dezember 2008

Vorwort

Die vorliegende Arbeit wurde in der Zeit von Juli 2005 bis Dezember 2008 an dem Lehrstuhl für mechanische Verfahrenstechnik der Technischen Universität Kaiserslautern durchgeführt.

Für das entgegengebrachte Vertrauen möchte ich besonders Herrn Prof. Siegfried Ripperger danken, der mir die Möglichkeit gegeben hat meine Doktorarbeit an seinem Lehrstuhl durchzuführen. Sein stetiges Interesse am Fortgang der Arbeit sowie die Bereitstellung des Arbeitsplatzes und des nötigen Freiraums für eigenständiges Forschen waren wichtige Bausteine zum Erfolg der Arbeit. Ebenso gilt mein herzlicher Dank Herrn Professor Bernd Sachweh, der mich durch seine konstruktiven Diskussionen und sein Vertrauen unterstützt hat. Herrn Professor JianFeng Chen möchte ich für seine ideelle Unterstützung sowie für die Übernahme des Koreferates danken.

Für die finazielle und materialle sowie die wissenschaftliche Förderung der Arbeit bedanke ich mich bei der BASF SE, die durch die Projektkooperation mit der TU Kaiserslautern meine Promotion ermöglicht hat. Mein Dank gilt auch der Palas GmbH für die fachlichen Diskussionen und materialle Unterstützung.

Mein Dank gilt auch allen Kollegen des Lehrstuhls für die schöne gemeinsame Zeit, die ich mit ihnen am Lehrstuhl verbringen durfte. Das hervorragende Arbeitsklima sowie die fachliche und persönliche Unterstützung ermöglichten mir ein zielorientiertes und effektives Arbeiten.

Zu guter Letzt danke ich meiner Familie für die persönliche und finanzielle Unterstützung während meines Studiums und der Promotion. Besonders inniger Dank gilt neben meiner Familie auch meinen Freunden. Sie gaben mir alle durch ihr Verständnis und ihren Zuspruch stets die nötige Sicherheit und Rückhalt.

Kaiserslautern Haomin Ding

Abstract

Sublimation (Evaporation) is widely used in different industrial applications. The important applications are the sublimation (evaporation) of small particles (solid and liquid), e.g., spray drying and fuel droplet evaporation. Since a few decades, sublimation technology has been used widely together with aerosol technology. This combination is aiming to get various products with desired compositions and morphologies. It can be used in the fields of nanoparticles generation, particle coating through physical vapor deposition (PVD) and particle structuring.

This doctoral thesis deals with the experimental and theoretical investigations of sublimation (evaporation) kinetics of fine aerosol particles (droplets). The experimental study was conducted in a test plant including on-line control of the most important paramters, such as heating temperature, gas flow and pressure. On-line and in-line particle measurements (Optical sensor, APS) were employed. Relevant parameters in sublimation (evaporation) such as heating temperature, particle concentration and aerosol residence time were investigated. Polydispersed particles (droplets) were introduced into the test plant as precursor aerosols. Two kinds of materials were used as test materials, including inorganic particles of NH_4Cl and organic particles of DEHS. NH_4Cl particles with smooth surface and porous structure were put into the experiments, respectively. The influence of the particle morphology on the sublimation process was studied.

Basing on the experiments, different theoretical models were developed. The simulation results under different parameters were compared with experimental results. The change of concentration of particles was specially discussed. The discussion was focused on the relationship of the total particle concentration and the change of single

particles with diverse initial diameters. The study of the sublimation kinetics of particles with different morphologies and different specific surface areas was carried out. The factor of increased surface area on the sublimation process was taken into the simulation and the results were compared with experimental results.

A sublimation (evaporation) kinetics was investigated in this thesis. Basing on the property of a material, such as molecular weight, molecular size and vapor pressure, the sublimation (evaporation) kinetics was described. The optimum sublimation (evaporation) conditions with respect to the material properties were advanced. A *Phase Transition Effect* during the sublimation (evaporation) was found, which describes the increase of the large particles on the cost of small particles. A similar effect is observed in crystal suspension (called Ostwald ripening) but with another physical background.

In order to meet the need of in-line particle measurement, a hot gas sensor (O.P.C.) was developed in this study, for measuring the particle size and the size distribution of an aerosol. With the newly developed measuring cell, the operating conditions of the aerosol could be increased up to 500 ^{o}C.

Zusammenfassung: Charakterisierung der Sublimationskinetik (Verdampfungskinetik) von feinen Aerosolpartikeln durch Experimente und Modellierung

Ziel der Arbeit

Das Ziel der vorliegenden Arbeit ist Sublimations- bzw. Verdampfungsprozesse von einem feinen Aerosol wie z.B. Harnstoff zu beschreiben damit Scale-up von Apparaten abgesichert und industrielle Prozesse gestaltet werden können. Die grundlegende Frage in diesem Zusammenhang ist das Verhalten der Partikeln während der Sublimation im Kollektiv. Diese Frage wird mit Experimenten und Simulationsrechnungen beantwortet. Sublimations- bzw. Verdampfungsprozesse treten u.a. in folgenden Prozessen auf:

1. Herstellung von Nanopartikeln durch Sublimation/Kondensation;
2. Dünnschichttechnologien durch physikalische Abscheidung eines Dampfes auf einer Trägerpartikel;
3. Abtrennung von Verunreinigungen aus Partikeln;
4. Verdunstung von Kraftstofftropfen in Brennräumen.

Experimentelle Untersuchung

Im Zuge des Forschungsvorhabens wurde eine Anlage aufgebaut, bei der Partikeln in einem Strömungsrohr aufgeheizt wurden. Die Sublimation bzw. Verdampfung wurde an polydispersen Partikeln im kontinuierlichen Partikelstrom on-line untersucht. Der Gasvolumenstrom, die Temperatur und der Druck wurden on-line kontrolliert. Die Partikelgrössenverteilungen wurden mit verschiedenen Messgeräten on-line bzw. in-line gemessen. Als organisches Material wurden DEHS Tropfen in einem Stickstoff Strom versprüht und als anorganisches Material wurden NH_4Cl Partikeln in Luft dispergiert. An der Versuchsanlage wurden alle für den Sublimations- bzw. Verdampfungsprozess relevanten Parameter (Temperatur, Partikelgrössenverteilung, Volumstrom, Partikelkonzentration) jeweils am Ein- und Austritt gemessen und registiert. An Hand von Proben wurde die Partikelmorphologie untersucht. Folgender Zusammenhang wurde ermittelt:

- Die Erwärmung der Partikeln im Gasstrom bestimmt in Verbindung mit dem Stoffaustausch wesentlich den Sublimations- bzw. Verdampfungsprozess.
- Die Sublimations- bzw. Verdampfungskinetik ist wesentlich von dem Anstieg der Gasphasenkonzentration des jeweiligen Stoffes, die von der Partikelkonzentration, der Partikelgrössenverteilung und der Partikelmorphologie beeinflusst wird, abhängig.
- Bei der Untersuchung feiner Partikel darf die Dampfdruckerhöhung aufgrund der stärker gekrümmten Partikeloberfläche nicht vernachlässigt werden (Kelvin Effekt).
- Die jeweiligen Stoffparameter (Dampfdruck, Diffusionskoeffizient, Verdampfungswärme) müssen berücksichtigt werden.

Der Einfluss der Partikelmorphologie auf die Sublimation wurde durch Vergleiche von NH_4Cl Partikeln mit glatter Oberfläche und entsprechenden Partikeln mit poröser Agglomeratstruktur untersucht. Im Temperaturbereich von 100^{o}C bis 130^{o}C wurde bei Partikeln mit glatter Oberflächenstruktur ein Wachstum der gemittelten Partikeldurchmesser beobachtet. Die Anzahlkonzentration der kleinen Partikeln ($d_p < 1\mu m$) nahm dabei

stark ab. Die Anzahlkonzentration der großen Partikeln blieb konstant. Im Temperaturbereich von 100^{o}C bis 130^{o}C wurde bei porösen Partikeln mit hoher spezifischer Oberfläche eine steigende Sublimationskinetik beobachtet. In dem entsprechenden Temperaturbereich nahm sowohl die Anzahlkonzentration der kleinen Partikeln als auch die Anzahlkonzentration der großen Partikeln ab. Mit weiter steigender Temperatur wurde bei beiden Partikelmorphologien die Partikelkonzentration insgesamt verringert.

Bei der Verdampfung der DEHS Tropfen wurde eine starke Reduzierung aller Partikeln gemessen, obwohl DEHS aus der Literatur als langsam verdampfend bekannt ist. (75) (78) (79)

Entwickelter Heissgassensor (HGS)

Bei der Untersuchung von Aerosolen ist die Partikelmesstechnik unverzichtbar. Im Vergleich zu anderen Messtechniken haben optische Sensoren den großen Vorteil, die Partikeln berührungslos unter den gegebenen chemischen und physikalischen Bedingungen zu vermessen. Die bisher zur Verfügung stehenden optischen Messsysteme sind stark temperaturbegrenzt. Die maximale Gastemperatur im Messvolumenstrom ist auf ca. 120^{o}C limitiert. Ein wichtiger Bestandteil der Arbeit war die Entwicklung eines Heißgassensors (HGS), der es möglich macht, in-line Messungen bei Temperaturen bis zu 500^{o}C durchzuführen.

Modellierung

Mit Bezug auf die Parameter der Experimente wurden verschiedene Simulationsmodelle entwickelt. Der Einfluss von Partikelmorphologie, Partikelanzahlkonzentration, Partikelgrößenverteilung und der Temperatur auf den Sublimations- bzw. Verdampfungsprozess wurden untersucht und die Simulationsergebnisse mit den Ergebnissen der Experimente verglichen. Die Sublimations- bzw. Verdampfungskinetik ist ausführlich disku-

tiert und bewertet geworden.

Ergebnissen und Diskussion

Im Sublimations- bzw. Verdampfungsprozess werden Moleküle an der Partikeloberfläche durch Wärmeinwirkung aktiviert, so das sie den Moleklverband verlassen können und frei beweglich sind. Nach Fuchs bildet sich eine sehr dünne Gasschicht um eine Partikel. Die Molekülkonzentration in der Gasschicht ist abhängig von der Dampfdruckkurve und dem Partikeldurchmesser. Wenn ein kontinuierlicher Übergang der Moleküle von der Gasschicht in die Gasphase stattfindet, nennt man das Sublimation bzw. Verdampfung. Die Sublimations- bzw. Verdampfungskinetik wird hauptsächlich von zwei Faktoren beeinflusst, dies sind der Diffusionskoeffizient und der Konzentrationsgradient (siehe Bild 0.1). Der Diffusionskoeffizient ist ein Maß für die Molekülbeweglichkeit und wird von der Temperatur, dem Gesamtdruck und der Molekülgröße bestimmt. Der Konzentrationsgradient ist abhängig vom Gleichgewicht der Phasen und der Konzentrationsdifferenz zwischen der dünnen Gasschicht und der umgebenden Gasphase.

Aufgrund der großen Moleküldurchmesser von DEHS (M_W=426,69 $kg/kmol$) besteht eine geringe Molekularbeweglichkeit bei der Verdampfung. Die Verdampfungskinetik der DEHS Tropfen wird daher im untersuchten Temperaturbereich und Partikelkonzentrationsbereich von der Molekülbeweglichkeit bestimmt. Für NH_4Cl gilt wegen des geringen Moleküldurchmessers (M_W=53,49 $kg/kmol$), dass der Diffusionskoeffizient vergleichsweise groß ist. Die Sublimation der NH_4Cl Partikeln wird bei einem nahezu gleichen Dampfdruck wie DEHS von dem kleinen Konzentrationsgradient bestimmt.

Die Sublimation bzw. Verdampfung eines Materials mit entweder kleinem Moleküldurchmesser, oder niedrigem Dampfdruck, wird durch die geringe Konzentrationsdifferenz festgelegt. Die Sublimation eines Materials mit entweder großem Moleküldurchmesser oder hohem Dampfdruck, wird durch die geringe Molekularbeweglichkeit festgelegt. Durch Erhöhung des Gesamtdrucks in der Gasphase wird die durch die Molekularbeweglichkeit bestimmte Sublimation bzw. Verdampfung stark vermindert. Dieser Effekt kann für die Abscheidung von Materialen mit ähnlichen Dampfdrücken genutzt

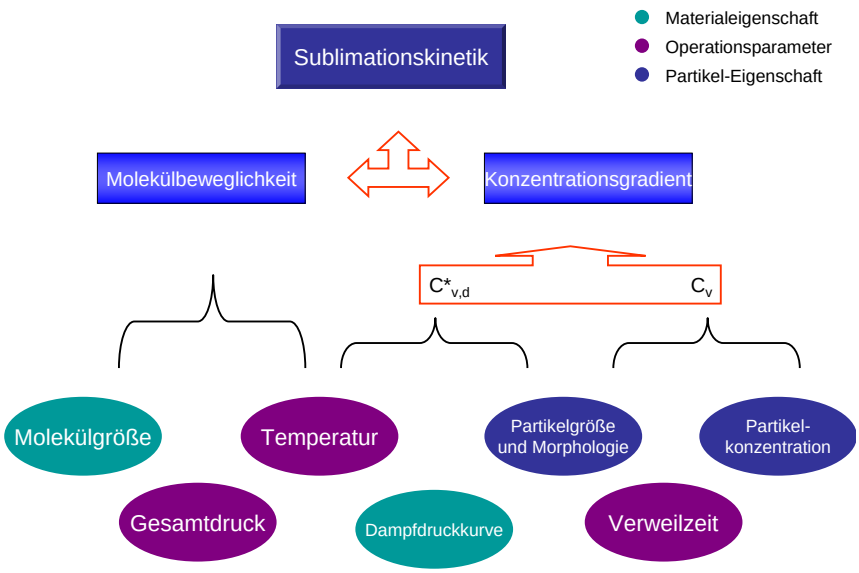

Figure 0.1: Schematische Demonstration der Sublimationskinetik

werden.

Wenn die Sublimations- bzw. Verdampfungskinetik wesentlich durch den Diffusionskoeffizient bestimmt wird, sublimieren alle Partikeln mit nahezu gleicher Geschwindigkeit.

Aufgrund des Kelvin-Effekts ist die Konzentrationsdifferenz vom Partikeldurchmesser abhängig. Kleine Partikeln haben infolge der stärker gekrümmten Oberfläche einen größeren Konzentrationsgradient. Wenn der Konzentrationsgradient die Sublimation bestimmt, haben die Partikeln mit verschiedenem Durchmesser unterschiedliche Sublimations- bzw. Verdampfungskinetik. Daher beobachtet man einen Effekt, den wir *Phase Transition Effekt* nennen. Dabei verdampfen kleine Partikeln und kondensieren auf den größen Partikeln unter folgenden Voraussetzungen:

- Partikeln/Tropfen sind polydispers und die Partikelgrößenverteilung ist breit.
- Es gibt genügend Material in dem Aerosol um die Gasphase zu sättigen.

- Der Partialdruck (Molekülkonzentration) in der Gasphase ist im Bereich des Sättgungsdrucks.

Um die freie Energie (Oberflächenspannung) des Systems zu minimieren, sublimieren die kleinen Partikeln schneller als die großen Partikeln. Wenn der Partialdruck in der Gasphase sich dem Sättigungsdruck nähert, diffundiert ein Molekülstrom von den kleinen Partikeln zu den großen Partikeln. Folglich schrumpfen die kleinen Partikeln, die großen Partikeln können wachsen. Der gemittelte Partikeldurchmesser im Aerosol wächst, wie im Experiment beobachtet.

Contents

List of Figures **xiii**

List of Tables **xvii**

1 Introduction **1**

2 Present Studies in Droplet Evaporation and Particle Sublimation **6**
2.1 Present Studies in Droplets Evaporation 7
2.2 Present Studies in Particle Sublimation 10

3 Theory **12**
3.1 Mean Free Path of Gases 12
3.2 Particle Reynolds Number (Re_p) 13
3.3 Sedimentation in a Gravitational Field 14
3.4 Stokes's Law 15
3.5 Partial Pressure 16
3.6 Vapor Pressure 16
3.7 Kelvin Effect 17
3.8 Thermodynamic Stability and Phase Change 17
3.9 Description of Droplets in Evaporation 18
3.9.1 Unidirectional Diffusion 19
3.9.2 Opposite Diffusion 21
3.10 Fuchs Effect 23
3.11 Heat and Mass Transfer Equilibrium 24
3.12 "Traveling" Effect 25
3.13 Diffusion Coefficient 26

4 Experiment Section and Measurement Technology 28
4.1 Experimental Setup . . . 28
4.1.1 Test Materials . . . 30
4.1.2 Aerosol Generators . . . 32
4.1.3 Operation Control . . . 33
4.2 Measurement Technology . . . 36
4.2.1 Aerodynamic Particle Sizer: APS . . . 36
4.2.2 Specific Surface Ratio . . . 37
4.2.3 Optical Particle Sensor . . . 37
4.2.4 HGS Properties and Calibrations . . . 44
4.2.5 Noise Effect . . . 49

5 Experimental Results 56
5.1 NH_4Cl Particles with Smooth Surface Sublimation Studies . . . 56
5.1.1 Experiments with Different Heating Temperature . . . 56
5.1.2 Experiments with Different Particle Concentrations . . . 60
5.2 NH_4Cl Particles with Porous Surface Sublimation Studies . . . 62
5.2.1 Experiments with Different Heating Temperature . . . 63
5.2.2 Different Particle Concentrations . . . 67
5.2.3 Different Residence time . . . 67
5.2.4 Analysis of Particle Surface Ratio . . . 69
5.3 Organic Droplets Evaporation Studies . . . 70
5.3.1 Influence of Different Heating Temperatures . . . 70
5.3.2 Influence of Different Droplets Concentrations . . . 70

6 Model Section 73
6.1 Evaporation Models . . . 74
6.1.1 Model for Low Volatile Materials: Model 1 . . . 75
6.1.2 Model for Volatile Materials . . . 77
6.1.3 Morphological Effect in the Particle evaporation . . . 78
6.2 Coagulation Model . . . 79
6.2.1 Kinematic Coagulation . . . 80
6.2.2 Thermal Coagulation . . . 81
6.3 Sublimation of Sedimentated Particles . . . 81

7 Simulation Results and Comparison **83**
7.1 Particles Coagulation in Flow 83
7.1.1 Kinematic Coagulation 83
7.1.2 Thermal Coagulation 83
7.2 Evaporation of Water Droplets 85
7.3 Simulation of NH_4Cl Sublimation at Experimental Conditions 87
7.3.1 Simulation of Spherical Particles 88
7.3.2 Sedimentation and Particles Sublimation 92
7.3.3 Morphological Effect on Particles Sublimation 95
7.3.4 Simulation of NH_4Cl Sublimation out of Experimental Conditions . 97
7.4 Simulations of DEHS Droplets Evaporations 99

8 Sublimation Kinetics and Phase Transition Effect **103**
8.1 Sublimation Kinetics 103
8.2 Phase Transition Effect 107

9 Summary **110**
9.1 Experiments 110
9.2 Hot Gas Sensor (HGS) 111
9.3 Simulations 112
9.4 Results and Discussion 112

A Determination of Surface Tension **115**
A.1 Application of the Young's Equation 115
A.2 Calculation of the Surface Tension 116
A.2.1 Method of Neumann 1 116
A.2.2 Method of Neumann 2 117
A.3 Practical Application 117

B SEM of NH_4Cl Particles Sublimation **119**
B.1 SEM of Porous NH_4Cl Particles before and after Sublimation 119
B.2 SEM Observation of NH_4Cl Particles Sublimation 119

List of Figures

0.1 Schematische Demonstration der Sublimationskinetik viii

1.1 Applications of phase transition in different industrial branches 2
1.2 Depiction of nanoparticles generation through sublimation and vapor deposition process. 4

2.1 Evaporation of a single suspended droplet 8
2.2 Water droplet temperature depression as a function of relative humidity for ambient temperatures $0 - 40^oC$ 10

4.1 Photo of the experimental setup 29
4.2 Flowsheet of the plant for sublimation investigation 30
4.3 Molecule structure of DEHS 31
4.4 Structure of the Collison nebulizer 32
4.5 Structure of the Brush feeder (LTG Model NDF 100) 33
4.6 The structure of aerosol generators AGK-2000 33
4.7 Front pane of the Labview controller of the whole experimental setup . . . 35
4.8 Scattered light used for the particle size analysis 39
4.9 The structure of the measuring cell in the sampling 40
4.10 Measured polydisperse NaCl from two Welas-3000s in the experimental setup 41
4.11 The structure of the HGS cell 42
4.12 Drawing of the detector head of the HGS 43
4.13 The experimental setup of the HGS cell, RM: Rotameter; MFC: Mass-flowcontroller 45
4.14 The digital control of the mass flow control and rotameter 46
4.15 Experimental setup of the HGS cell in the heating plant 47

4.16 HGS calibration setup, both of the two Welas-3000s and HGS are setup in the heating tube 47
4.17 PSD of Latex particles measured from Sensor 1 and HGS respectively . . 48
4.18 PSD of polydispersed NaCl particles measured from Sensor 1 and HGS respectively 49
4.19 PSD of polydispersed NH_4Cl particles measured from Sensor 1 and HGS at room temperature, respectively 50
4.20 PSD of polydispersed NH_4Cl particles measured from Sensor 2 and HGS at 120 ^oC. 51
4.21 The controlled test of the three sensors (Sensor 1, HGS and Sensor 2) under the measuring range of HGS, Sensor 2 is directly after the HGS to see the particle loss through aerosol flowing. 52
4.22 The intensity of the noise with different heating temperatures 53
4.23 Comparison of the noise intensity and the molecules concentration at the same temperature 54
4.24 Experimental setup for the research of the HGS's noice; a) the NH_4Cl powder place; b) heater of the plant; c) heater of the HGS 54
4.25 Indication of the temperature changes of flows in canal 1 and canal 2. . . 55

5.1 SEM of ground NH_4Cl particles, which is sent into test plant through a brushfeeder 57
5.2 The temperature distribution in the heating tube, at the exit the gas flow was heated to 120 ^oC. Temperature were measured at different temperature sensor sites. 58
5.3 Sublimation experiments with the particles of sample of ground NH_4Cl, which has solid structures and smooth surfaces. Two identical Welas-3000s are used and test aerosols are heated up to 120 ^oC. 59
5.4 Sublimation experiments with the particles of sample of ground NH_4Cl. HGS was used here and the aerosol was heated up to 180 ^oC 60
5.5 Sublimation experiments with higher particles concentration 61
5.6 Residual particles concentrations at different heating temperature 61
5.7 SEM of NH_4Cl generated from collison nebulizer. 63
5.8 Experimental setup for particle characterization 64

5.9 Aerodynamic diameter and optical diameter of particles from collison nebulizer . . . 64
5.10 Sublimation experiments with the particles from collison nebulizer. Two identical Welas-3000s are used and test aerosols are heated up to 120 ^oC . . . 65
5.11 Sublimation experiments with the particles from collison nebulizer. HGS is used here and the aerosol is heated up to 200 ^oC . . . 66
5.12 Percent of sublimated particle at different initial particle concentration at $V = 2.5m^3/h$ . . . 68
5.13 Particles sublimation at different residence time at $V = 1.2m^3/h$ and $V = 0.8m^3/h$, respectively . . . 68
5.14 Evaporation study of organic droplets DEHS at $V = 2.5m^3/h$ . . . 71
5.15 Evaporation of DEHS droplets with different concentration at different temperature . . . 72

6.1 The balance between gas/particle phase in the process of evaporation . . 74
6.2 Temperature and material concentration profile of low volatile materials on the particle surface . . . 76
6.3 Temperature and material concentration profiles of volatile materials on the particle surface . . . 77

7.1 The reduction of particle concentration from Kinematic coagulation 84
7.2 Thermal coagulation (120 ^oC) of aerosol particles at different residence time . . . 85
7.3 Comparison of the heating temperature from experimental measurement and calculation. The relationship between the heating temperature on the wall and the outlet temperature at the site of the hot sensor is presented. 88
7.4 Simulation of spherical NH_4Cl particles evaporation at the experimental conditions . . . 89
7.5 The change of single NH_4Cl particle's diameter through the heating process 90
7.6 Comparison of experimental results and simulation results of ground NH_4Cl 91
7.7 Comparison of different particles settling time with residence time in the heating tube . . . 93
7.8 NH_4Cl sublimation taking sedimentation into consideration . . . 94

7.9 Simulated sublimation of NH_4Cl particles from collison nebulizer at 90 ^oC and 120 ^oC $V = 2.5m^3/h$ 96
7.10 Comparison of the experimental results and the simulation results at the same sublimation conditions $V = 2.5m^3/h$ 97
7.11 Simulated sublimation of ground NH_4Cl particles at high concentration $\Sigma Cn = 4.7 \times 10^6 P/cm^3$, $V = 2.5m^3/h$ 101
7.12 Comparison of experimental and simulation results of DEHS evaporation 102

8.1 Indication of the driving force of particle evaporation. 104
8.2 Simulated evaporation of DEHS and sublimation of NH_4Cl under different total pressure. 105
8.3 Molecule concentration and the corresponding vapor pressure at different temperature 106
8.4 Indication of Phase Transition Effect during aerosol evaporation 108

9.1 Schematic demonstration of sublimation kinetics 113

B.1 The SEM photographs of porous NH_4Cl particles before sublimation: (1) and (2); after sublimation: (3) and (4). 120
B.2 The observed NH_4Cl particle sublimation in the vacuum chamber of SEM. 121

List of Tables

2.1 Researches in the study of Droplet Evaporation and Particle Sublimation . 6

3.1 Diffusion Volumes in Fuller-Schettler-Giddings Correlation Parameters . . 27

4.1 Physical properties of NH_4Cl and DEHS $*$ 31

5.1 Experimental conditions of ground NH_4Cl particles sublimation 58
5.2 Experimental conditions on sublimation with different particle concentrations 67
5.3 Measuring results of particle specific surface area with two measuring methods 69

7.1 Comparison of models results and literature data 86
7.2 Surface factors for different particles in sublimation simulation 95

1 Introduction

Historically, aerosol science has focused on environmental or health effects of aerosols, e.g., the effects of particles formed by combustion of coal and other fossil fuels in power plants, burning of gasoline in automobiles, and so on (1), (2). Until recently, a few aerosol routes for the formation of materials were developed for use in industrial applications. Several new aerosol methods for the generation of materials have been commercialized recently (3), (4), (5). These routes were developed to meet the needs of producing particles with controlled size distribution, morphology and crystallinity or coating films with controlled composition. One important realization is the conversion of a gaseous component to nanoparticles, which is carried out by sublimation and followed vapor deposition (6), (7), (8).

Aerosol methods for generating nanoparticles can involve a variety of fundamental physicochemical phenomena:

- Gas-particle chemical reactions;
- Single-particle chemical processes such as surface and intraparticle chemical reactions;
- Physical processes such as sublimation, nucleation, and condensation;
- Multiparticle physical processes such as collision, coalescence, and agglomeration;
- Transport and deposition of vapors and particles by a variety of mechanisms;
- Mass transport, heat transport and fluid flow leading to non-uniform temperature, mass and velocity fields
- Effects associated with plasmas, photons electric fields, and supercritical fluids;

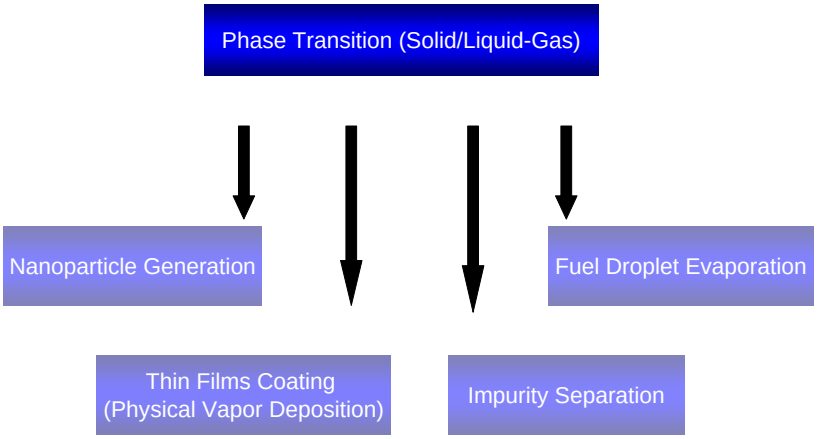

Figure 1.1: Applications of phase transition in different industrial branches

- Particle ejection or entrainment from surface.

Phase transition between gas and solid (liquid) phases is very important in aerosol routes, which includes atomization, sublimation and condensation, etc. They are involved in broad application fields (see in Fig.1.1), such as nanoparticle generation, thin film coating, impurity separation, and fuel droplets evaporation. Sublimation and subsequent vapor deposition is a technique widely used, especially, in the generation of organic nanoparticles because of the specific advantages: high product purity and precise control of particle size distribution. Basically, there are two steps in the process: formation of a vapor phase; and gas-to-particle conversion process by forming a supersaturated vapor of condensable gaseous species. The process is depicted in Fig.1.2. After sublimation, a vapor phase is formed. With sufficient high supersaturation of the vapor phase, either solid or liquid particles are formed by homogeneous nucleation. The higher the supersaturation, the smaller the radius of the particles will be served as a stable nucleus for condensation of vapor. Once a supersaturated species has been

formed in the gas phase, the system is in a nonequilibrium state. It may pass toward the equilibrium condition either by generation of new nuclei or by condensation on existing particles. With existing particles, the supersaturated state collapses by condensation on existing particles and homogeneous nucleation is suppressed. The desired size of the nanoparticles cannot be produced any more. Thus, it is important to have a clean vapor phase without residual particles, before gas to particles conversion. Besides the generation of nanoparticles, phase transition is also used in the coating process, such as physical vapor deposition (PVD) (10)(9)(11). The coating with PVD has many advantages: 1) almost any type of inorganic material can be used as well as many kinds of organic materials; 2) the process is more environmentally friendly than processes such as electroplating. Another application of phase transition is separation of impurities. Separation is carried out according to the different sublimation temperatures of different materials in mixtures (12)(13). With proper control, very high purity of target material can be achieved. Phase transitions also involve in the fuel droplet evaporation. Fuel droplet evaporation is a study with the object of generating a homogeneous mixture of fuel vapor and air which provides a stable combustion with low pollutant emission for the complete operating range of the engine (14)(15)(16)(17). The combustion performance and emission is greatly influenced by the atomization of the liquid fuel, evaporation of the fuel droplets and mixing of fuel and air.

Sublimation and evaporation are the common methods to get vapor phases of desired species. Although different industrial routes involving sublimation (evaporation) are already being developed, still the theoretical knowledge governing the phase transition (sublimation or evaporation) is not fully understood. The fundamental understanding is of great importance to improving the process, for example in the nanoparticles generation. Heating temperature and residence time are conventionally considered to be two important process parameters in the sublimation (evaporation). When the residence time or the heating temperature is too low, the sublimation will not be completely implemented and the residual particles are introduced to the following processes. On the contrary, when the temperature is too high the material decompose in the heating process, which leads to a commercial loss. Besides heating temperature, there are many parameters that decide the sublimation/evaporation process. The investigation of phase transition to control the sublimation process is of great importance in the relevant industrial applications including nanoparticles generations.

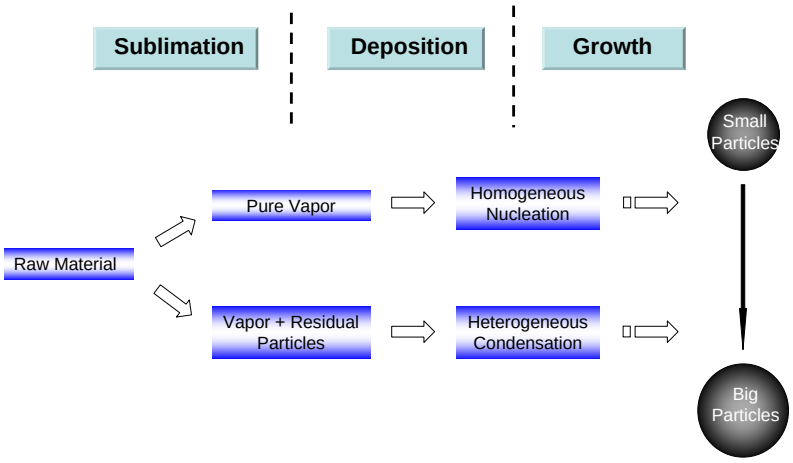

Figure 1.2: Depiction of nanoparticles generation through sublimation and vapor deposition process.

In this work, the physical processes of particle-to-gas phase transition are mainly discussed. In order to meet the demand of industrial practices, the factors of heating temperature, particle concentration, particle size distribution (PSD), particle morphology and particle residence time in the heating process are investigated. Two kinds of materials are tested: 1) particles of Ammonium Chloride (NH_4Cl); 2) droplets of Di-Ethyl-Hexyl-Sebacat (DEHS).

For many of the commercially important materials, there are no reliable data of vapor pressure curve, diffusion coefficient, etc. available, which are necessary to calculate the phase transitions. In this work an advanced experimental setup with on-line control was built, where gas flows and temperatures were controlled, and the pressures were monitored. Particle sublimation or droplet evaporation were observed through measuring the change of particle size distribution (PSD) before and after heating.

Based on the thermodynamic theory, numerical models are developed. With such models, aerosol sublimation can be predicted without expensive experiments. The mass (molecules) transition between gas and particles phases was thoroughly investigated. A new effect was discovered, which helps us understand the process better.

Particle sensors are very important in the aerosol study to measure the particle size distributions and concentrations. Optical particle sensors are used widely, in order to avoid any influence on the sample by probing. Optical sensors are used in this work to measure the change in the particle size distribution during the particle sublimation or the droplet evaporation. Optical sensors are, however, very sensitive, especially to high temperature. The present commercial optical sensors cannot work under high temperature. It is also the biggest obstruction in the particle sublimation study. In this work a new optical sensor is developed, which can work under 500 ^oC. With the help of the new sensor, in line particle measurement can be realized.

2 Present Studies in Droplet Evaporation and Particle Sublimation

Tab.2.1 exhibits the representative studies of droplet evaporation and particle sublimation. These studies were focused on the single droplets/particles or monodispersed droplets/particles. Different parameters such as temperature, relative humidity and particle size were taken into account. However, there is still less investigations contributed into the multiparticles influence in the particle sublimation process. The present work in this thesis is concentrated on the study of multiparticles sublimation.

Table 2.1: Researches in the study of Droplet Evaporation and Particle Sublimation

	Single Particle/Droplet Size			
	nm	μm	$\mu m \sim mm$	mm
Droplet		Taflin (63) and so on	Prommersberger (24), Schiffter (35) and so on	Davis (23), Lee (40) Hegseth (43)
Particle	Mori (34), Nanda (39) Lee (41)	Savage (36)	Swanson (44)	

2.1 Present Studies in Droplets Evaporation

Numerous investigators have studies the full range of water vaporization phenomena since Maxwell (18) analyzed quasi-steady state diffusion-controlled evaporation from a wet bulb. Many of studies contributed to the evaporation of water film or water droplet on high temperature materials, such as metal and ceramics (19), (20), (21) and (22).

Fundamental studies on liquid droplet evaporation were performed by Froessling (54). On the basis of a dimensionless analysis he derived the well-known relationship for the Sherwood number as a function of the Reynolds and Schmidt number. For the determination of the constant of the relationship, he investigated the evaporation of water, nitrobenzene, and aniline droplets suspended in air. Experiments were carried out at room temperature for Reynolds number ranging from 2 to 800 and droplet diameters from 0.1 to 0.9 mm.

Many researchers already addressed the phenomena associated with evaporation of single droplets. The suspended-droplet technique has been widely employed in experimental studies of droplet evaporation. The experimental results from suspended-droplet studies have been employed to predict the vaporization characteristics of convecting droplet. Many researches (23) (17) described an experimental configuration of droplet, which involved suspension of a single droplet from a fiber or a thermocouple bead (Fig.2.1). A liquid-fuel droplet assumes a spherical shape around the bead. The solid bead and the droplet are assumed to remain concentric. The whole system is in a laminar, hot air stream flow. The configuration is very idealized.

A study on droplet evaporation in hot ambient with different water vapor concentration has been conducted by Lee, et.al.(40). "Big droplets" with diameters about 1$\sim$2 mm were introduced into the study. The squared droplet diameter (droplet surface area) decreases almost linearly as the time lapse ($\frac{dd_p^2}{dt} = Const$). It is also observed in the work that the different water vapor humidity has not significantly effected the evaporation of those "big droplets". The same tendency has also been observed by Hiromistu (42).

Hegseth et.al.(43) studied the evaporation of methanol droplet. The droplet with a diam-

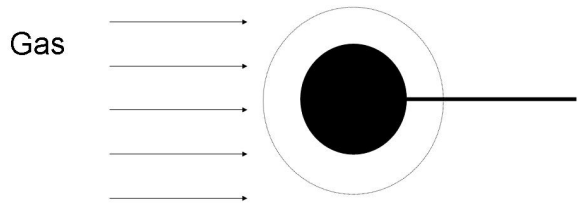

Figure 2.1: Evaporation of a single suspended droplet

eter of about 2 mm was observed by a charge coupled device video camera. Reflected light from the droplet edge is focused into the camera. Occuring of vigorous convection inside of an evaporating droplet was observed. This convection was driven by surface tension gradient in the droplet. As the droplet evaporated the relative humidity (RH) of methanol increased. The evaporation rate ($\frac{dd_p^2}{dt}$) decreased with increasing RH.

With the emergence of lasers, new measurement techniques evolved which allowed the determination of the droplet size with a higher accuracy than by photographic imaging. Ravindran et. al. (62) measured the size of droplets suspended in an electric field. The initial droplet diameters were between 1.2 and 2.4 μm. The droplet liquids were pure organics with very low volatilities. The carrier gases were helium, nitrogen, or carbon dioxide. The experiments were performed at standard atmospheric pressure and at temperatures ranging from 7 ^oC to 32 ^oC. During the measurement period, the droplets changed their size significantly. Plotting the square of the droplet radius versus time yielded straight lines showing that the evaporation process was diffusion-controlled.

Taflin et.al. (63) reported evaporation measurements of single water droplets that showed non-isothermal effects. They trapped single water droplets in an electrodynamic balance and made angular light scattering measurements to determine the droplet size as a function of time by comparing the data with Mie theory. The smallest droplet

in the experiment was bigger than 10 μm. A linear relationship between the reduce of droplet's surface and time was discovered.

Many experiments and calculations have already been performed on a single free-falling water droplet. Prommersberger et.al.(24) introduced an experimental setup where the evaporation of free falling droplets was investigated. Monodisperse droplets were generated in the upper part of the test rig while fall separately due to gravity, through a gas phase under constant pressure. The distance between the evaporating droplets is far, there is no interaction between the droplets. The initial droplet diameter varied between 640 μm and 820 μm. The droplet diameter and the droplet velocity are measured simultaneously by means of video technique and a stroboscope lamp.

El Golli et al.(25) measured the evaporation of drops of double distilled water, while recording the scattering light of droplet in a fine spray at various distances from the spray nozzle. The mean droplet radii varied from 7.4μm at 20cm distance from the nozzle to 1.3μm at 100cm. The time of evaporation was of the order of 100 $milliseconds$. The mean radii were used without reference to the size distribution which must have changed during evaporation.

Ranz and Marshall (28) measured the rates of evaporation of pure liquids and solutions in droplets at ca. 0.1 cm in diameter, which were exposed to air stream velocities up to 300 cm/s. In nominally still air gravitational convection may take place, thus increasing the rate of evaporation due to the air movement; clearly this will only be possible when the evaporative cooling is large.

Kincaid and Longley (26) described the evaporation measurement of single droplet. The photographic technique have been used to measure the change of droplet size. The evaporation loss from droplets between 0.3 and 1.5 mm diameter were measured. With decreasing of the water droplet the loss rate was increased. It was also addressed that a more accurate particle measuring technique was needed in the study.

General studies of the relationship between humidity and equilibrium droplet radius have also been carried out a lot (30), (31). The effect of the temperature depression is to reduce the partial pressure of vapor at the droplet surface and slow the rate of

evaporation. Fig.2.2 indicates the temperature depression for water droplets at different ambient conditions. An important action is that it may prevent the growth of fine hygroscopic particles in moist air (32), (33). There is negligible temperature depression when the atmosphere surrounding the droplet is saturated with vapor.

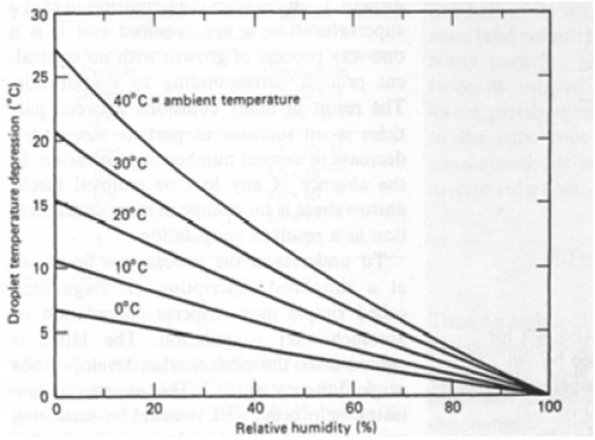

Figure 2.2: Water droplet temperature depression as a function of relative humidity for ambient temperatures $0 - 40^oC$

Most of the studies were focused on the effects of temperature and pressure in droplets evaporation. Single droplet evaporation was carried out a lot. Some researches were performed on the equilibrium between the droplets and air humidity (circumstance vapor pressure). But in industrial applications, the droplets involved in evaporation have a high concentration, which makes the instance much different from that of the single particle. In case of droplets with wide size distribution, the interaction between droplets with different diameter cannot be neglected.

2.2 Present Studies in Particle Sublimation

A crystalline-to-gas transition in a nanometer-sized silver particle (9 nm) on a graphite substrate was carried by Mori, et.al.(34) A high resolution electron microscope (HREM) was used to observe the change of particle size in a vacuum chamber (pressure was

below $7 \times 10^{-7} Pa$). Particles were heated slowly to 950 K and kept at that temperature. No melting of the particle was observed during the process.

Savage et.al (36) studied the kinetics of sublimation of monodispersed polystyrene spheres with 1.4 μm in diameter. It was observed that crystallites sublimate at a steady rate from their perimeter until they reach a characteristic size, after which they vaporize very rapidly.

The size-dependent evaporation of free-spherical PbS and Ag nanoparticles has been investigated by Nanda et.al (39) by size-classified aerosols. The temperature at which the particle size decreases due to evaporation is found to be size-dependent and decreases with decreasing particle size.

Swanson et.al (44) used electrodynamic levitation techniques to measure sublimation rate of single ice particles. The changes of particle size were inferred from i) light-scattering phase functions, ii) balance voltage measurements, and iii) optical images. In the experiments, an irregularly shaped frost particle ($\sim 50 \mu m$) sublimated to a sphere after a while. They have observed that particles lose their initial sharp corners at first. The breaking off of small protuberances from the surface of all types of frost particles were observed.

In the study of solid particle sublimation, most of the works were performed in the research of monodisperse particles. The effects of aerosol's concentration and particle size distribution on the sublimation process were still not fully studied. However, these effects are very important in the industrial applications. Different from droplets, solid particles are usually not in the shape of ideal spheres, which plays a great role in the sublimation process. Few studies are focused on this point.

3 Theory

For molecules of a droplet (or a particle) to evaporate, they must be located near the interface, be moving in the proper direction, and have sufficient kinetic energy to overcome liquid-phase (or solid-phase) intermolecular forces. At low temperature, only a small proportion of the molecules meet these criteria, so the rate of evaporation is limited. (29)

3.1 Mean Free Path of Gases

There are many situations in aerosol technology where there is an interaction between the particles and the gases and one must take into account the discontinuous nature of the gas. The gas cannot be treated as a continuous fluid but must be considered a collection of rapidly moving molecules randomly colliding with the particles. The criterion for such an approach depends on the particle size relative to the spacing between the gas molecules. Rather than using the average spacing between molecules, a more useful concept is the *mean free path*, which is defined as the average distance traveled by a molecule between successive collisions. From the kinetic gas theory the *mean free path* can be calculated by (30):

$$\lambda = \frac{k_B T}{\pi \sqrt{2} d_m^2 p}, \tag{3.1}$$

where d_m is the collision diameter of the molecule, defined as the distance between the

centers of two molecules at the instant of collision. For air the collision diameter is 3.7 $\mathring{A}$. The mean free path for air at 1 atm and 20 C is 0.066 μm.

A dimensionless number–Knudsen number is commonly used to describe the interaction of gases and particles, which is the ratio of the mean free path of diffusing species, λ, to the particle diameter, d_p.

$$Kn = \frac{2\lambda}{d_p} \tag{3.2}$$

The limiting cases of continuum theory and free-molecule theory apply for $Kn \to 0$ and $Kn \to \infty$, respectively. The regime between the two extremes is frequently referred to as the transition region. In general, for practical purposes the transition region is defined as $0.25 < Kn < 10$; $Kn > 10$ is free molecule region; $Kn < 0.25$ is continuum region (46).

At normal atmospheric pressure the mean free paths of gas and vapor molecules are much smaller than a micrometer. In this condition, sublimation/condensation processes for micrometer-size aerosols are in the continuum regime, where Cunningham corrector is necessary in the description of gas flow (see Section.3.3).

3.2 Particle Reynolds Number (Re_p)

A key to understanding of the aerodynamic properties of aerosols is the particle Reynolds number, a dimensionless number that characterizes fluid flow around an obstacle such as an aerosol particle.

$$Re_p = \frac{\rho V_{pg} d_p}{\mu} \tag{3.3}$$

Laminar flow around a particle occurs at low Re_p ($Re_p < 1$) where viscous forces are

much greater than inertial forces. As Reynolds number (Re_p) increases above 1.0, eddies form downstream of the particle, gradually becoming more numerous and vigorous.

3.3 Sedimentation in a Gravitational Field

Sedimentation, or settling, refers to the steady particle motion resulting from the balance of gravity and gas resistance (drag) forces. The gravity force is important only when large, dense particles are involved. Applications include the the collection of high agglomerated particle or large particles in large chambers with long residence times. Sedimentation can also play a role in the deposition of droplets when the droplet size and density are sufficiently large. (51) (53) (52)

The gravitational force that drives the settling velocity is

$$F_G = m_p g = \frac{\pi d_p^3}{6}(\rho_p - \rho_g)g, \tag{3.4}$$

when $\rho_p \gg \rho_g$, then $\rho_p - \rho_g \approx \rho_p$.

The resistance force (drag) on the particle in the direction of gravitational is

$$F_D = \frac{C_D}{C_c}\frac{\pi}{8}\rho_g d_p^2 v_s^2 \tag{3.5}$$

where v_s is the settling velocity of the particle, C_c is the Cunningham correction factor, and C_D is the drag coefficient of the particle, which depends on its Reynolds number Re_p.

In physical terms, the dependencies on pressure and particle size are primarily due to the ”slip” of the particles as their size approaches the gas mean free path. In terms of

pressure and particle diameter, the Cunningham correction factor is (30)

$$C_c = 1 + (2/pd_p)[6.32 + 2.01exp(-0.1095pd_p)] \tag{3.6}$$

where p is the absolute pressure ($cm\ Hg$ in this equation) and d_p is particle diameter (μm in this equation).

Particles commonly encountered in materials synthesis are of micron and submicron sizes. For these particles, Re_p is usually less than 0.1, for which

$$C_D = 24/Re_p \tag{3.7}$$

The sedimentation, or settling, velocity of particles in the Stokes regime ($Re_p < 1$) can be obtained by combining Eq.3.4 to Eq.3.7 and observing that $\rho_p \gg \rho_g$ for aerosol:

$$v_s = \frac{\rho_p d_p^2 g C_c}{18\mu} \tag{3.8}$$

3.4 Stokes's Law

If taking the drag force on the particle in the direction of the gas flow into account, there is the *Stokes's law*. According to *Stokes's law*, the total resisting force on a spherical particle due to its relative velocity (V_{pg}) to the fluid in the direction of gas flow is given by:

$$F_D = \frac{3}{C_c}\pi\mu V_{pg} d_p \tag{3.9}$$

3.5 Partial Pressure

In a mixture of idea gas, each gas has a partial pressure, p_i, which is the pressure that the gas would have if it alone occupied the volume. The total pressure of a gas mixture is the sum of the partial pressures of each individual gas in the mixture.

$$p = \sum_{i=1}^{n} p_i \tag{3.10}$$

The partial pressure of a gas dissolved in a liquid is the partial pressure of that gas which would be generated in a gas phase in equilibrium with the liquid at the same temperature. The partial pressure of a gas is a measure of thermodynamic activity of the gas's molecules. Gases will always flow from a region of higher partial pressure to one of lower pressure; the larger this difference, the faster the flow. Gases dissolve, diffuse, and react according to their partial pressures.

3.6 Vapor Pressure

Vapor pressure, p_i^* is the pressure of a vapor in equilibrium with its non-vapor phases. All liquids and solids have a tendency to a gaseous form, and all gases have a tendency to condense back to their original form (either liquid or solid). At any given temperature, for a particular substance, there is a pressure at which the gas of that substance is in dynamic equilibrium with its liquid or solid forms. This is the vapor pressure of that substance at that temperature. The equilibrium vapor pressure is an indication of a liquid's (or solid) evaporation rate. It relates to the tendency of molecules and atoms to escape from a liquid or a solid.

The ratio of the actual vapor pressure to the saturated vapor pressure at the same temperature is saturation ratio.

$$S = \frac{p_i}{p_i^*} \tag{3.11}$$

3.7 Kelvin Effect

The vapor pressure of material in equilibrium, $p_{i,d}^*$ with a spherical drop at a given temperature depends on the material and on the size of the particle (47), (48). This size dependence, resulting from the surface tension of the particle-air interface, is known as Kelvin effect (50). Saturation vapor pressure, p_i^*, is defined as the equilibrium partial pressure for a plane (flat) surface at a given temperature. For small particles the surfaces are mostly convex, the partial pressures required to maintain equilibrium are greater than that for a flat surface. To maintain mass equilibrium, the partial pressure of vapor must be greater than the saturation vapor pressure, p_i^*. The relationship between the saturation ratio (p_i/p_i^*) required for equilibrium (no growth or sublimation) and droplet (particle) size for pure materials is given by the well-known Kelvin equation:

$$\frac{p_{i,d}^*}{p_i^*} = \exp \frac{4\gamma M}{\rho R T_d d^*} \tag{3.12}$$

where γ, M and ρ are the surface tension, molecular weight, and density of the material and d^* is the Kelvin diameter. The droplet (particle) will neither grow nor evaporate when the saturation ratio of the partial pressure is $p_i = p_{i,d}^*$ and $S = p_{i,d}^*/p_i^*$. Each droplet (particle) size needs a different partial pressure p_i that maintains the droplet (particle) size.

3.8 Thermodynamic Stability and Phase Change

In the thermodynamic opinion, there are three possibilities of phase status:

(a) *Stable equilibrium* in which the initial phase is stable with respect to all phases different from the initial phase.

(b) *Metastable equilibrium* wherein the initial phase is stable with respect to all phases infinitesimally different from it. However, there is at least one other phases, which is not stable, with respect to the initial on.

(c) *Unstable equilibrium* in which the initial phase is unstable in relation to all phases infinitesimally different from it.

As vapor saturation is exceeded, clusters or embryos will form in the supersaturated medium. Because of their small size, their surface-free energy is critical to their stability. These submicroscopic agglomerates thermodynamically have greater probability of splitting apart than continuing to grow in the weakly supersaturated vapor. The vapor then may remain in a metastable gaseous state (macroscopically) until higher supersaturations are attained. With continued increase in supersaturation, the molecular clusters of condensed phase are created on a microscale, giving rise to appreciable condensation to form particles as an aerosol cloud.(57)

3.9 Description of Droplets in Evaporation

In this section the evaporation of a droplet, which has a same velocity of the gas flow, is described. The particle's Reynolds number Re_p is nearly zero. The basic equations used are derived from the microscopic theory of dilute gases (58) except that terms representing vapor condensation and evaporation are included

$$N_v = x_v(N_v + N_g) - cD_{vg}\nabla x_v. \tag{3.13}$$

3.9.1 Unidirectional Diffusion

One direction diffusion of droplet molecules into gas phase: droplet molecules evaporate into the gas phase; then, the vapor, N_v, go through a stationary gas layer into the gas phase. There is a net motion of particle vapor away from the droplet surface and the carrier gas is stationary $N_g = 0$. The molar flux in the direction of particle diameter is considered:

$$N_v = -\frac{cD_{vg}}{1 - x_v} \cdot \frac{dx_v}{dr}, \tag{3.14}$$

and

$$N_v dr = -\frac{cD_{vg}}{1 - x_v} \cdot dx_v. \tag{3.15}$$

If we take the assumption that the gas and vapor both behave as perfect gases. Then,

$$c = \frac{p}{RT}. \tag{3.16}$$

In a steady state we have $\frac{d\mathbf{N_v}}{dt} = 0$ and in a spherically symmetric geometry this equation can be integrated immediately from $r = \frac{d_p}{2}$ to $r = \infty$ to give the total mass flux away from the droplet as

$$\dot{m}_c = \pi d_p^2 \frac{M_p p}{RT} D_{vg} \frac{d}{dr} \ln(p - p_v) = 2\pi d_p \frac{M_p p}{RT} D_{vg} [\ln(p - p_v) - \ln(p - p^*_{v,d})]. \tag{3.17}$$

The mass flux $\dot{m}$ ($= \dot{m}_c$ in the present continuum case) is related to the droplet growth rate by

$$\dot{m} = -\pi \rho_p d_p^2 \frac{1}{2} \frac{dd_p}{dt}. \tag{3.18}$$

To determine $\frac{dd_p}{dt}$, first we have to find the total heat flux, Q, away from the particle and use energy conservation to relate Q to $\dot{m}$ to find T_d. In the steady state the total constant heat flux vector relative to the particle surface

$$Q_c = -\pi d_p^2 k_g \frac{dT}{dr} + h_v(T)\dot{m}_c, \tag{3.19}$$

if we take h_v to be $h_v(T_d)$, the value on the droplet surface, it is then easy to integrate Eq. 3.19 to obtain

$$Q_c = h_v(T_d)\dot{m}_c + 2\pi d_p k_g (T_d - T_\infty), \tag{3.20}$$

where

$$T_\infty = T(r = \infty). \tag{3.21}$$

Since it involves with absolute enthalpies, the heat removal rate is also given by the reduction in energy content of the particle from its loss of mass

$$Q_c = h_p(T_d)\dot{m}_c. \tag{3.22}$$

In terms of the particle and vapor enthalpies, h_p and h_v, respectively, the latent heat of vaporization is given by

$$\triangle H_v(T_d) = h_v(T_d) - h_p(T_d), \tag{3.23}$$

so that Eq.3.20 give

$$\dot{m}_c = -\frac{2\pi d_p k_g (T_d - T_\infty)}{\triangle H_v}. \tag{3.24}$$

Given T_∞ and p_v or S ($S = p_v/p^*_{v,d}(T_\infty)$), the Eq.3.17 and Eq.3.24 are sufficient to determine the m_c and thus $\frac{dd_p}{dt}$.

$$\frac{dd_p}{dt} = \frac{4(S-1)}{\rho_p d_p [\frac{\Delta H_v^2}{k_g R T_\infty^2} + \frac{p - S p^*_{v,d}(T_\infty)}{p D_{vg} \rho_g(T_\infty)}]}. \tag{3.25}$$

If we take the Kelvin effect into account, Eq.3.25 gets into

$$\frac{dd_p}{dt} = \frac{4(S-1-\frac{4\gamma_{pg} M_p}{\rho_p R T d_p})}{\rho_p d_p [\frac{\Delta H_v^2}{k_g R T_\infty^2} + \frac{p - S p^*_{v,d}(T_\infty)}{p D_{vg} \rho_g(T_\infty)}]}. \tag{3.26}$$

The same expression is also adopted by Barrett (59) and Sachweh (60) to describe the growth of liquid drops in a cloud.

3.9.2 Opposite Diffusion

There is another theoretical approximation of droplet evaporation: opposition diffusion. In the opposition diffusion, the evaporated molecules on the droplet surface diffuse into gas phase (N_v); at the same time, the gas molecules diffuse in the opposition direction to the droplet surface (N_g). In this case, at the phase interface of the droplet and the gas phase is $N_v = N_g$. Eq.3.13 turns out to be:

$$N_v = -cD_{vg} \nabla x_v = -D_{vg} \nabla c_v. \tag{3.27}$$

The solution of this equation is depending on the boundary conditions. At the droplet surface the vapor concentration is noted as c_d; in the gas phase is considered as c_∞. Hence:

$$c_d - c_\infty = \frac{\dot{m}}{4\pi D_{vg}} \int_{\frac{d_p}{2}}^{\infty} \frac{dr}{r^2} = -\frac{\dot{m}}{2\pi D_{vg} d_p}, \tag{3.28}$$

or

$$\dot{m} = -2\pi d_p D_{vg}(c_d - c_\infty). \tag{3.29}$$

For low volatility particles $T_d = T_\infty$:

$$\frac{dd_p}{dt} = \frac{4D_{vg}M_p}{R\rho_p d_p}(\frac{p_v - p^*_{v,d}}{T_\infty}). \tag{3.30}$$

Strictly speaking, either sublimation or condensation of particles has to be accompanied by thermal changes resulting from release or absorption of latent heat. The simultaneous transfer of thermal energy and material to or from a particle can be calculated.

If the particle is fairly volatile it cools while evaporating because of loss of latent heat ($T_d < T_\infty$). Being cooler than the surrounding air, heat is conducted to it from the air. The Eq. 3.29 comes to be:

$$\frac{dd_p}{dt} = \frac{4D_{vg}M_p}{R\rho_p d_p}(\frac{p_v}{T_\infty} - \frac{p^*_{v,d}}{T_d}). \tag{3.31}$$

It is important here to get the particle temperature, T_d.

- Rate of conduction of heat to the particle $= \pi d_p^2 \cdot k_g \cdot (\frac{dT}{dr})_{\frac{d_p}{2}}$

- Rate of loss of heat by evaporation $= \triangle H_v \dot{m} = \pi d_p^2 D_{vg} \triangle H_v (\frac{dc}{dr})_{\frac{d_p}{2}}$

when both the temperature and the rate of evaporation are steady:

$$k_g (\frac{dT}{dr})_{\frac{d_p}{2}} + D_{vg} \triangle H_v (\frac{dc}{dr})_{\frac{d_p}{2}} = 0, \tag{3.32}$$

the resulting steady-state temperature depression, $T_\infty - T_d$, can be given by:

$$T_\infty - T_d = \frac{D_{vg} M_p \triangle H_v}{R k_g} (\frac{p^*_{v,d}}{T_d} - \frac{p_v}{T_\infty}). \tag{3.33}$$

The latent heat of vaporization can be gotten from Clausius-Clapeyron relation,

$$\frac{1}{p^*_v} dp = \frac{\triangle H_v}{RT^2} dT. \tag{3.34}$$

The temperature depression seems to be independent of the particle size (23). When we see the Eq.3.33 clearly, however, it can be seen that the particle surface saturated pressure, $p^*_{v,d}$, is dependent on the particle size (according to the Kelvin effect). In this case a small particle has a big temperature depression due to the high particle surface pressure.

On the other hand because of the dependence of $p^*_{v,d}$ on T_d Eq.3.33 cannot be solved explicitly and an iteration method must be used here.

3.10 Fuchs Effect

Fuchs (45) reasoned that the transport of vapor molecules from the surface of a particle to an imaginary concentric sphere of diameter $d_p + 4/3\lambda$ is controlled by the kinetic

theory of gases. Beyond this sphere, the sublimation is controlled by diffusion. This is called Fuchs effect. Davies (23) developed an expression for the rate of mass transfer by the combined mechanisms. The rate of decrease in particle size becomes:

$$\frac{dd_p}{dt} = \frac{4D_{vg}M_p}{R\rho_p d_p}(\frac{p_v}{T_\infty} - \frac{p^*_{v,d}}{T_d})[\frac{2\lambda + d_p}{d_p + 5.33(\lambda^2/d_p) + 3.42\lambda}]. \tag{3.35}$$

For large particles there is not much of a difference between sublimation as predicted by Eq.3.31/Eq.3.35 because most of the time required for sublimation is spent while the particles are large. Corrections for the Kelvin effect and the Fuchs effect are important for the simulations with small particles (30).

3.11 Heat and Mass Transfer Equilibrium

Equilibrium between an aerosol and its surrounding vapor is shown to be generally fast so that vapor supersaturations are small. Diffusion and conduction control evaporation and condensation on aerosols so that the sign of the aerosol growth term can be determined by the ratio of their relative rates. Lewis number, Le, where $Le < 1$, as for water vapor-air mixtures, aerosol may evaporate as the mixture is cooled. A "condensation number" $Cn(T)$ representing the ratio of the rate of heat transport to that of latent heat by vapor diffusion, and which is a strong function of temperature, is introduced to describe the other main controlling physical effect in aerosol formation, $Cn(T) \ll 1$ (as for high temperature water vapor-air mixtures). The proportion of vapor that can condense as an aerosol is very small. For a fixed total heat transport rate, the maximum aerosol formation rate occurs near $Cn(T) = 1$, which is at $T \approx 4^\circ C$ for water vapor-air mixtures at 1atm pressure.

$$Le = \frac{Sc}{Pr} = \frac{rate\ of\ heat\ transport\ by\ conduction}{rate\ of\ mass\ transport\ by\ diffusion} \tag{3.36}$$

$$Cn = \frac{rate\ of\ heat\ transport}{rate\ of\ latent\ heat\ transport\ by\ vapor\ diffusion} \tag{3.37}$$

Equilibrium between an aerosol and its surrounding vapor will often be so fast that concerning heat and mass transfer, it will be a very good approximation to take the local vapor concentration and have its equilibrium value at local temperature. This is also a basic assumption by Hills (1964) and Clement (1985).

$$Cn \gg 1, \tag{3.38}$$

when droplets growth and condensation are limited by diffusion to the droplet, and

$$Cn \ll 1, \tag{3.39}$$

when the limiting factor is the ability of surrounding gas plus vapor conducting away the latent heat.

3.12 "Traveling" Effect

Under some situations such as droplet traveling through still air or the flowing of very big droplets (above millimeter in diameter) in gas flow, the relative velocity of droplets and gas phase cannot be ignored. The particle Reynolds number Re_p must be taken into account.

In case of a droplet flowing through a moving airstream, forced convection is the process under which evaporation takes place. For this situation, Froessling (54) developed a empirical relation for the mass transfer number, Sherwood number (Sh)

$$Sh = 2.0 + 0.60 Sc^{1/3} Re_p^{1/2}, \tag{3.40}$$

where $Sc = \nu_g / D_{vg}$ is Schmidt number. According to the heat transfer analogy proposed by Ranz and Marshall (28), the heat transfer number (Nusselt number) should be correlated with heat transfer data according to:

$$Nu = 2.0 + 0.60 Pr^{1/3} Re_p^{1/2}, \tag{3.41}$$

where $Pr = C_p \mu / k$ is Prandtl number. These equations meet the requirement that $Sh = Nu = 2$ at $Re_p = 0$.

Marshall (55) and Goering et.al (56) made a modification using geometric and mass definitions for the rate of diameter change for an evaporating droplet:

$$\frac{dd_p}{dt} = \frac{2 D_{vg} M_p}{R \rho_p d_p} \left(\frac{p_v}{T_\infty} - \frac{p^*_{v,d}}{T_d} \right) Sh. \tag{3.42}$$

When the relative velocity of the droplet $V_{pg} = 0$ Eq.3.42 is equal to Eq.3.31.

3.13 Diffusion Coefficient

D_{AB} in Eq.3.43 is the gas mixtures diffusion coefficient. A number of empirical or semi-empirical correlations for estimating gaseous diffusion coefficient have been developed. A widely used equation is recommended by Reid et.al. and by Danner and Daubert (38).

$$D_{AB} = C T^{1.75} \frac{\sqrt{[(M_A + M_B)/M_A M_B]}}{p[\sqrt[3]{V_A} + \sqrt[3]{V_B}]^2} \tag{3.43}$$

with T in Kelvin (K), p in pascal (Pa), M_A and M_B in gramme per mole (g/mol) and $C = 1.013 \times 10^{-2}$, D in square meters per second (m^2/s). The terms V_A and V_B are molecular diffusion volumes and are calculated by summation of the atomic contributions in Table 3.1.

Table 3.1: *Diffusion Volumes in Fuller-Schettler-Giddings Correlation Parameters*

Diffusion Volumes for Some Atomic and Molecules						
He	Cl	S	C	H	O	N
2.67	21.0	22.9	15.9	2.31	6.11	4.54
O_2	Air	CO_2	H_2O	NH_3	N_2	H_2
16.3	19.7	26.7	13.1	20.7	18.5	6.12

4 Experiment Section and Measurement Technology

4.1 Experimental Setup

For the experimental study of the particles sublimation, a plant with a tube furnace was set up where aerosol particles sublimation under well-defined conditions was carried out. Fig.4.1 is a photograph of the experimental setup, Fig.4.2 indicates the flowsheet. The main part of the test plant was an aerosol transport tube with a diameter of 38 mm. There are two sections in the tube. A set of flow adjustment section was followed by a 1 m long heating section , where aerosol particles were heated and sublimated. In the heating section the wall of the tube was heated and the wall temperature is controlled. Clean air or N_2 was used as carrier gas to get particles out of the aerosol generator into the test tube (clean air was used in the sublimation of NH_4Cl; clean N_2 was used in the evaporation of DEHS). The particle concentration and gas flow velocity in the heating tube were adjusted by a dilution path, which controlled the mass flow and pressure through valves. The total flow was measured through a flow meter (HFM-200, Teledyne). A flow controller (Flowcontroller 300, Teledyne) was used to get the regulated flow of the main path. The pressure before the aerosol generator was controlled with an electrical valve (Rexroth). The particle concentrations in aerosols were regulated by the dilute flow. Electrical heating bands (Horst, Temperature(max): 900^oC; Power: 500W) and oven (Thermolyne 21100 Tube furnace) were used to heat the tube. The temperature regulation was realized through a timercard, controlled by the voltage of the heating bands. On-line control of the whole set-up was carried out by a Labview program through a control computer. The temperature of the gas flow in the

tube was measured though thermistor elements (K-type, Omega). Pressure in the tube was measured through pressure transmitters (Danfoss). The flow out of the sublimation experiment was sent into a cooler and a set of filters.

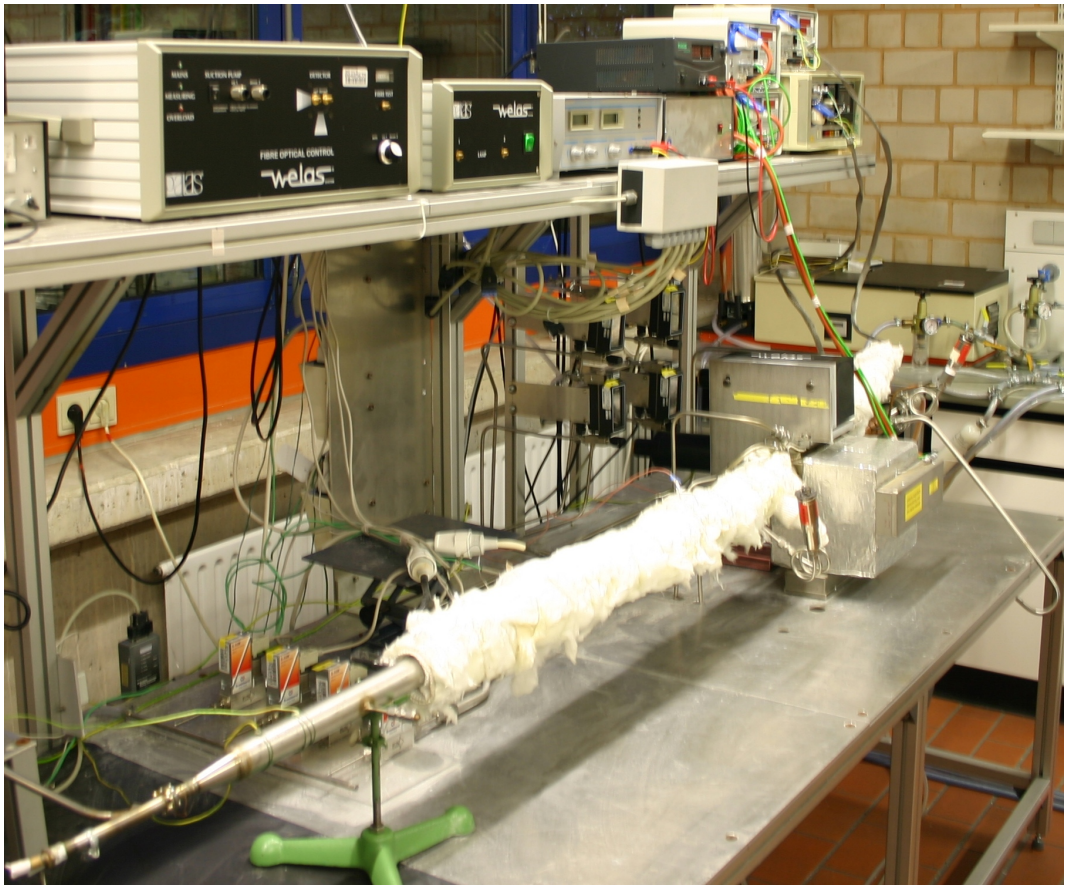

Figure 4.1: Photo of the experimental setup

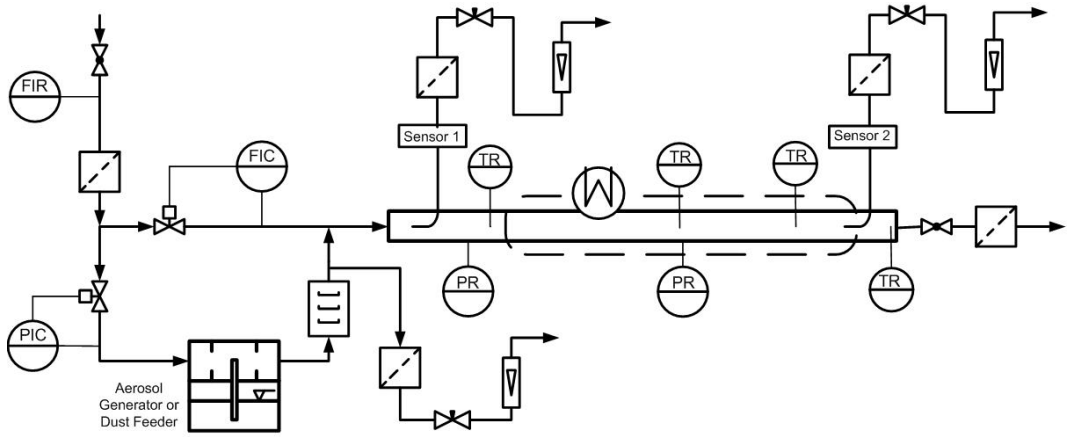

Figure 4.2: Flowsheet of the plant for sublimation investigation

Optical particle counters were used to measure the change of particle size distribution and particle concentration before and after sublimation. In the first part of the experiments, two commercial optical sensors (Welas-3000, Palas GmbH) were used. Two isokinetic on-line samplings were installed for the two sensors. Sensor 1 was installed in the 'cool' section of the tube, where the initial particles were measured. Sensor 2 was installed at the end of the heating section, where the particles after sublimation were measured. An additional heating band and an insulation were introduced to the sensor to keep the temperature constant. These particle counters, however, can measure the aerosols only up to 120^oC, which is too low to meet the needs of the sublimation study. In this case a new optical particle counter was developed, which can measure aerosol up to 500^oC in situ. In the second part of experiments, the new developed Hot Gas Sensor (HGS) was installed in the test plant, an in-situ particle measurement would be realized. The detailed description of the measurement technology in the experiments is presented in Section.4.2.

4.1.1 Test Materials

Inorganic material Ammonium Chloride (NH_4Cl) and organic material Di-Ethyl-Hexyl-Sebacat (DEHS) were used as test materials to study aerosols evaporation. NH_4Cl

is at room temperature a white powder and DEHS is a colorless liquid. The physical properties are shown in Table 4.1. The DEHS is a kind of organic material with a big Mole weight and big molecule size.

Table 4.1: Physical properties of NH_4Cl and DEHS $*$

Formulae	Mol.wt	Surface Tension	Density	Subl. Boiling point
	M/(kg/kmol)	γ/(mN/m)	ρ_p/(kg/m^3)	$T/^\circ$C
NH_4Cl	53.49	70†	1527	Subl. 340
DEHS‡	426.69	32	912	–

$*$ *Data listed in CRC Handbook of Chemistry and Physics (66)*
† *Calculation of NH_4Cl's surface tension is shown in Appendix A*
‡ *Molecule Structure of DEHS see Fig.4.3*

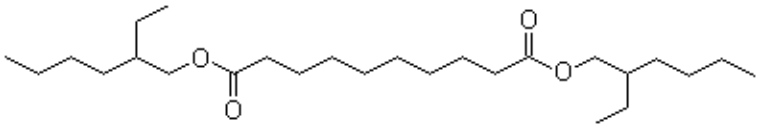

Figure 4.3: Molecule structure of DEHS

Vapor pressures, p_v^*, of NH_4Cl and DEHS can be calculated with Eq.4.1(67) and Eq.4.2(68), respectively. They are

$$\lg p_v^*(T) = 14.5 - \frac{7454.86}{446.58 + T}, \tag{4.1}$$

and

$$\lg p_v^*(T) = 14.3 - \frac{5590}{273.15 + T}, \tag{4.2}$$

where $P_v^*(T)$ in Pa, T in ^oC.

4.1.2 Aerosol Generators

Different aerosol generators were adopted to meet the different needs of the experiments. Three kinds of aerosol generators were used to get NH_4Cl particles or DEHS droplets into the heating tube.

1. Collison nebulizer (see Fig.4.4). NH_4Cl droplets were generated from the NH_4Cl-water solution in the container. Then, the NH_4Cl droplets were sent through a silica diffusion tube to get drying NH_4Cl particles.
2. Brush feeder (LTG Model NDF 100) (see Fig.4.5). Ground NH_4Cl particles were put into the brushfeeder's container. They were dispersed equably onto a rotary brush and then brought into the test plant.
3. AGK-2000 (Palas GmbH) (see Fig.4.6) was used for the generation of DEHS droplets. The compressed N_2 transported the droplets into the test plant.

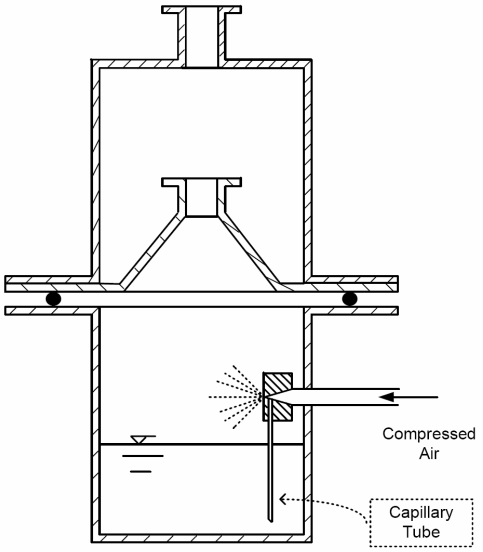

Figure 4.4: Structure of the Collison nebulizer

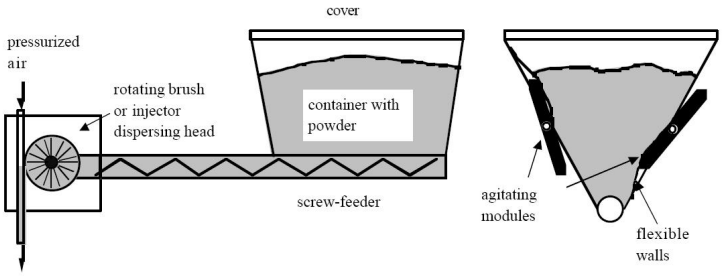

Figure 4.5: Structure of the Brush feeder (LTG Model NDF 100)

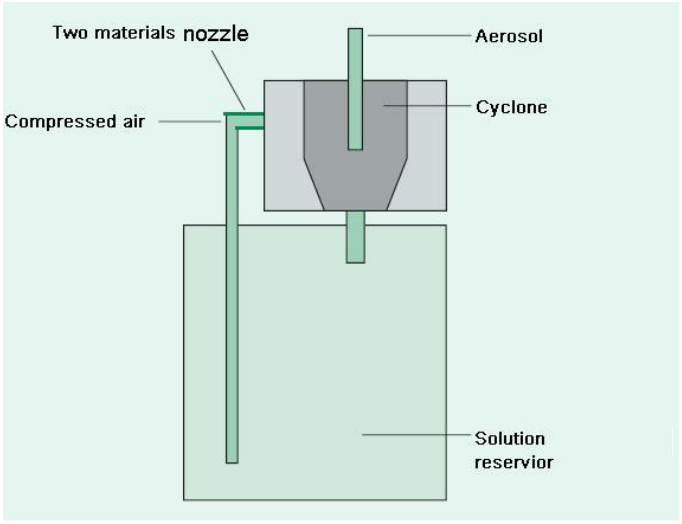

Figure 4.6: The structure of aerosol generators AGK-2000

4.1.3 Operation Control

Function and control of the test plant were realized by Labview program. Fig.4.7 shows the control panel of Labview, where the experimental parameters can be adjusted and collected. In order to control the test plant, measurement apparatus were regulated through a computer, including setting of the gas flow and pressure (aerosol genera-

tors and dilute path) in the heating tube. The measured temperatures and pressures in the test plant were shown in the Labview window and all the experimental parameters were registered in a corresponding text. There were four temperature measuring sites, which are exhibited in Fig.4.7: temperature before heating, temperature at the beginning of heating, temperature at the end of heating (corresponding to the second particle sensor) and temperature of the gas flow to the end filter. In the sublimation experiments, the temperature at the end of the heating section was considered as the aerosol temperature. There were two pressure measuring sites in the aerosol transport tube: pressure within the heating section and pressure outside the heating section. The pressure before aerosol generators was regulated. The gas flow in the dilute path was controlled. The total gas flow through the heating tube was measured.

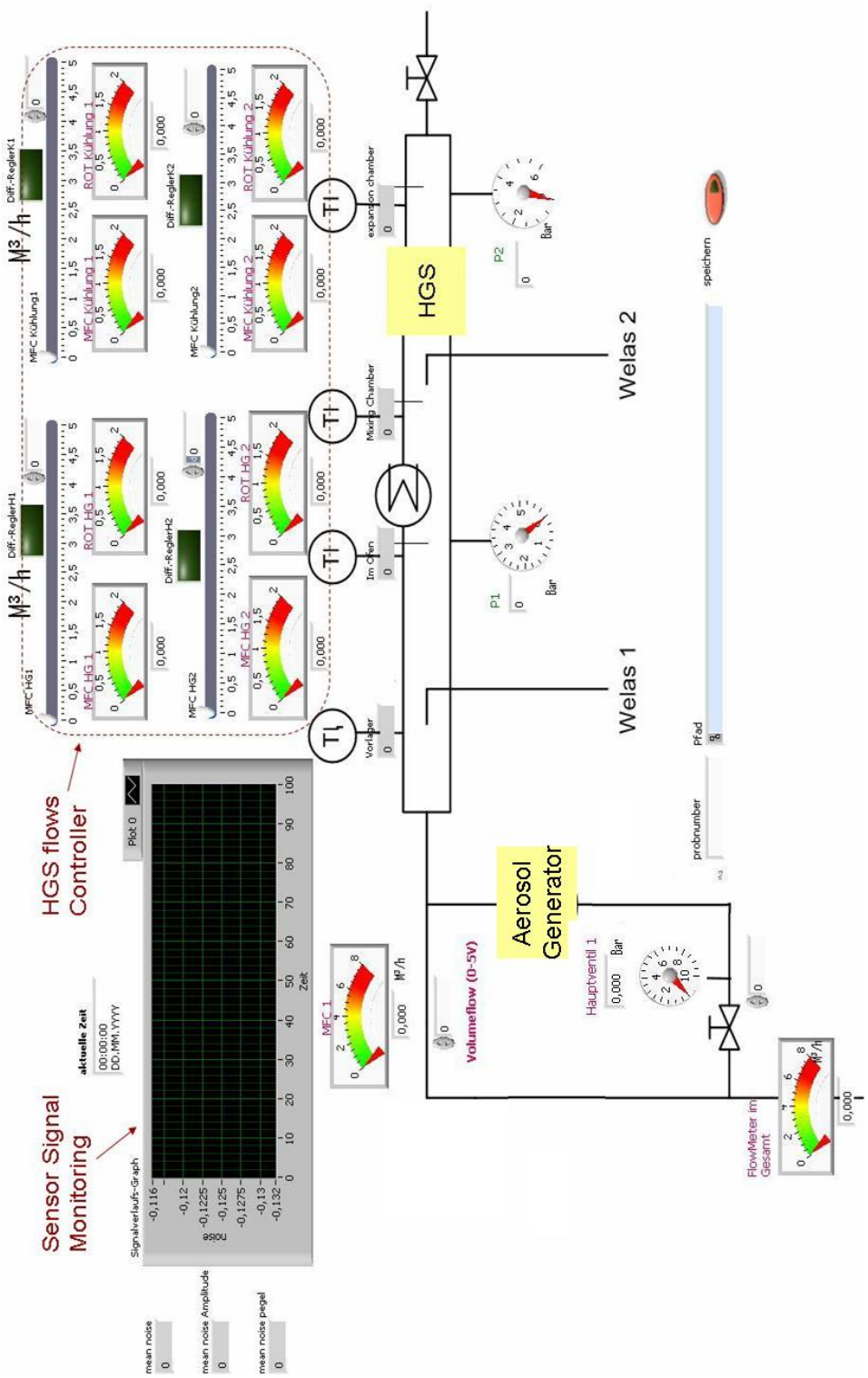

Figure 4.7: Front pane of the Labview controller of the whole experimental setup

4.2 Measurement Technology

4.2.1 Aerodynamic Particle Sizer: APS

APS spectrometer (Model 3321, TSI) measures both aerodynamic diameter and light-scattering intensity of particles. It counts size distribution for particles with aerodynamic diameters from 0.5 to 20 μm. It detects light-scattering intensity for particles from 0.3 to 20 μm. APS (Model 3321, TSI) is specifically engineered to perform aerodynamic size measurements in real time using low particle accelerations. Time-of-flight particle sizing technology involves measuring the acceleration of aerosol particles in response to the accelerated flow of the sample aerosol through a nozzle. The aerodynamic size of a particle determines its rate of acceleration, with larger particles accelerating more slowly due to increased inertia. As particles exit the nozzle, the time of flight between the APS's two laser beams is recorded and converted to aerodynamic diameter using a calibration curve. APS (Model 3321, TSI) measures light-scatterings by examining each particle's side-scatter signal intensity. This measurement produces a second distribution that can be plotted against aerodynamic size to gain additional information about the aerosol sample.

Aerodynamic diameter, d_a is defined as the diameter of a sphere of unit density that attains the same terminal (steady state) settling velocity, v_s at low Reynolds number in still air as the actual particle under consideration. It is more likely that the particle is moving in a gaseous medium and the inflight or aerodynamic nature is the property observed. Aerodynamic diameter may or may not equal true diameter. Inertial impaction and gravitational forces are proportional to the particle mass and in these cases aerodynamic diameter is the particle size that governs particle motion. When $Re_p > 3 \times 10^{-7}$ the terminal settling velocity can be found using Eq.4.3

$$v_s = \frac{d_a^2 g \rho_p C_c}{18\mu}, \tag{4.3}$$

where the aerodynamic diameter d_a of a particle can be decided.

The major difference between this instrument and an optical single-particle counter is that instead of measuring the intensities of the scattered light pulses, the aerodynamic particle sensor measures the velocities of particles exiting from an acceleration nozzle. These velocities are then related to particle size. The major disadvantage of the technique is that only low particle concentrations can be handled, due to coincidence errors.

4.2.2 Specific Surface Ratio

Two kinds of measuring methods were carried out to decide the specific surface ratio of particles. 1) **Monosorb** (Quantachrome) measurement is based on a high sensitivity, thermal conductivity detector, which measures the change in concentration of an adsorbate/inert carrier gas mixture (N_2 and H_2) as adsorption and desorption proceed. When integrated by the on-board electronics and compared to calibration, the detector provides the volume of gas adsorbed or desorbed. The specific surface ratio is decided. 2) **Autosorb-1** (Quantachrome) needs a sample preparation before measurement. The sample is heated at leat to 50 ^oC in vacuum to active the surface area of the particles completely (getting rid of water and O_2 in the samples). The specific surface ratio is decided according to the BET (Brunauer Emmett and Teller).

4.2.3 Optical Particle Sensor

There are two optical methods commonly used for detecting and measuring particle size or size distribution: Light blocking and Light scattering. The light blocking optical particle counter method is typical useful for detecting and sizing big particles and is based upon the amount of light a particle blocks when passing through the detection area of particle counter. The light blocking optical particle counter is used to measure small particles. Single particle optical sensor (OPC) is an important application of light scattering particle counter. It is found widespread use in aerosol studies because of their ability to make in situ measurement of the concentrations and size distribution of

particles suspended in the air. A beam of incident light is focused on to a ”measuring volume” through with the air borne particles pass one at a time. The amount of light scattered from each individual particle is measured by a photosensitive detector. Each signal corresponds to a particle count and this incremented in the appropriated size category to obtain particle concentration in a given size interval. There are three major sections in an OPC: i) the air flow system (sampling); ii) the optical system; iii) electronics system.

Theoretical Fundamentals of Optical Particle Sensor

When aerosol particles interact with light, the energy received can be reradiated by the particle in the same wavelength. The reradiation may take place in all directions but usually at different intensities in different directions. This process is called *scattering*. The angular distribution of intensity of the scattered light depends on the size, shape, orientation, composition, and structure of the particle. The scattered light thus carries information about these characteristics of the particle (69). If the particles are irregular in shape, the scattering will be different because a particle of a given size will have a scattering effect that will depend on its orientation. A number of irregular particles of the same size, randomly oriented with respect to the incident beam, will scatter light in a somewhat more diffuse manner than the same concentrations of spheres.

The scattering light of particle is proportional to its size. For particles much smaller than wavelength, $x \ll 1 (x = \pi d_p/\lambda)$, particles scatter light proportional to diameter to sixth power ($I \propto d_p^6$). This type of scattering is called *Rayleigh scattering*. For particles much larger than the wavelength of the incident light $(x \gg 1)$, the particles scatter light proportional to their diameter squared ($I \propto d_p^2$).

Rayleigh scattering for $x \ll 1$ and the large particle extinction law for $x \gg 1$ provide useful limiting relationships for the efficiency factor. It is necessary to make use of a much more complicated theory due to Mie, which treats the general problem of scattering and absorption of a plane wave by a particle between the two applications above.

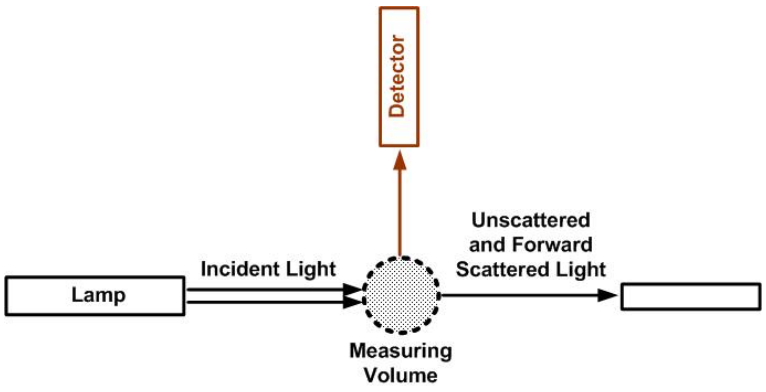

Figure 4.8: Scattered light used for the particle size analysis

A brief overview of Lorenz-Mie theory (61) is in order to permit interpretation of light-scattering data. For a sphere of radius r and refractive index m illuminated with a vertically polarized light beam with wavelength λ, the intensity of the light scattered in the horizontal plane is given by

$$I_l = \sum_{n=1}^{\infty} \frac{2n+1}{n(n+1)} [a_n \frac{P_n^l(\cos\theta)}{\sin\theta} + b_n \frac{d}{d\theta} P_n^l(\cos\theta)]^2 \tag{4.4}$$

where $P_n^l(\cos\theta)$ is the associated Legendre function, and θ is the scattering angle measured from the back side of the sphere. a_n and b_n are function of the optical size x ($x = 2\pi r/\lambda$)(63)

Fundamental Components of Optical Sensor

In order to realize the on-line particle measuring, particles are led into a measuring cell through a sampling. The incident light shoots through a measuring volume inside the measuring cell. When a particle flies through the cell, the incident light is scattered into all directions. The scattered (see in Fig.4.8) light after certain degree from the incident light will be gathered and sent to analyze. Particle size and size distribution in aerosol can be obtained. The structure of the measuring cell is shown in Fig.4.9.

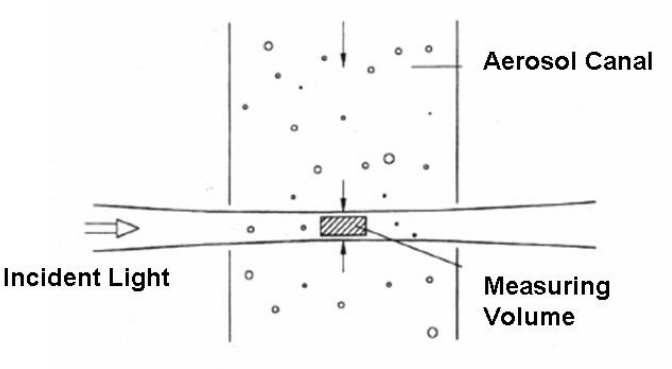

Figure 4.9: The structure of the measuring cell in the sampling

In this work, Welas-3000 (Palas GmbH) is used to measure the PSD in aerosol. White light is adopted in this sensor as incident light and scattered light after 90^o from the incident light are detected. Welas-3000 has a heating in the measuring cell (sampling), which can be heated to 120^oC. Due to the limitation of the optical system, however, the measured aerosol temperature cannot be above 120^oC. It is also the limitation of all the present optical particle sensors. It also restricts the development of the characterization of particle sublimation/evaporation behaviors by now.

The two sensors were calibrated using monodisperse latex particles independently, before the two sensors were built up in the test plant (Fig.4.2).

A high boiling point material–NaCl were used to control the calibration of the two sensors. Polydisperse NaCl particles were then introduced into the test plant. The particle size distributions were measured before and after the heating tube at room temperature. The sublimation effect of the particles can be ignored. Fig.4.10 indicates that the two sensors measure almost the same particle concentrations and particle size distributions at the two sites.

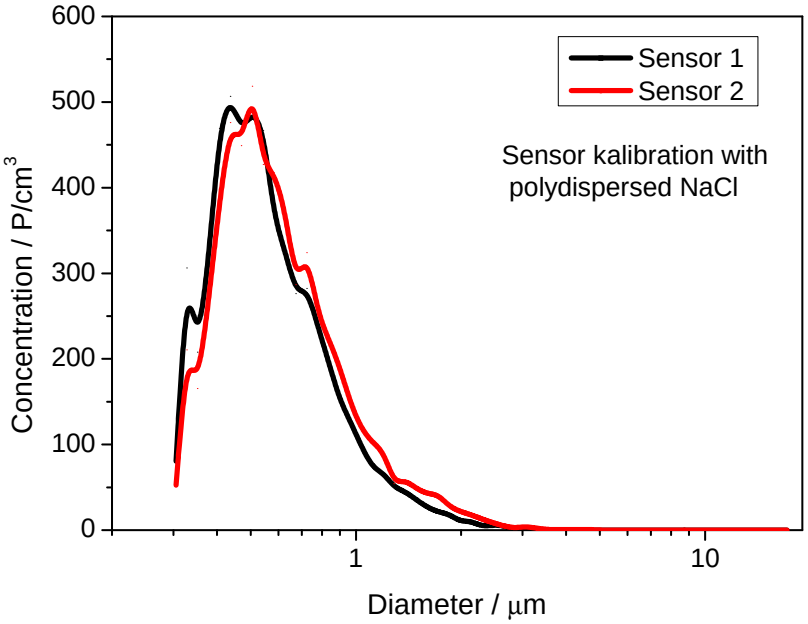

Figure 4.10: Measured polydisperse NaCl from two Welas-3000s in the experimental setup

New Development of Hot Gas Sensor and Correspond Experimental Setup

In order to meet the need of the aerosol development, a new optical in-line sensor was developed to measure the particle size and size distribution in a hot gas environment. The detector head in optical sensors is temperature-sensitive, which cannot be directly in contact with the high temperature medium. The present work was focused on the sampling in the sensor to avoid the contract of gas media with optical and electronic system. A new flow cell was developed in this work. The aim of the development was to avoid the direct contact between the sensor and hot gas. Two isolation flows were introduced in the measuring cell (Fig.4.11) of the hot gas sensor (HGS), which was designed for the applications of HGS specially.

As show in Fig.4.12, in the middle of the cell there is the main flow channel, where

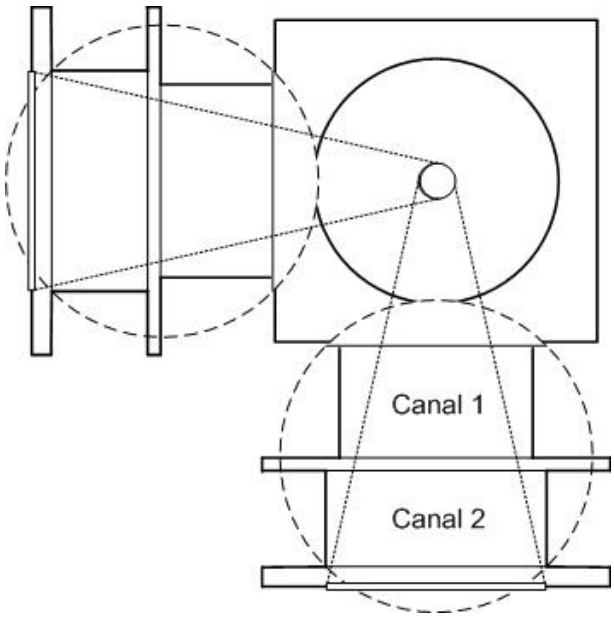

(a) Structure of hot gas sensor cell

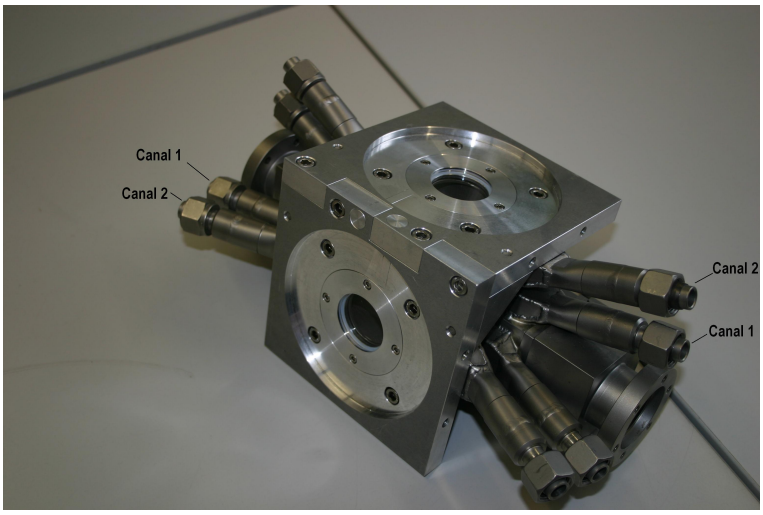

(b) Photo of the hot gas sensor cell

Figure 4.11: The structure of the HGS cell

the hot gas and aerosol pass through. The cell has two windows, which are in the two sides vertical to each other. The incident light gets into the cell from one side and the

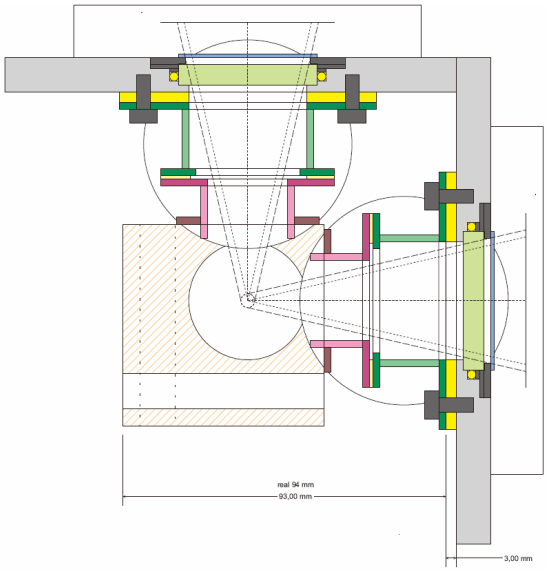

(a) Drawing of the detector head, designed for optical sensor

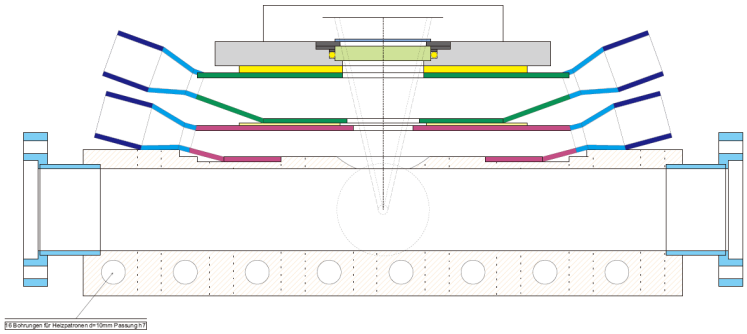

(b) Drawing of the detector head, working with two isolation flows

Figure 4.12: Drawing of the detector head of the HGS

scattered light after 90^o can go out of the cell through another window. At each side of the windows there are two pipelines: Canal 1 and Canal 2, which are built between the

main flow channel and windows (see in Fig.4.11-4.12). Incident light transfers from the glass window through the two isolation flows into the main flow, where the hot aerosol passes through. The scattered light from the aerosol after 90 ^{o} transfers to the detector of the sensor at another side window.

The extra canals in the cell are working as isolations between the hot gas flow and the sensor's lenses. The flows in canal 1 (the canals next to the main flow) are heated to the same temperature with the main flow, which is a particle isolation. The flows in canal 2 remain at room temperature, which is a heat isolation. Canal 2 remains at room temperature, then, the hot should not be conducted to the sensor.

In order to avoid mixing of the flows in the cell, the four isolation flows must be precisely controlled. The flows in Canal 1 and Canal 2 are controlled by mass flow controllers (ss316, Bronkhorst) before going into the cell and regulated by rotameters (DK37/M8E, Krohne) after the cell. The flows in Canal 1 are going into a cooler after the sensor cell, to cool down the temperature. All of the flows in Canals are going through the cell in the opposition direction from the main flow, reducing the contact time between mainflow and isolation flows. The cell is set up in the plant as Fig.4.13. All the massflow controllers and rotameters are controlled through a Labview program Fig.4.7 in PC. A digital regulator (Fig.4.14) is built up between each mass flow controller and a corresponding rotameter to exactly regulate each flow in the canals not mixing with each other.

The HGS cell and accessories are built in the experimental setup (Fig.4.15). Aerosols are heated through the residence time in the heating tube. The particle concentration and PSD are measured directly in the tube.

4.2.4 HGS Properties and Calibrations

Comparing with commercial optical particle sensor, (Welas-3000), the new developed HGS has a relatively big measuring volume and the focalized light in this measuring volume has a lower density. The intensity of the scattered light is weakened, especially for the small particles. This makes the HGS a low resolution of small particles

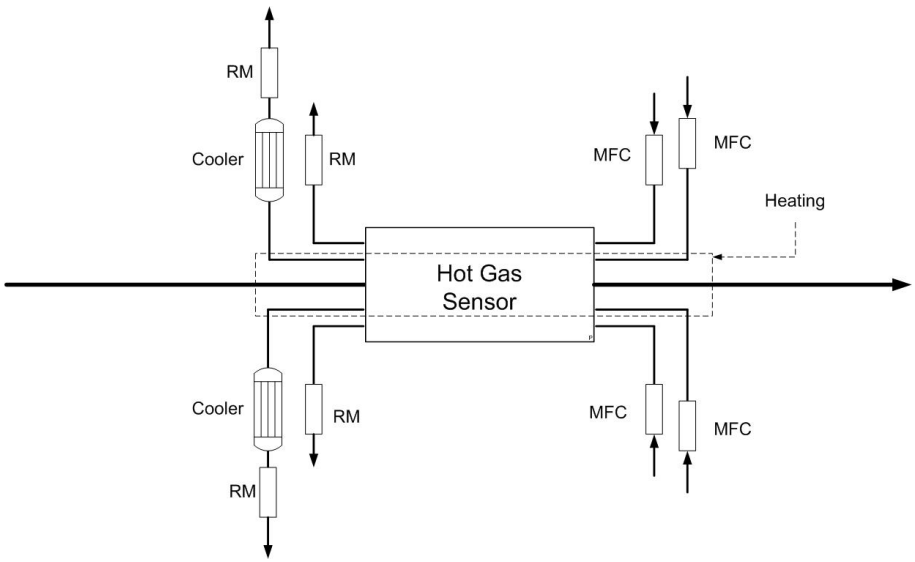

Figure 4.13: The experimental setup of the HGS cell, RM: Rotameter; MFC: Massflowcontroller

measuring. In the HGS and measuring cell, 'in situ' particles measurement is realized. Measurement sampling is avoided and this part of the error can also be avoided.

The HGS, however, cannot be calibrated independently. It was built in the test plant (experimental setup see in Fig.4.16). In this test plant, the sensor 1 measured the particles direct after the aerosol generator and dilute system. HGS measured the particles after the heating tube inline. Sensor 2 measured the particles directly after the HGS, to control the loss of the particles after flowing through the HGS. Calibration was carried out with particles out of aerosol generator. Monodispersed latex particles suspension with particle diameter of 1 μm was used. The "Rohdaten" in the sensor must be corrected. Together with the HGS calibration, a control measurement was conducted by sensor 1. The calibration results of HGS and control measuring results of sensor 1 (Welas-3000) were compared.

Sensor 1 (Welas-3000) and HGS have the same measuring results for monodispersed latex particles, which have a diameter of 1 μm (Fig.4.17). Then, a control measurement

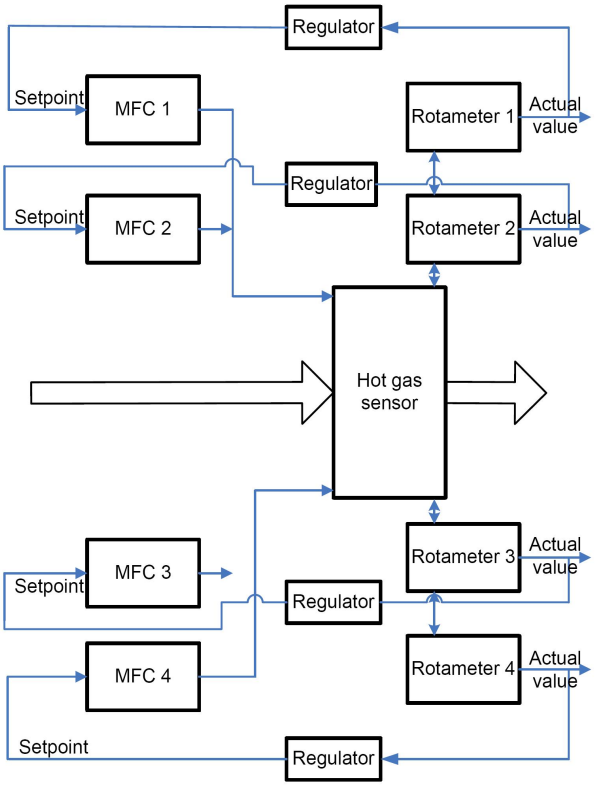

Figure 4.14: The digital control of the mass flow control and rotameter

was conducted with polydispersed NaCl particles. The comparison measurement with sensor 1 was also carried out at the same time. HGS has a lower resolving power, due to the limitation of the large measuring volume and white light intensity in HGS. Thus, the measurement range of HGS in case of NaCl particles begins at 0.5 μm (Fig.4.18). In the range of particles bigger than 0.7 μm, the two sensors have identical measuring results.

In the sublimation experiments, NH_4Cl particles were used. The controlling measurement of HGS is also carried out with the polydispersed NH_4Cl particles. The compared measurement of sensor 1 (Welas-3000) and HGS is conducted and shown in Fig.4.19. It can be seen that the Welas-3000 and HGS have the same measuring results in the

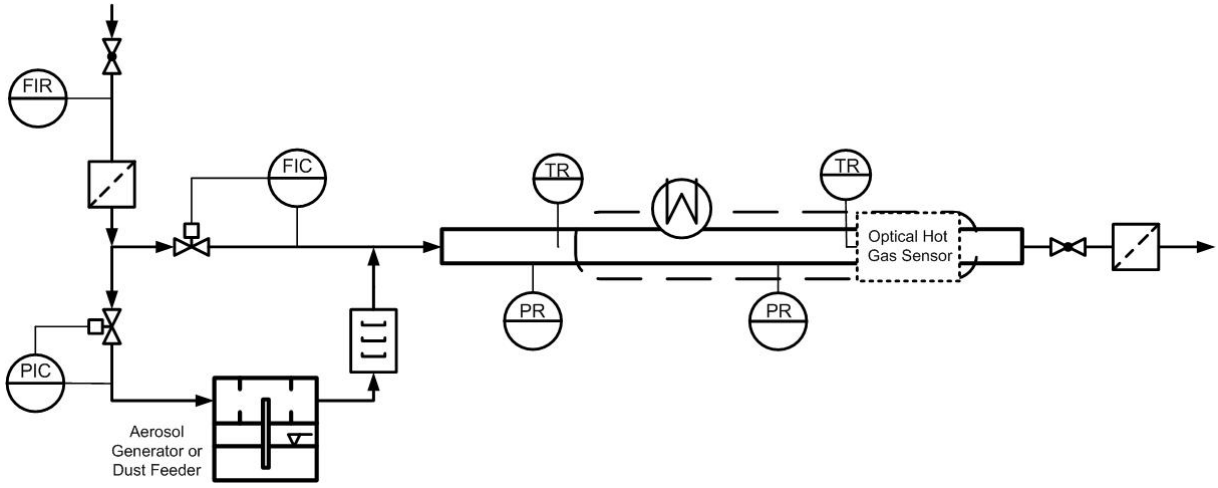

Figure 4.15: Experimental setup of the HGS cell in the heating plant

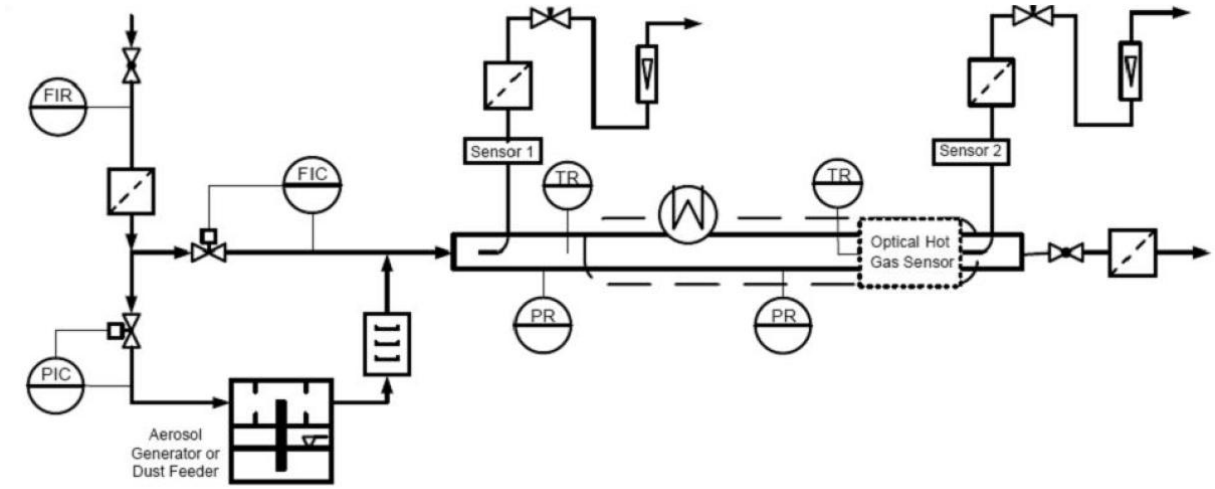

Figure 4.16: HGS calibration setup, both of the two Welas-3000s and HGS are setup in the heating tube

particle range of bigger than 0.7 μm.

The controlling measurement of HGS at high temperature is also carried out. Due to the temperature factor on the volume flow, the particles' residence time in the measur-

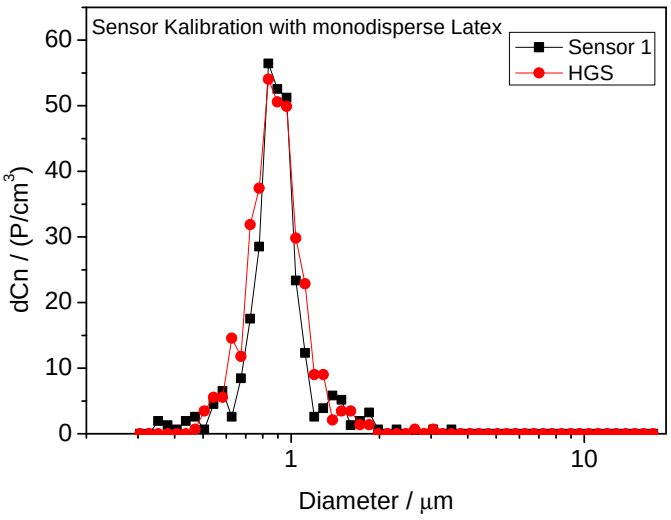

Figure 4.17: PSD of Latex particles measured from Sensor 1 and HGS respectively

ing volume must be measured (This measurement is carried out by the sensor itself) and the particles' mean velocity must be calculated by each measurement (Measuring volume of the sensor is given in the software already). The measuring result of HGS is compared with that of Sensor 2 (Welas-3000) at the same time. The measuring of HGS and sensor 2 are conducted at the same temperature 120 ^oC. The NH_4Cl particles out of aerosol generator were used. The results are shown in Fig.4.20. In the range of big particles the two sensors have accordant results, whereas small particles cannot be countered by HGS.

The control measurement of polydisperse NH_4Cl was carried out with Sensor 1, HGS and Sensor 2 at the same time. In order to focus on the measuring range of HGS, the range was selected at from 0.6 μm to 40 μm. The measurement results are shown in Fig.4.21. The bimodal in the figure is coming from the miss of large amount of particles under the measuring range. Looking at the measuring range of the HGS, the three sensors have almost the identical results. The loss of the particles by flowing through the HGS cell is not detectable by these sensors.

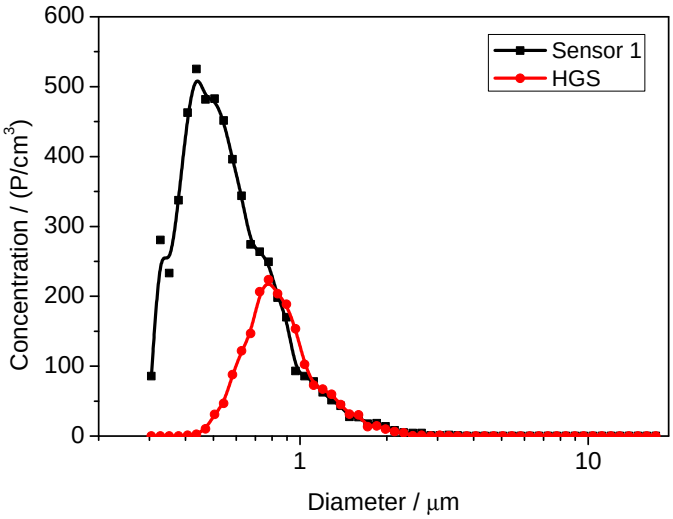

Figure 4.18: PSD of polydispersed NaCl particles measured from Sensor 1 and HGS respectively

4.2.5 Noise Effect

In the course of the particles sublimation, noise was measured from the HGS, which displacing an overload signal of particle measuring. Together with the measurement of NH_4Cl particles, the noise was measured at different heating temperatures. In order to see the noise quantitatively, an oscilloscope was connected with the photomultiplier in HGS. An increased noise was tested with increased heating temperature (Fig.4.22-Fig.4.23). But when the heating temperature was over 300^oC, the noise is depressed. It is interesting to see that the increasing of the noise intensity with increased heating temperature has the same tendency with the molecule concentration in the gas phase (Fig.4.23). The molecule concentration is calculated according to the saturated vapor pressure in the gas phase, $p_v^*(T)$.

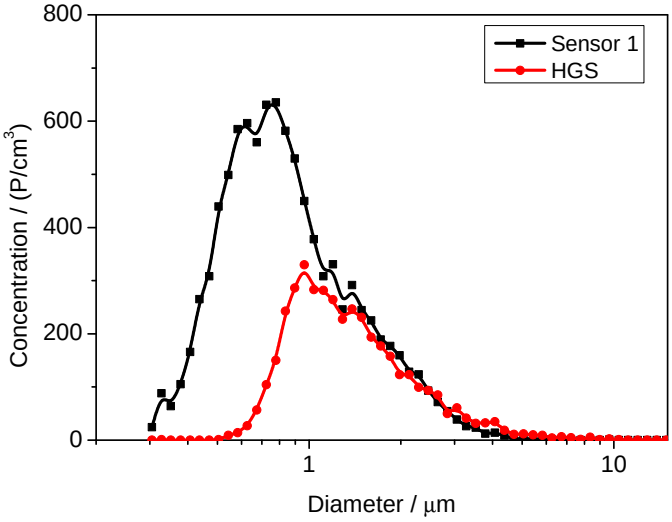

Figure 4.19: PSD of polydispersed NH_4Cl particles measured from Sensor 1 and HGS at room temperature, respectively

Experiments

In order to see clearly the properties of the noise, a set of experiments were conducted in an experimental setup (Fig.4.24). The heating systems in the experimental setup were controlled separatively. NH_4Cl particles were used as test materials to see the noise. NH_4Cl was introduced into the heating tube at place a (Fig.4.24), instead of the utilization of an aerosol generator. The air flow in the tube was heated to different temperatures.

The following processes were carried out to test the noise effect.

1. Activated heating zone b and activated sensor heating c, putting gas flow through the tube, without particles in Place a;
2. Activated heating zone b and deactivated sensor heating, putting gas flow through the tube, with particles in Place a;

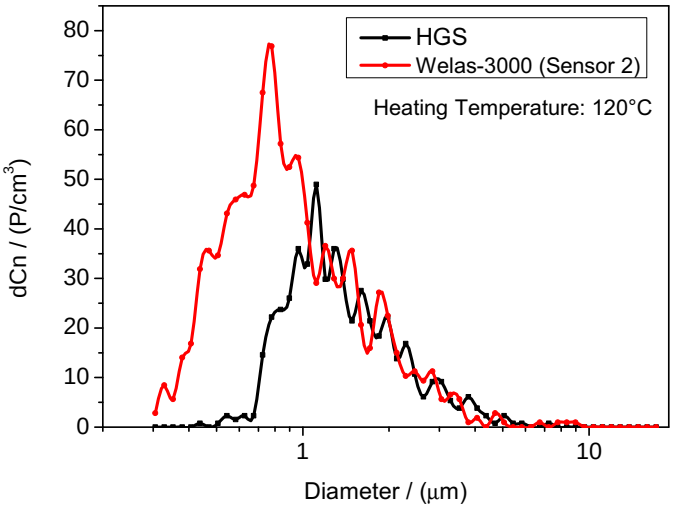

Figure 4.20: PSD of polydispersed NH_4Cl particles measured from Sensor 2 and HGS at 120 ^oC.

then, activating sensor heating

3. Deactivated heating zone b and activated sensor heating, putting gas flow through the tube, with particles in Place a;
   then, activating heating zone b and deactivating sensor heating

Experimental Results

1. Without particles in the plant, there was no significant noise signal detected by the oscilloscope;
2. With particles in the plant, activating the heating zone b, there was noise coming out of the HGS; activating sensor heating, there was also the noise at first. After a while, however, the noise was going down, then disappeared completely;
3. With particles in the plant, activating heating zone c, there was no noise coming out of the HGS; deactivating sensor heating and activating heating zone b, there was noise coming out.

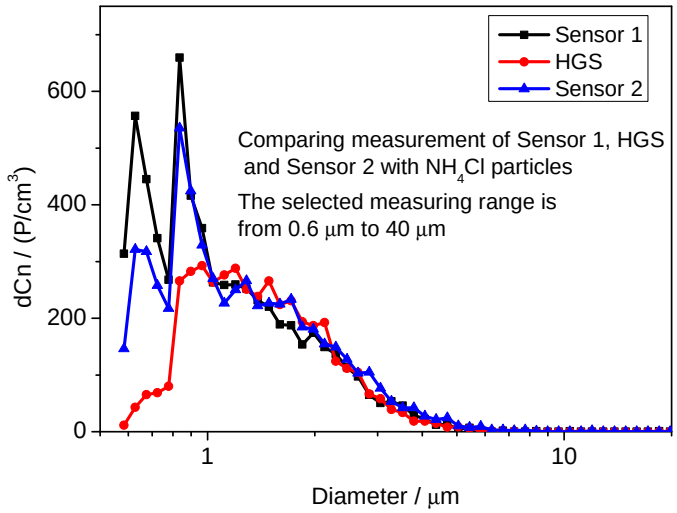

Figure 4.21: The controlled test of the three sensors (Sensor 1, HGS and Sensor 2) under the measuring range of HGS, Sensor 2 is directly after the HGS to see the particle loss through aerosol flowing.

Discussion

According to the experiments above, the significant noise signal occurs only when enough materials are sublimated into gas phase and there is a temperature difference between HGS cell and transport tube. The significant noise signal is based on the overloaded desublimated molecular clusters or nanoparticles in gas phase. The 'noise' is supposed to be coming from the different temperature of the gas phase before HGS and the gas temperatures in the sensor. The two isolation flows in canal 1 are heated before the flows go into the cell of HGS. The temperature in the canal 1 in the cell may be lower than the temperature at the heating tube. Due to the limitation of HGS, it is impossible to set a temperature sensor in the path of the light scattering. There may be a temperature difference between the HGS cell and the heating tube before the cell. The temperature distribution is shown in Fig.4.25. If the gas temperature in the HGS cell is lower, a oversaturation, S, is generated in short time. The sublimated molecule in the gas phase is going to nucleate or condensate, which can change the transparency

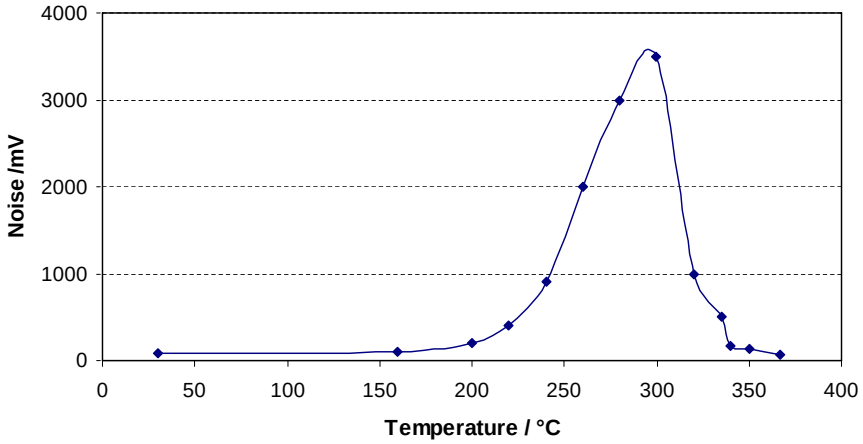

Figure 4.22: The intensity of the noise with different heating temperatures

of the gas phase in HGS. When a set of light is going through the gas flow, the nuclei in the flow scatter light in every direction. Some scattered light then goes into the detector of the sensor, eventhrough there is no initial particles in the gas flow. It is also important to note that, the nuclei are very small, which are not detectable for HGS actually. In this case, it is measured by oscilloscope as noise, which cannot be translated into particle signals.

In this case, in the operation of HGS the heating temperature in the HGS cell should be adjusted slightly higher than the temperature in the heating tube.

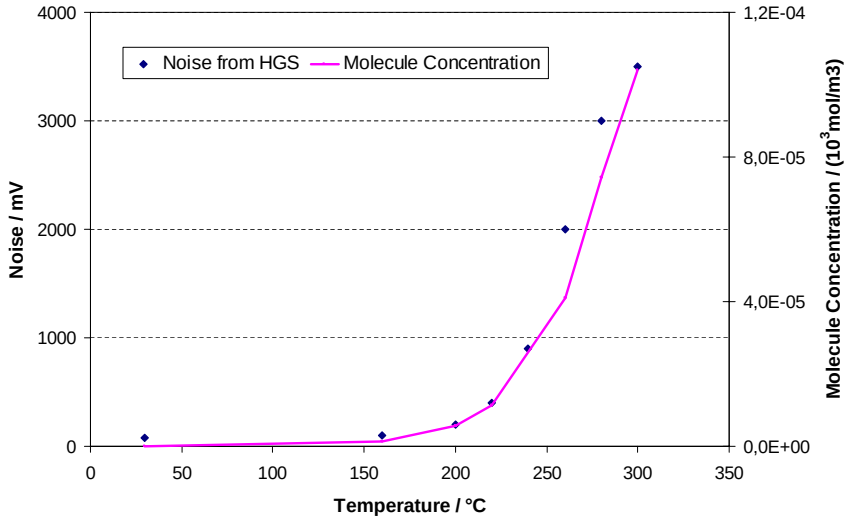

Figure 4.23: Comparison of the noise intensity and the molecules concentration at the same temperature

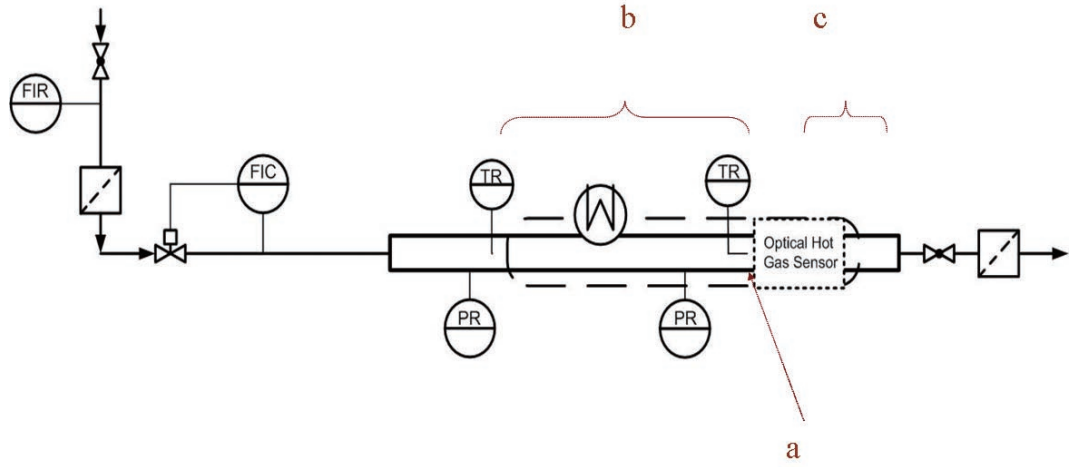

Figure 4.24: Experimental setup for the research of the HGS's noice; a) the NH_4Cl powder place; b) heater of the plant; c) heater of the HGS

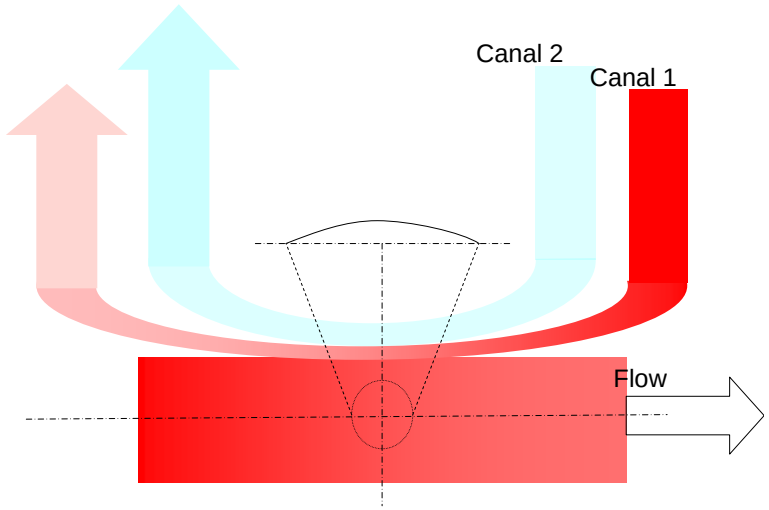

Figure 4.25: Indication of the temperature changes of flows in canal 1 and canal 2.

5 Experimental Results

In this chapter the experimental results of NH_4Cl particles sublimation and DEHS droplets evaporation are presented. In the particle sublimation study, two kind of NH_4Cl particles with different smooth surface and porous surface were taken into account.

5.1 NH_4Cl Particles with Smooth Surface Sublimation Studies

Brushfeeder (LTG Model NDF 100) was built in the test plant (see Fig.4.5) and used as an aerosol generator to transport ground NH_4Cl particles into the test plant. The SEM photos of the ground NH_4Cl particles are shown in Fig.5.1. These particles have relative smooth surfaces and solid particle structures. The change of the particle size distribution and particle concentrations were measured in the test plant through the experiments.

5.1.1 Experiments with Different Heating Temperature

Heating temperature is supposed to be the most important factor in particles sublimation. Vapor pressure of the material $p_v^*(T)$ increases with heating temperature. Enhancing the heating temperature more materials can be sublimated into the gas phase from particles. There is an increased molecule concentration in the gas phase. The conducted experimental conditions are shown in Tab.5.1.

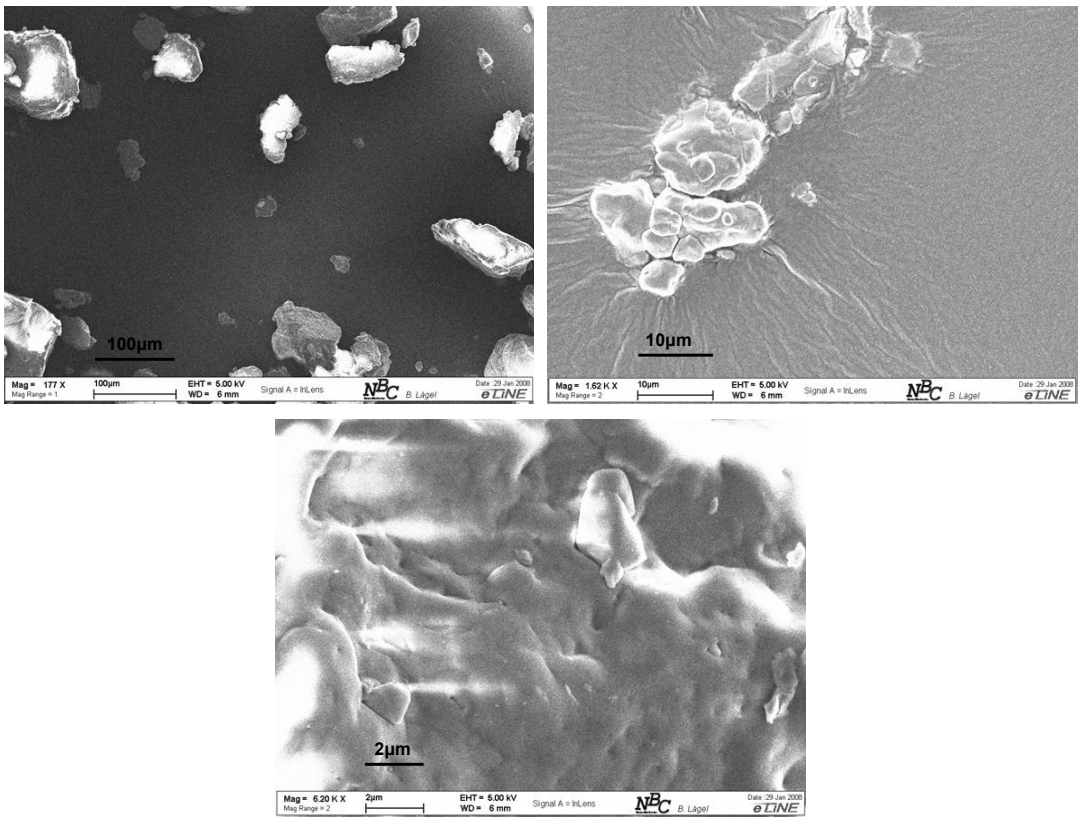

Figure 5.1: SEM of ground NH_4Cl particles, which is sent into test plant through a brushfeeder

In this section, the experiments were carried out at a constant gas flow, but different heating temperatures. At first two identical optical sensors (Welas-3000) were used to measure aerosol's PSD before and after heating. Due to the limitation of the sensor, the object aerosol can only be heated up to 120 ^oC. In order to measure aerosol under higher temperature, the new developed HGS was employed, where the aerosol is heated to 180 ^oC. Due to the character of HGS (see in Section 4.2.4), very small particles in aerosol ($< 0.5\mu m$) cannot be measured.

The temperature profile in the tube from Sensor 1 to Sensor 2 is shown in Fig.5.2, where the gas in Sensor 2 is heated to 120 ^oC. Three temperature sensors were introduced in the heating tube to measure the temperature profile. The first measured inlet temperature of the gas flow. The second measured the temperature in the heating tube

Table 5.1: Experimental conditions of ground NH_4Cl particles sublimation

Heating Temperature		Gas Flow	Pressure
Welas-3000	HGS		
Up to 120 ^oC	Up to 180 ^oC	2.5 m^3/h	1.1∼1.3 bar

($L = 60cm$) the third one measured the temperature at the sensor 2 ($L = 100cm$). It can be seen that the calculated temperature profile was in accordance with the measuring results.

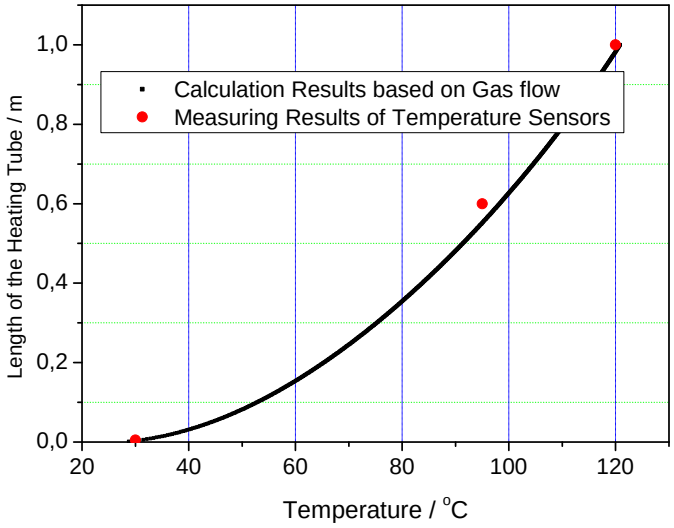

Figure 5.2: The temperature distribution in the heating tube, at the exit the gas flow was heated to 120 ^oC. Temperature were measured at different temperature sensor sites.

Fig.5.3 shows the experimental measuring results with Welas-3000, where the aerosols were heated up to 120 ^oC. The total particles concentration decreases intensively with increased heating temperature. There is a special decrease in the small particles concentration. The big particles ($> 1\mu m$) concentration, however, is almost constant with increased heating temperature.

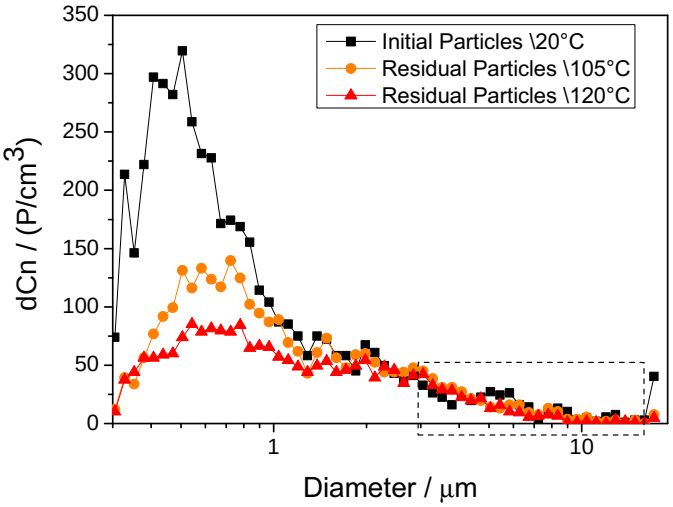

Figure 5.3: Sublimation experiments with the particles of sample of ground NH_4Cl, which has solid structures and smooth surfaces. Two identical Welas-3000s are used and test aerosols are heated up to 120 ^oC.

Then, the particles sublimation measurement was conducted with HGS. The results are shown in Fig.5.4, where the aerosol at the measuring site was heated up to 180 ^oC. Because the measuring range of HGS begins at 0.5 μm, the change of very small particles concentrations in aerosols cannot be monitored. Increasing heating temperature the particles smaller as 1 μm decreases, whereas the concentration of big particles is nearly constant (or decrease slightly at high temperature).

Comparing Fig.5.3 and Fig.5.4, we can see that in the sublimation process small particles concentration decreases at first, big particles concentration keeps constant. With increased heating temperature, there is remarkable decrease in the small particles concentration. When the particles concentration is already very low, the concentration of big particles reduces too.

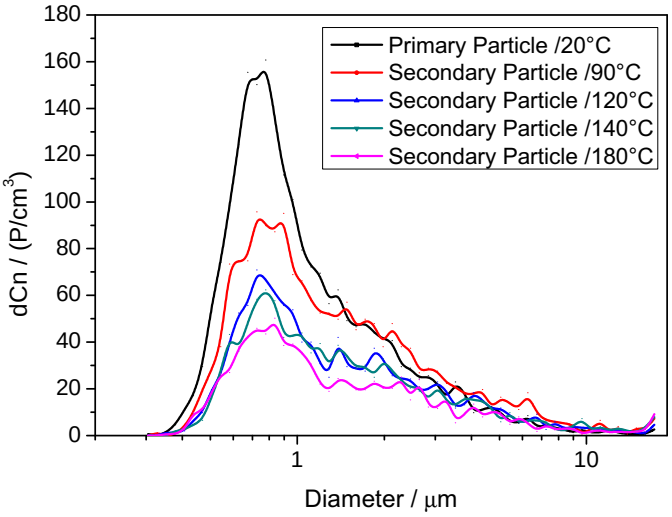

Figure 5.4: Sublimation experiments with the particles of sample of ground NH_4Cl. HGS was used here and the aerosol was heated up to 180 ^oC

5.1.2 Experiments with Different Particle Concentrations

Particle concentration in the initial aerosol is also an important parameter in the sublimation process. With high particle concentration, more particles can be sublimated into the gas phase. The partial pressure p_v increases faster. Fig.5.5 shows the aerosol sublimation at higher particles concentration. The particles concentration increases about 5 times. The concentration of the small particles apparently decreases whereas the concentration of the big particles remains nearly constant.

Fig.5.6 shows, the comparison of aerosol sublimation at low and high particle concentrations. The reduce of the aerosol particles at different heating temperatures are compared. At high particles concentration, less percent of particles are sublimated into gas phase. At a certain heating temperature, there is a certain vapor pressure p_v^* in the gas phase. The amount of material that can be sublimated into gas phase is also decided by this vapor pressure p_v^*. Increasing the particle concentration, less percent of particles can be sublimated into the gas phase.

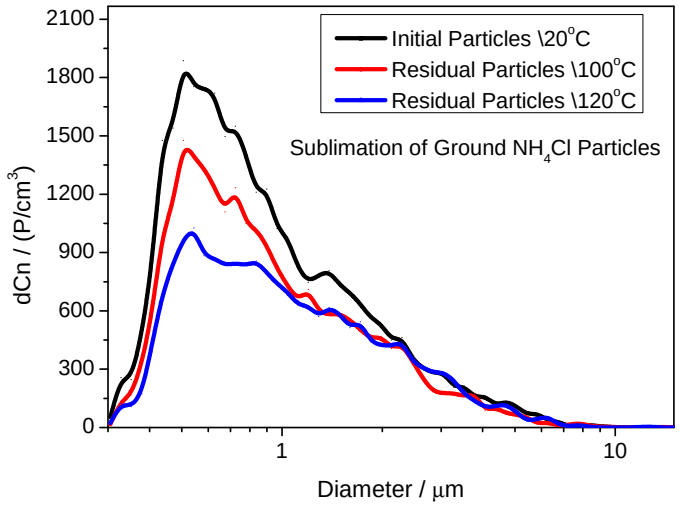

Figure 5.5: Sublimation experiments with higher particles concentration

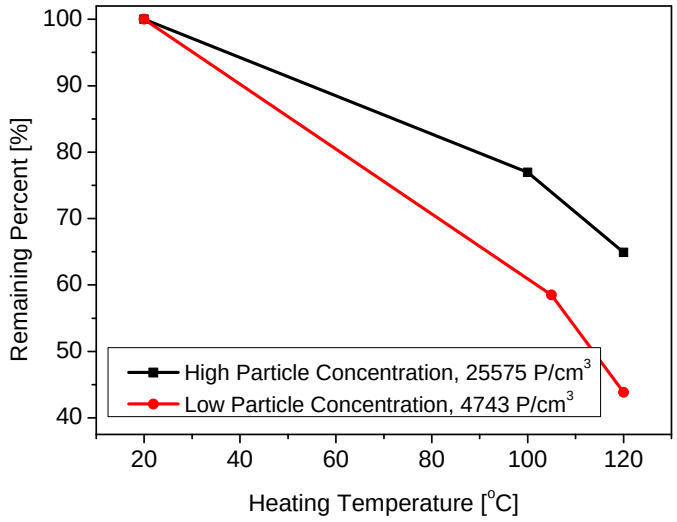

Figure 5.6: Residual particles concentrations at different heating temperature

5.2 NH_4Cl Particles with Porous Surface Sublimation Studies

Aerosols involved in the sublimation process have commonly different structures instead of perfect spheres. Particles have usually irregular morphologies, such as slices, needles or even porous structures, and also different surface. Because of the irregular forms, the properties of solid particles such as the surface ratio or the deposit density are variable. So that the sublimation behaviors of particles are also different. Thus, the different particles morphologies can induce to different sublimation behavior.

Another kind of NH_4Cl particles can be generated by collison nebulizer. The NH_4Cl solution droplets were produced from NH_4Cl-water solution in a container. The droplets were conveyed into a dryer, where water was evaporated. NH_4Cl particles were sent into the test plant.

The particles directly out of the collison nebulizer were supposed to be some small primary particles. These primary particles have a high concentration, so in the course of drying and transport the high concentrated particles tend to collide and coagulate to bigger particles with complex/irregulated structures. The SEM photographs of the particles are shown in Fig.5.7. It can be seen that these particles have porous structure and high surface ratios. These particles were used in this section of experiments to see the effect of particles morphologies on the sublimation process.

Due to the unregulated forms of this sample, it is important to distinguish the influence of particle morphology on measuring results of the particle counters. A test setup was built to measure the particle size of the sample with different instruments. Two kinds of particle sensors were adopted here. A comparison between optical diameter and aerodynamic diameter was conducted. Welas-3000 (Palas, GmbH) and APS (Model 3321, TSI) were used to measure the aerosol particles diameter. In the test setup (Fig.5.8), the aerosol particles out of the collison nebulizer (Fig.4.4) are tested with the two kinds of particle sensors.

Fig.5.9 shows the comparison of aerodynamic diameter and optical diameter of the

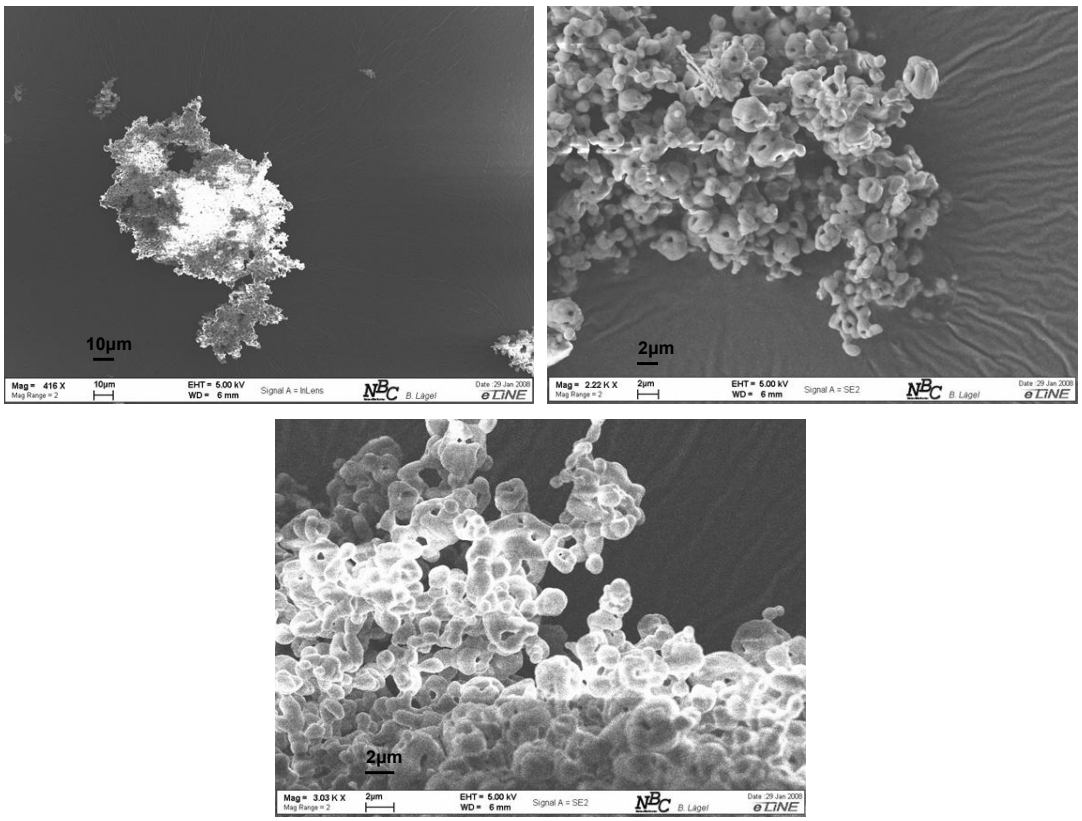

Figure 5.7: SEM of NH_4Cl generated from collison nebulizer.

particles with porous structures. It can be seen that the particle's mean diameters from the two kinds of measurements are most identical. The optical sensor shows a slightly broader PSD in aerosol than APS. Through the experiments in this section, optical particle counter: Welas-3000 and HGS were used to measure the change of particle size and size distribution before and after heating.

5.2.1 Experiments with Different Heating Temperature

Sublimation of the NH_4Cl with porous structure was also carried under different temperatures with the two sensors (Welas-3000 and HGS). The sublimation study was carried

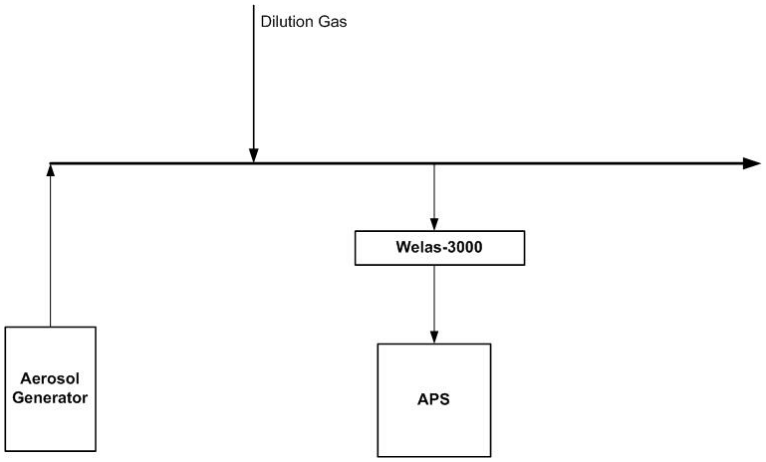

Figure 5.8: Experimental setup for particle characterization

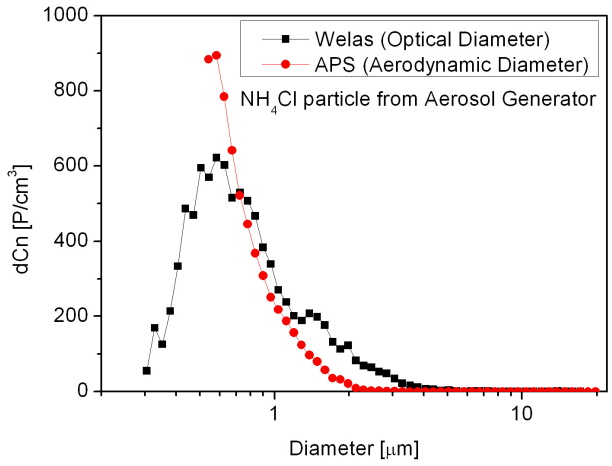

Figure 5.9: Aerodynamic diameter and optical diameter of particles from collison nebulizer

out in two parts. At first PSD was measured by two identical Welas-3000s up to 120 ^oC. Then, the HGS was used to measure aerosol sublimation under higher temperature up to 200 ^oC.

Particle concentration decreases with increased heating temperature (see in Fig.5.10-

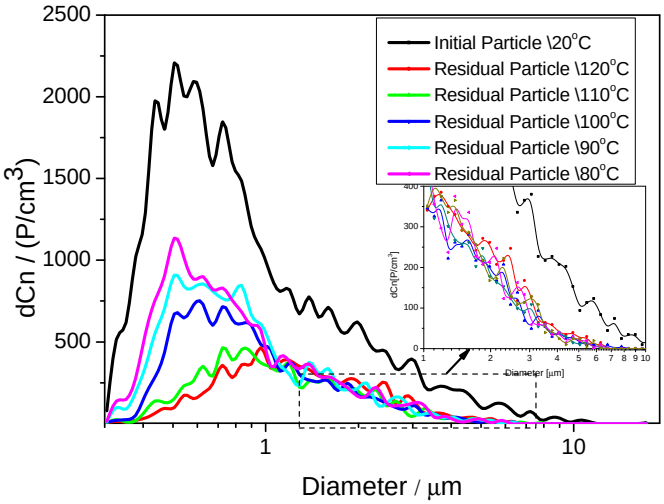

Figure 5.10: Sublimation experiments with the particles from collison nebulizer. Two identical Welas-3000s are used and test aerosols are heated up to 120 ^oC

5.11). In Fig.5.10, increasing the heating temperature increased amount of small particles sublimate into the gas phase. Meanwhile, the concentration of big particles ($d_p > 1\mu m$) decreases and then remains at a certain level.

In Fig.5.11, the test aerosol was heated to 200 ^oC and the measurement was carried out by HGS. Small particles' concentration always decreases with increasing temperature. The concentration of big particles reduces further, if the heating temperature is high enough. At 200 ^oC, all the particles sublimate into the gas phase.

Compared to the experiments of sample with ground particles, there are some common properties but even great differences in the sublimation processes of the two kinds of particles. The common property is, sublimation of small particles ($< 1\mu m$) takes precedence over big particles for both kinds of samples. In the sublimation of porous particles, the concentration of big particles at first reduces to an extent (Fig.5.10). Increasing the heating temperature to 120 ^oC (Fig.5.10), the small particles' concentration keeps on decreasing whereas the big particles' concentration remains to the same extent. In-

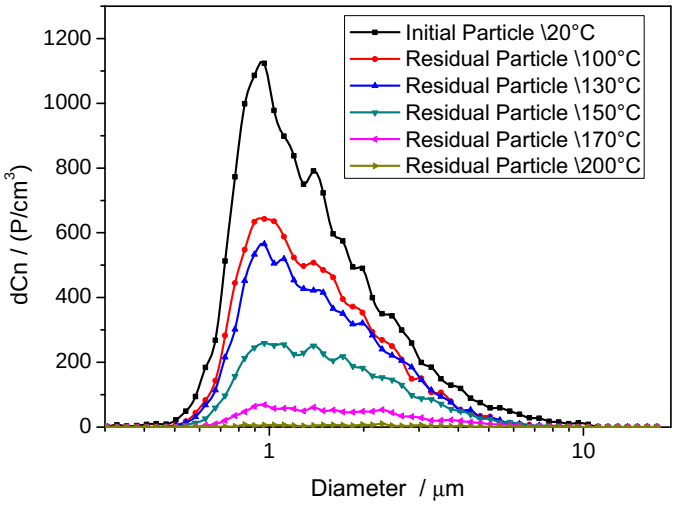

Figure 5.11: Sublimation experiments with the particles from collison nebulizer. HGS is used here and the aerosol is heated up to 200 ^oC

creasing the heating temperature to 150 ^oC (Fig.5.11), the concentration of small particles is already very low (The total particle concentration is very low); the big particles concentration begins to reduce further. The ground particles have solid structures and low surface ratio. In this sample, small particles' concentration decreases at the beginning of heating process, whereas big particles concentration stays constant (Fig.5.3). Further increasing the heating temperature, the big particles concentration reduces only slightly. In the present experiments, the aerosol particles with porous structures can be mostly sublimated into the gas phase at the heating temperature of 180^oC; whereas the aerosol particles with solid structure can not. Generally, the porous surface accelerates the particles' sublimation; the porous structure of the particles reduces also the heating temperature for sublimation. If looking at the the SEM observation (Fig.5.1 and Fig.5.7) in detail, it can be seen: particles out of collison nebulizer has a lower apparent density and higher surface ratio than the ground particles, which makes the decrease of particles concentration through sublimation faster. The detailed analysis of particles specific surface ratios of the two kinds of particles is carried out in the modeling section (Section 5.2.4).

5.2.2 Different Particle Concentrations

Sublimation experiments of the particles with irregular (porous) structures, based on different particle concentrations, were carried out. Two Welas-3000s were adopted here. Aerosols with different particle concentrations were heated to the same temperature, 120 ^oC. Tab.5.2 gives the detailed experimental information.

Table 5.2: *Experimental conditions on sublimation with different particle concentrations*

Material	NH_4Cl out of collison nebulizer			
Volume Flow (m^3/h)	2.5			
Heating Temperature (^oC)	120			
Particle Concentration (P/cm^3)	2735	3658	12429	24836

Experiments of particles sublimation at different concentrations were carried out at the same heating temperature and the same residence time. The results are shown in Fig.5.12. There is an increased percent of particles sublimated into gas phase with decreased particle concentration.

5.2.3 Different Residence time

Sublimation of NH_4Cl particles at different residence time were tested. Due to the limitation of the test plant, the flow of the carrier gas was changed to get different residence time in the heating tube. With the help of a bypath, the particles concentration was controlled to be constant. The experimental results are shown in Fig.5.13. Increasing the residence time (decreasing the gas flow), more particles were sublimated into the gas phase. The particle concentration in the residual aerosol decreased accordingly.

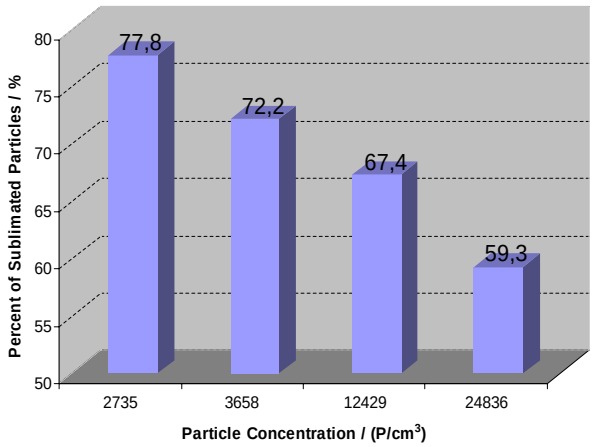

Figure 5.12: Percent of sublimated particle at different initial particle concentration at $V = 2.5m^3/h$

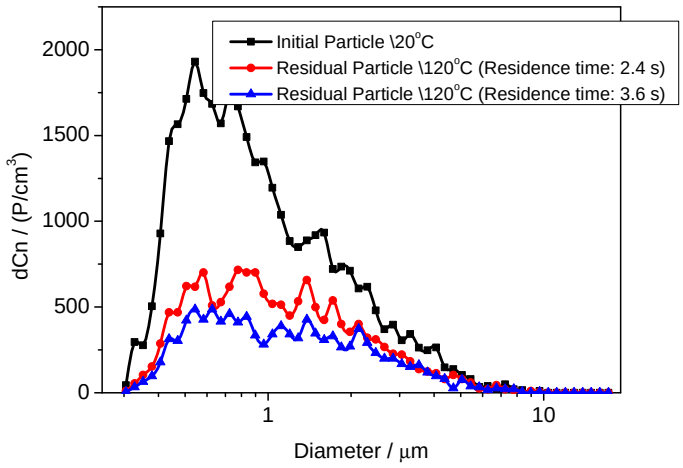

Figure 5.13: Particles sublimation at different residence time at $V = 1.2m^3/h$ and $V = 0.8m^3/h$, respectively

5.2.4 Analysis of Particle Surface Ratio

From the experimental results above, it can be seen that the particle's morphology is very important in the sublimation process. The specific surface ratio is a direct index on the morphology. In this case the specific surface ratios of the two kinds of particles were measured. Monosorb©was used at first to test the surface ratio of the two samples, where the adsorption and desorption of mix gas (N_2/He) were measured. It is important to note that the sample was not activated before measurement. Then, Autosorb©was used to decide the specific surface area of samples, where the sample was activated at first. In the activation, the sample was heated up to 50 ^oC in vacuum. In the process of activation, small amount of particles sublimation was observed. The results of the two measurements are shown in Tab.5.3

Table 5.3: *Measuring results of particle specific surface area with two measuring methods*

Measurement Method	Monosorb©	Autosorb©
Ground Particles	0.23 m^2/g	13.27 m^2/g
Particles from Collison nebulizer	0.59 m^2/g	37.64 m^2/g

It is seen that the Autosorb©measures always higher specific surface area than Monosorb©by the same sample. Before the surface ratio measuring with Monosorb©, the particles were not activated. In this case the water molecules and O_2 molecules were still on the particle surface in the measurement. The adsorption of N_2 was going to be reduced due to the limited particle area in activation. A very low particle surface area was measured. In the measurement with Autosorb©, the activated samples were tested, where the samples were heated in vacuum. A much higher particle surface area was measured by Autosorb©comparing with the results from Monosorb©. In the activation (under the conditions of heating and vacuum), however, a sublimation of NH_4Cl particles was observed. In this case, the morphology of the particles was changed in the activation, which may induce to a decrease of the particle surface ratio. The real particle surface area is supposed to be still higher than the results of Autosorb©measurement.

5.3 Organic Droplets Evaporation Studies

In this section, the evaporation of organic droplets DEHS was taken into research. Comparing with aerosol particles, droplets usually have spherical forms. In this case, the morphological influence can be ignored in this study. The study is based on different heating temperatures and different particle concentrations.

5.3.1 Influence of Different Heating Temperatures

Droplets have usually a uniform morphology. The aerosol generator AGK-2000 have a cyclone at the outlet, which classifies the DEHS droplets to a narrow size distribution. The size distribution of initial DEHS droplets is shown in Fig.5.14. The mean droplet diameter is between 0.7 μm and 0.8 μm. In the evaporation study of DEHS, the HGS was used to measure the change of aerosol PSD at different heating temperatures. In the evaporation experiment, the aerosol was heated up to 122 ^oC (Fig.5.14). With increased heating temperature, a decreased droplets concentration was detected. The concentrations of the big droplets ($d_p > 1\mu m$) and small droplets decrease with increased heating temperature.

5.3.2 Influence of Different Droplets Concentrations

DEHS evaporation study at droplets concentration was carried out. The remaining droplets' percentage with different heating temperatures is shown in Fig.5.15. Increasing the heating temperature more droplets were evaporated into gas phase. At low droplet concentration, the decrease of droplet concentration after heating is stronger than that at high droplet concentration. At relative low heating temperature $T < 60^oC$, the evaporation of DEHS droplets was weak. Increasing the heating temperature, there was an intensive concentration decrease at heating temperature of 70 ^oC to 100 ^oC. Comparing with the vapor pressure, $c_v^*(T) = \frac{p_v^*(T)}{RT}$, this temperature range corresponds to the intensive increase of DEHS vapor pressure. Vapor pressure is the driving force of

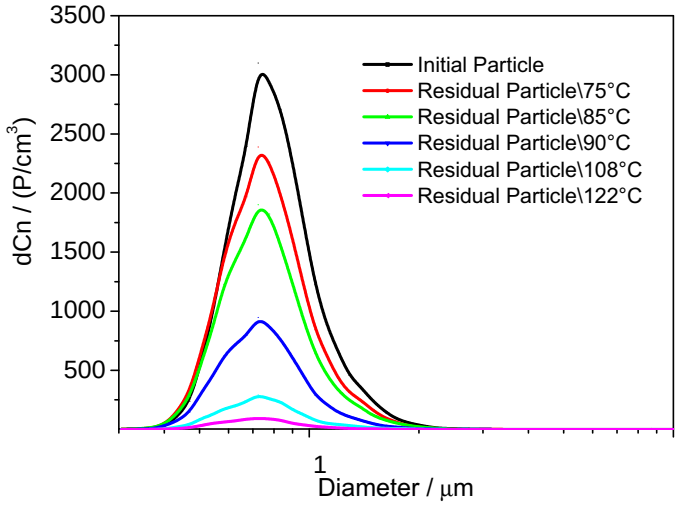

Figure 5.14: Evaporation study of organic droplets DEHS at $V = 2.5m^3/h$

the droplets' evaporation. An abrupt increase in vapor pressure (vapor concentration) results in an intensive droplets' evaporation at the temperature range.

In short conclusion, in this chapter the sublimation of NH_4Cl particles and evaporation DEHS droplets are described. The NH_4Cl particles with different morphologies are taken into account. The sublimation behaviors of big particles and small particles are different. In order to explain these phenomenon in the experiments thoroughly, the kinetics of sublimation and evaporation is further discussed in the computational model section.

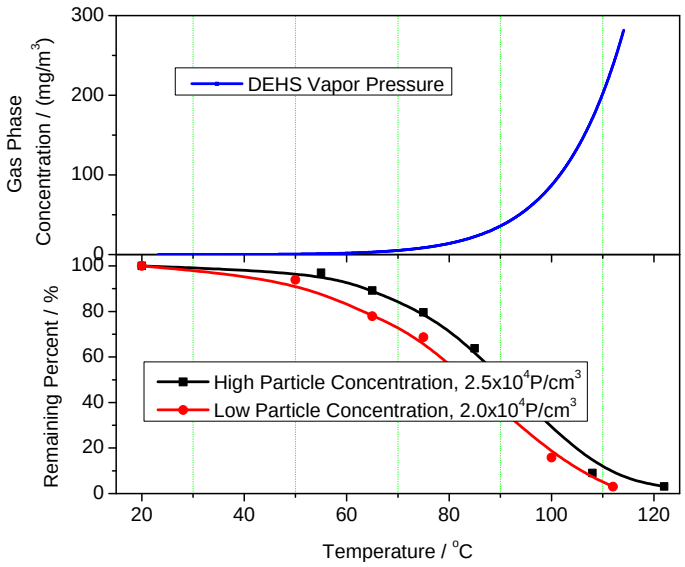

Figure 5.15: Evaporation of DEHS droplets with different concentration at different temperature

6 Model Section

In the experimental section, it can be seen that sublimation/evaporation are strongly dependent on the vapor pressure (Heating temperature), $p_v^*(T)$, the particle size distribution (PSD), particle concentration and particle morphology. During sublimation of NH_4Cl particles, small particles' concentration decreased whereas big particles did not. Droplets, however, have a uniform diameter and narrow size distribution. In order to describe these phenomenon clearly, simulation work was carried out. Based on the experimental results above, theoretical models were established and validated in this chapter, which can help us see the essential of sublimation/evaporation process.

Up to now, most of the studies are focused on the evaporation of single particle or monodispersed aerosols (see Chapter 2). In this work, the particle size distribution is regarded as an important parameter in the simulation work. Based on the theory in Chapter 3 several models are set up. Different process parameters are taken into account. The initial particle size distributions, which are measured in the experiments, are introduced in the models. Experimental conditions are employed in the models such as: heating process, gas volume flow, residence and so on. The comparison of modeling results and experimental results are presented in the next chapter.

Particle coagulation in the gas flow is another important reason for the change of particle size distribution in aerosol, whereby aerosol particles collide with one another and adhere together to form large particles. The net result is a continuous decrease in number concentration and an increase in particle size. The effect of coagulation in the experimental gas flow is discussed in this chapter too.

6.1 Evaporation Models

There are two phases in aerosol: gas phase and particle phase. The gas phase gets energy from outside via heating. The particles in aerosol get heat from the surrounding gas. When the molecules on the particles surface receive enough energy, it is going to be 'free' from the particles. The free molecules go into the gas phase. The molecule concentration in the gas phase increases. In this case, the sublimation process can be considered as a transition of energy and molecules between the gas and particles' phases (see in Fig.6.1).

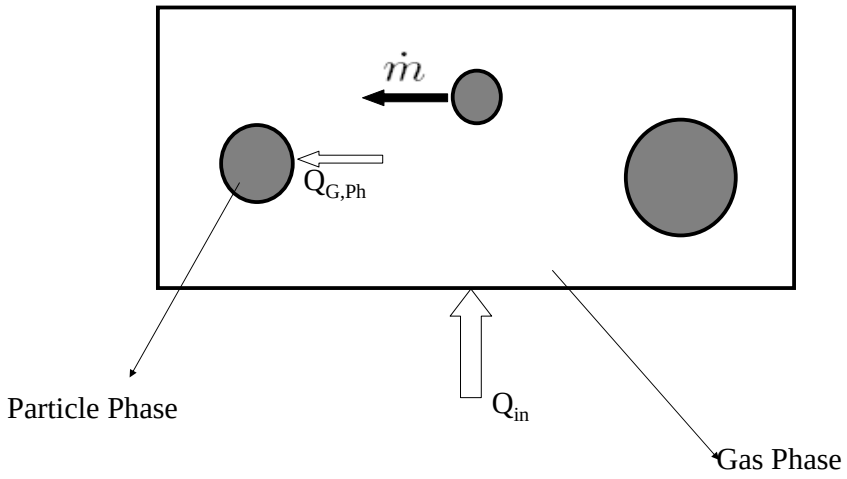

Figure 6.1: The balance between gas/particle phase in the process of evaporation

In order to simulate the phase transition between the particle and gas phases, the following materials' parameters are necessary:

a Surface tension of droplets or particles, γ;

b Diffusion coefficient of vapor molecules in air or nitrogen, D_{vg};

c Vapor pressure of the material at different temperatures, $p_v^*(T)$;

d Vaporization enthalpy of the material, ΔH;

e Real heat and mass transfer surface of particle phase, A_i.

There are few literatures about the surface tension of desired materials. The experiment to determine the particle surface tension is described in the annexe. Diffusion coefficients are calculated according to Eq.3.43 in Chapter 3. The vapor pressure of the sublimation material can be gotten from literature.

In the simulation work, several preconditions were assumed:

1. Aerosol gets into the heating tube after a defined regulation area. According to the calculation based on Stokes law (30), aerosol particles and gas flow have nearly the same speed ($u_g = u_p$ is used in the modeling work).
2. The heating tube is heated from outside. There is a temperature profile in the tube and the temperature of the wall is constant.
3. Experimental conditions (measured particle concentration and PSD at room temperature) are used in the models for the initial stage of the aerosol.

6.1.1 Model for Low Volatile Materials: Model 1

In this model the temperature on particle surface is supposed to be the same as that of gas phase, which is shown in Fig.6.2. The cooling of the particle due to the latent heat of evaporation is ignored. Thus, after molecules on the particle surface sublimate into the gas phase, the particle temperature remains constant.

For particles larger than the mean free path, the rate of sublimation is controlled by the rate at which vapor can diffuse away from the droplet. This rate is given by Eq.3.30.

When the partial pressure of vapor, well away from the droplet, p_v, is less than the vapor pressure at the particle surface, $p_{v,d}^*$, the right side of Eq.3.30 will be negative and parti-

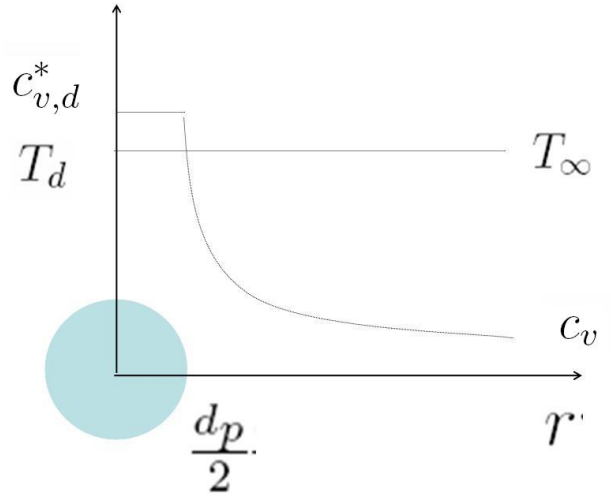

Figure 6.2: Temperature and material concentration profile of low volatile materials on the particle surface

cle size will decrease with time, i.e., net evaporation is occurring. The vapor pressure at the particle surface, $p^*_{v,d}$, is determined by 1) the temperature at the particle surface T_d 2) the diameter of the droplet d_p. The partial pressure required to maintain equilibrium of a small droplet, $p^*_{v,d}$ is greater than that of a flat surface, p^*_v. The relationship between the saturation ratio ($p^*_v/p^*_{v,d}$) required for equilibrium and droplet size for pure liquids is given by the Kelvin Equation (Eq.3.12).

The partial pressure of vapor away from the droplet in the gas phase, p_v, is very important to determine the sublimation speed of the droplet. It can be calculated through the amount of sublimated particles by Eq.6.1

$$p_v(t) = p_v(t - dt) + \sum_{i=1}^{n} \frac{\pi}{6} \frac{\rho_p}{M_p} \cdot R \cdot T_\infty \cdot n(d_{pi})(d^3_{pi}(t) - d^3_{pi}(t - dt)). \tag{6.1}$$

The partial pressure increases when more droplets are evaporated into the gas phase.

The reduce of particle surface is present by Eq.6.2

$$\frac{dA}{dt} = -\pi \frac{8 D_{vg} M_p}{R \rho_p} \left(\frac{p_v - p^*_{v,d}}{T_\infty} \right). \tag{6.2}$$

According to the Kelvin effect (Eq.3.12), the partial pressure at small particle surface is greater than at big particle surface. In this case, the reduction of the particle surface is also faster than that of the big particles.

6.1.2 Model for Volatile Materials

For volatile materials, such as water or alcohol, an additional correction must be applied to account for the cooling of the particle due to the latent heat. After molecules sublimate into the gas phase from particle surface, the temperature of particle decreases. An equilibrium droplet temperature is established by balancing the heat, required for sublimation and the heat gained by conduction from the warmer surrounding air, then $T_\infty > T_d$. It is depicted in Fig.6.3.

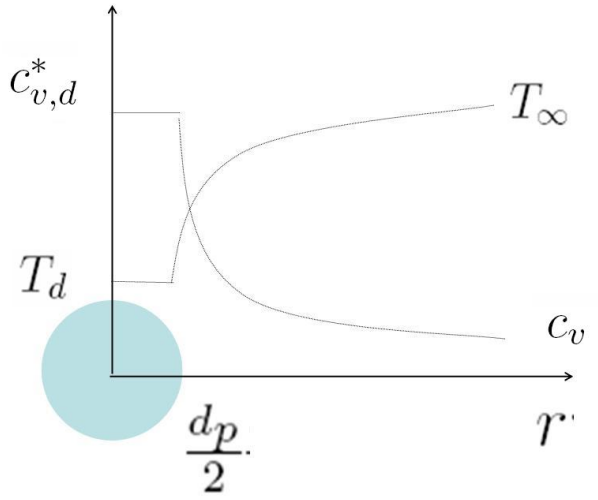

Figure 6.3: Temperature and material concentration profiles of volatile materials on the particle surface

The particle surface temperature is very important in this model to calculate the sublimation kinetics.

Model 2

The steady-state temperature depression, $T_\infty - T_d$, is calculated by Eq.3.33. The sublimation speed is given by Eq.3.31. Taking the Fuchs effect into account the particle sublimation can be calculated by Eq.3.35. The reduce of particle surface is present by Eq.6.3

$$\frac{dA}{dt} = -\pi \frac{8 D_{vg} M_p}{R \rho_p} \left(\frac{p_v}{T_\infty} - \frac{p^*_{v,d}}{T_d}\right). \tag{6.3}$$

Model 3

In the unidirectional diffusion model, the molecule diffusion happens at one direction: particle molecules into the gas phase. The particle sublimation speed is described by Eq.3.26 (detailed description see in Chapter.3), which is also used in Habilitation of Sachweh (60).

6.1.3 Morphological Effect in the Particle evaporation

Usually solid particles have great diversity in their particle morphology. All the present models, however, are based on the sublimation of spherical particles. The irregular mass and heat transfer surface area and apparent density are not taken into account. These models cannot describe the actual conditions of the sublimation of particles, which have irregular morpholoies. In this section a new model is proposed, where a surface ratio factor (f_i) is introduced, and the change of the apparent density, ρ_p^d, due to morphological effect is considered.

Particles, such as needle, cube, cylinder, or even hollow structures, have bigger surface ratios than that of the spheres

$$A_i = f_i A_{si}. \tag{6.4}$$

where A_i is the surface area of the particle; A_{si} is the surface area of a corresponding sphere, which has the same optical properties during the measurement of the optical sensor to the particle; $f_i > 1$. The surface area of the particles should be expressed in

$$\frac{dA_i}{dt} = f_i \frac{dA_{si}}{dt} = -f_i \pi \frac{8 D_{vg} M_p}{R \rho_p} \left(\frac{p_v}{T_\infty} - \frac{p^*_{v,d}}{T_d}\right). \tag{6.5}$$

If the particles have porous structures, the change of the particle density with the porosity ε should be taken into account too,

$$\frac{dA_i}{dt} = f_i \frac{dA_{si}}{dt} = -f_i \pi \frac{8 D_{vg} M_p}{R \rho^d_p} \left(\frac{p_v}{T_\infty} - \frac{p^*_{v,d}}{T_d}\right). \tag{6.6}$$

and

$$\rho^d_p = \rho_p (1 - \varepsilon), \tag{6.7}$$

where ρ^d_p is apparent density.

6.2 Coagulation Model

Coagulation of aerosols comes from relative motions of particles and results in a decrease of the particle concentration and an increase in the particle size. (64) (65) When the relative motion between particles is Brownian type the process is called *thermal*

coagulation. When the relative motion arises from external forces such as gravity or electrical force or aerodynamic effects, the process is called *kinematic coagulation*. Thermal coagulation occurs for small particles ($< 10\mu m$). The objective of the theory of coagulation is to describe how particles' concentration and particle size change as a function of time.

6.2.1 Kinematic Coagulation

In the experiments, there is no external induced electrical force. Therefore the gravity is considered as the only driving force of kinematic coagulation.

The change of the particle concentration in the flow through residence time can be considered as:

$$c_n(t) = \frac{c_n(t=0)}{1+\frac{t}{\tau_c}}, \tag{6.8}$$

where $\tau_c = 2/(K \cdot c_n(t=0))$ is the characteristic time of coagulation with a constant coagulation coefficient K.

For the particles smaller than $(10\mu m)$, the model of Saffmann and Turner (37) is adopted:

$$K_{ij} = 1/2\sqrt{2\pi}(d_{pi}-d_{pj})^2[(1-\frac{\rho_g}{\rho_p})^2(\tau_{pi}-\tau_{pj})^2 g^2 + \frac{1}{36}(d_{pi}-d_{pj})^2\frac{\varepsilon}{\nu_g}]^{0.5} \tag{6.9}$$

where ε is the energy dissipation rate in the flow which can be calculated through $\varepsilon \approx 0.16\frac{\overline{u}^3}{D_{tube}}Re^{-1/4}$, $\overline{u}$ is the middle speed of the flow.

τ_{pi} is the particle relaxation time, which is defined by:

$$\tau_{pi} = \frac{1}{18}\frac{d_{pi}^2 \rho_p}{\nu_g \rho_g}. \tag{6.10}$$

6.2.2 Thermal Coagulation

There are a lot of models considering the coagulation during Brownian motion. Here the Friedlander (49) famous models used. When the Stokes-Einstein relation holds for the diffusion coefficient and $d_p \gg \lambda_g$ (λ_g is gas mean free path) then the following equation can be used:

$$K_{ij} = \frac{2k_B T}{3\mu}(\frac{1}{v_i^{1/3}} + \frac{1}{v_j^{1/3}})(v_i^{1/3} + v_j^{1/3}) \tag{6.11}$$

For particles much smaller than the mean free path of the gas, the collision frequency is obtained from the expression derived in the kinetic theory of gases. For collision among molecules that behave as rigid elastic spheres the following equation holds:

$$K_{ij} = (\frac{3}{4\pi})^{1/6}(\frac{6k_B T}{\rho_p})^{1/2}(\frac{1}{v_i} + \frac{1}{v_j})^{1/2}(v_i^{1/3} + v_j^{1/3})^2. \tag{6.12}$$

6.3 Sublimation of Sedimentated Particles

External force fields such as gravitation can influence the particle motion. The particle motion rather quickly becomes steady (reaching a constant migration velocity, v_s), because of the balance between the field forces and aerodynamic resistance (drag) from the gas. Determination of this velocity (Eq.3.8) can help us calculate the particles loss in a horizonal transport tube. Taken the influence of particles shapes into account, the settling velocity of aerosol particles is given by:

$$v_s = \frac{\rho_p^d d_p^2 g C_c}{18 k_i \mu}, \tag{6.13}$$

where k_i is the shape factor with regard to the settling velocity. It is calculated due to the increased touching area with the drag gas. The apparent density ρ_p^d should be used here. The influence of the particle form is taken into account.

Sedimentation is not fully avoidable in the transport process. When the sedimentation time, τ_s, of particle is longer than the residence time in the heating tube, the particle do not sedimentate on the wall; otherwise it sedimentates on the heating wall. The particles on the wall of the heating tube sublimate into gas phase and increase the partial pressure (p_v). In a heating tube , the wall of the tube is heated to a constant temperature. The sedimentation particles are heated to this temperature.

The mole flux of NH_4Cl away from the sublimation surface is given by:

$$N_v = \frac{p D_{vg}}{R_{tube} R T} ln(\frac{p - p(T_g)}{p - p(T_w)}). \tag{6.14}$$

The increase of the partial pressure in the gas phase due to the sublimation of sedimenting particles is:

$$p_{v,sedim} = \frac{N_v A_{p,w} \Delta t}{\Delta V} RT, \tag{6.15}$$

where Δt is the time interval of the aerosol in the volume of ΔV.

7 Simulation Results and Comparison

7.1 Particles Coagulation in Flow

The particles coagulation is inevitable in aerosol flow. The particle coagulation effect is discussed at first to evaluate the change of PSD due to this effect.

7.1.1 Kinematic Coagulation

Particles of $<$0.4 μm, 0.8 $\mu m>$ are used as an example to show the particles coagulation effect through the heating process. The coagulation under high particle concentration of $10^5\ P/cm^3$ is tested to see the maximal kinematic coagulation. The kinematic coagulation is dependent on the velocity of the gas flow and residence time of the particles. The simulation is carried out at different velocity and the heating temperature of 120^oC. When the aerosol flows through a set of 1 m long tube, the coagulations at different Reynolds numbers (flow velocities) are calculated. The results are shown in Fig.7.1. At low Reynolds number the coagulation is high, which induces a reduction in the particle concentration at about 3.5 $\%$.

7.1.2 Thermal Coagulation

Thermal coagulations of different particle groups $<$10 μm, 1 $\mu m>$, $<$1 μm, 1 $\mu m>$ and $<$0.4 μm, 0.8 $\mu m>$ at high particle concentration $10^5\ P/cm^3$ are calculated and shown

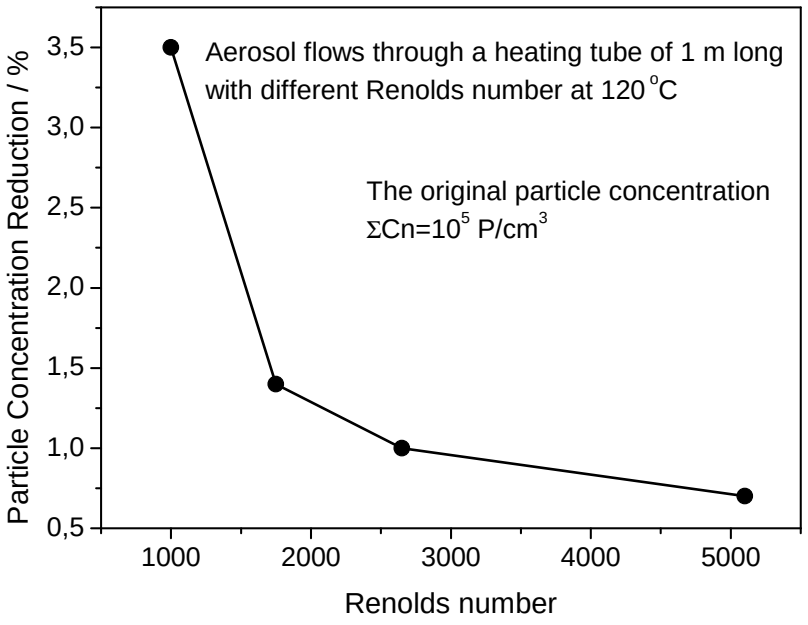

Figure 7.1: The reduction of particle concentration from Kinematic coagulation

in Fig.7.2. Increasing the residence time, there is an increased thermal coagulation effect. The coagulation between big particles and small particles is stronger. Among the examples, the largest coagulation is between particles of 10 μm and 1 μm, where the reduction of particle concentration is even under 0.5 $\%$ through long residence time (4 s).

When taking the two kinds of coagulations into account, it can be found that the maximal coagulation effect in the experiments induces to a reduction of particle concentration under 4 $\%$. In the experiments there is much bigger decrease in the particle concentration after heating process.

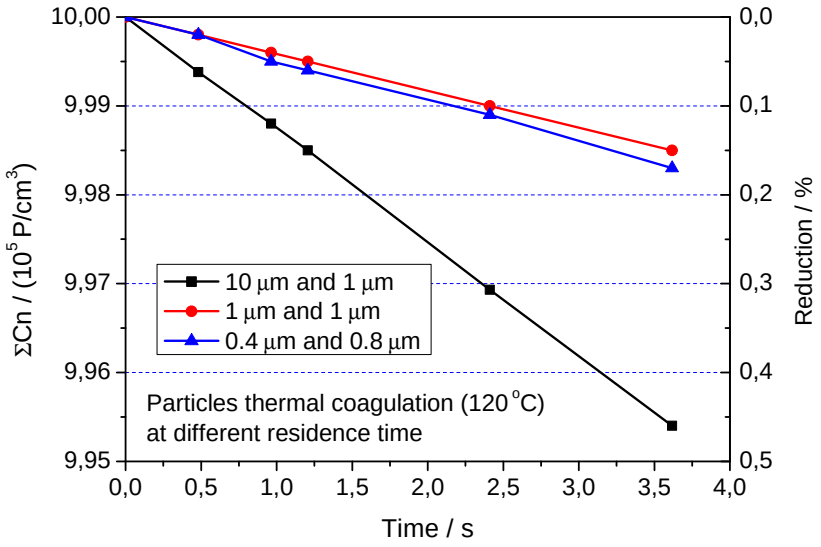

Figure 7.2: Thermal coagulation ($120\ ^oC$) of aerosol particles at different residence time

7.2 Evaporation of Water Droplets

The changes in the size and life time of the particles and droplets are calculated by three numerical models. In the three models, the evaporation of spherical droplets are described. *Model 1* is focused on the evaporation of no volatile materials, where the latent heat do not change the droplet temperature after evaporation. *Model 2* describes the evaporation of volatile materials, where the evaporation of molecules on droplet surface decreases the surface temperature. *Model 3* contributes to the description of evaporation under unidirection molecule diffusion, where only the vapor molecules diffuse into the gas phase from the particle surface. The lifetime of water droplets is calculated and controlled with literature data(30). The comparison is in Tab.7.1. The same heating temperature as indicated in the literature conditions is set in the theoretical models. However, the literature data is based on the evaporation of a single droplet. In this case the difference between the present theoretical model and literature conditions are:

1. The data of literature used in (30) were calculated based on the single water droplets evaporation in a constant relative humidity ($S = 0.5$), i.e., the evaporation of the droplet had no influence on the boundary conditions.
2. In present models, the condition of particle concentration is considered. The relative humidity of gas phase is changing from $S = 0.5$ to $S = 0.52$. The diffusion coefficient and surface tension of water used in the theoretical model are $0.201 \times 10^{-4} m^2/s$ and 76 mN/m, respectively.

Table 7.1: Comparison of models results and literature data

Particle Diameter (μm)	Water Droplet Lifetime at 20^oC (s)				
	Volatile Material			No Volatile Material	
	Iteration Correction		Model 3	Model 1	Literature
	Model 2	Literature			
0.04	2.9×10^{-5}	1.4×10^{-5}	7.7×10^{-6}	9.6×10^{-6}	6.6×10^{-6}
0.1	7.7×10^{-5}	4.7×10^{-5}	1.5×10^{-5}	2.6×10^{-5}	2.1×10^{-5}
0.4	3.65×10^{-4}	3.6×10^{-4}	3.62×10^{-4}	2.2×10^{-4}	1.5×10^{-4}
1.0	1.85×10^{-3}	1.7×10^{-3}	1.44×10^{-3}	9.9×10^{-4}	7.4×10^{-4}
4.0	0.027	0.024	0.0169	0.015	0.01
10	0.14	0.15	0.09525	0.083	0.062

Literature is Aerosol Technology, W.C. Hinds.

Imput parameter of models: $Re_p = 0;\ S = 0.5 \sim 0.52;\ T = 20^oC;$
Literature data are calculated: $Re_p = 0; S = 0.5.$

In Tab.7.1 it can be seen that there is some small discrepancies between theoretical and literature results. Comparing the results of theoretical models and literature data, the life time of water droplet is longer than the one in literature. The small difference derives from different simulation conditions such as droplet concentration and change of humidity. Increasing the relative humidity, the evaporation speed of droplet decreases accordingly. In the literature, single droplet evaporation was calculated and in this case the humidity was constant. In the present model, the droplet concentration is considered so that the humidity increases with the evaporation process.

It Tab.7.1, it can be seen that single water droplet's life time is very short, even for the very big droplets ($\geq 10\mu m$) the lift time is shorter than 1 s. Under the present laboratory technologies, it is impossible to observe the shrinkage of a single aerosol droplet in such a short time. Therefore, theoretical models are need to predict the change in the size distribution and particle concentration during the evaporation process. Comparison of simulation and experimental results were carried out in this work to verify the theoretical models.

One of the material in experiments was NH_4Cl, which is considered as a volatile material. The temperature decrease of particles, due to latent heat should be taken into account. The molecule diffusion between the particle and gas phase is considered as a two direction flux. Model 2 is used in this work to compare the experimental with the simulation results.

7.3 Simulation of NH_4Cl Sublimation at Experimental Conditions

The experimental conditions such as heating temperature, gas flow and residence time in heating tube were used during simulation. The measured PSDs at room temperature from Sensor 1 (Welas-3000) were used to represent initial particle conditions in the simulations. The particle size distributions after different sublimation conditions were calculated through the theoretical model. The simulation results were compared with those results of the experiments at the same parameters.

The temperature profile of the test plant was calculated according to the gas flow and heating temperature on the wall of heating tube. The relationships between the heating temperature on the wall of the tube and the outlet temperature at the site of sensor 2 are shown in Fig.7.3 . The measured temperature in the experiment is accordant with the calculated result.

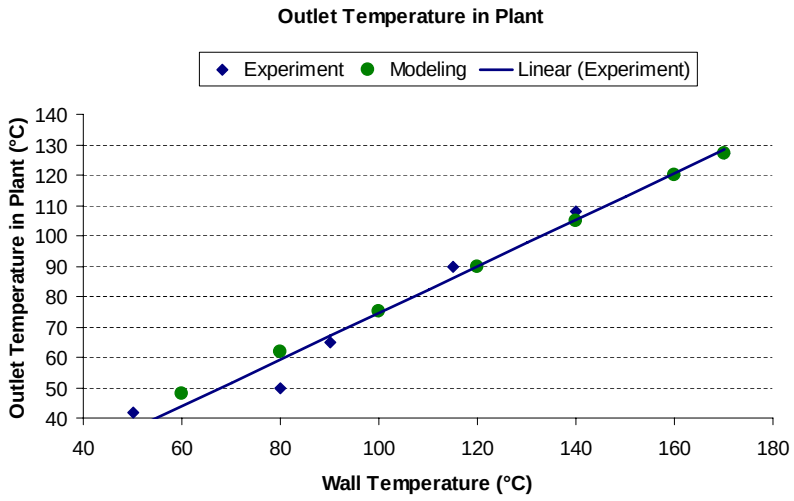

Figure 7.3: Comparison of the heating temperature from experimental measurement and calculation. The relationship between the heating temperature on the wall and the outlet temperature at the site of the hot sensor is presented.

7.3.1 Simulation of Spherical Particles

In this section, NH_4Cl particles were considered as spherical particles where the change of the surface ratio and structure of the particle were not taken into account. Experimental conditions for the sublimation of the ground NH_4Cl (see in Tab.5.1) were used in the theoretical model.

The measured particle concentration and particle size distribution at room temperature were introduced in the model. The simulated particle size distribution after sublimation is shown in Fig.7.4. It can be seen that there is a greater decrease in the small particles' concentration than in the bigger one. The concentration of the big particles (particles bigger than 2 μm) is, however, almost constant. Increasing the heating temperature from 100 ^oC to 120 ^oC, more small particles are sublimated into the gas phase. However, big particles concentration is almost constant.

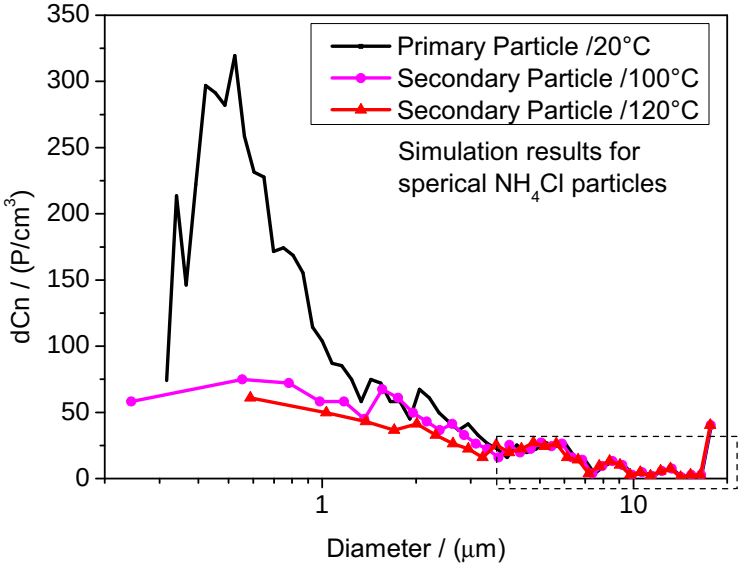

Figure 7.4: Simulation of spherical NH_4Cl particles evaporation at the experimental conditions

.

The shrinkage of a single particle in aerosol cannot be detected under present labor technologies. In the simulation work, however, a single particle's life time can be calculated; the change of particle size through heating process can be simulated. Aerosol sublimation at the heating temperature up to 100 ^oC and 120 ^oC are simulated in the theoretical model. The results are shown in Fig.7.5. At the same heating temperature, decrease of the small particles' diameter is faster than that of the big particles. During the residence time in the heating tube, small particles are completely sublimated into the gas phase, whereas big particles are still residual aerosol. Increasing the heating temperature (from 100^oC to 120 ^oC), the particle sublimation speed is also increased. The sublimation of big particles, however, is not accelerated very much at higher heating temperature. Thus, there is a great decrease in the small particles concentration; meanwhile the big particles are almost constant at the two heating temperatures (Fig.5.3).

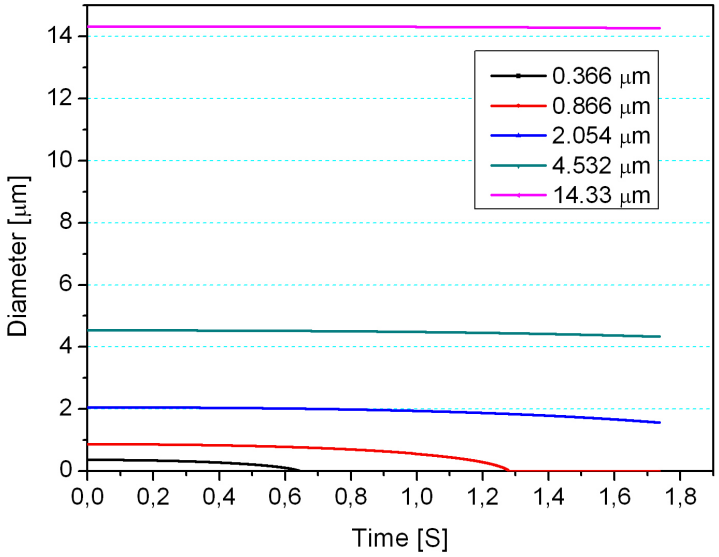

(a) Heating temperature up to 100 ^oC

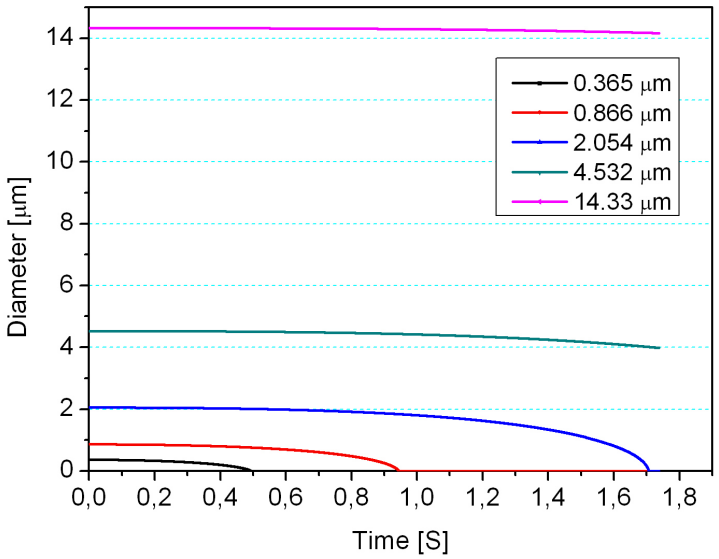

(b) Heating temperature up to 120 ^oC

Figure 7.5: The change of single NH_4Cl particle's diameter through the heating process

The comparison of experimental and simulation results are shown in Fig.7.6. The commonness in the both cases is, small particles are sublimated first, whereas most big particles still remain in aerosols.

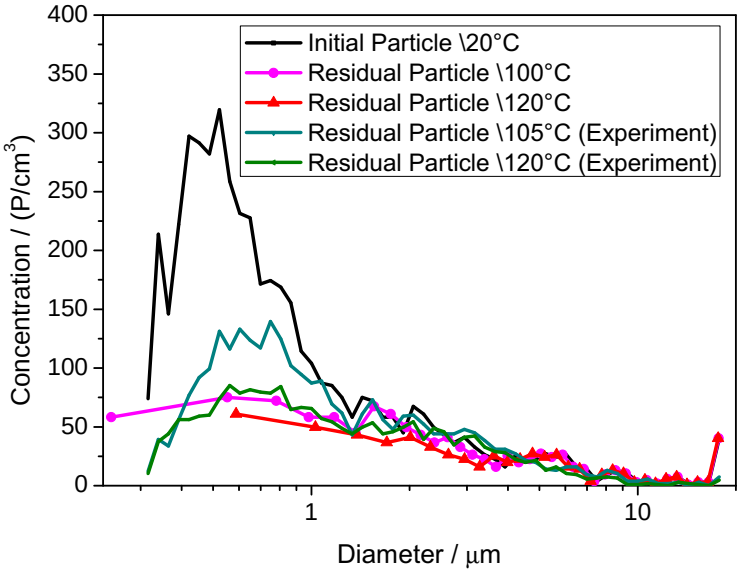

Figure 7.6: Comparison of experimental results and simulation results of ground NH_4Cl

.

There are some discrepancies between the experimental and simulated results. The simulated results show a lower particle concentration in the residual aerosol than the experimental results. According to simulation results, more particles are sublimated into the gas phase than measured. The simulated particles sublimation is faster than experiments. From the SEM of the particles (Fig.5.1), it can be seen that the particles have solid structure and wide PSD. The sedimentation effect of aerosol particles may lead to the difference between the simulation and experimental results. On the other side, the measuring range of the optical sensor, used in the present experiments, is up to 0.3 μm. Very fine particles with a diameter lower than this range cannot be detected. This also introduces the discrepancy between the measuring results and simulation results.

7.3.2 Sedimentation and Particles Sublimation

The sedimentation of aerosol particles can be calculated according to Eq.6.13 ($\rho_p^d = \rho_p, k_i = 1$). The settling time is calculated as the particles sedimentate from the middle of the heating tube to the wall of the tube. The settling time of each particle can be compared with the residence time in the heating tube. If the settling time is longer than the residence time, the particle flows through the heating tube with the carrier gas. If the settling time is shorter than the residence time, the particle sedimentates on the wall of the heating tube. Fig.7.7 shows the settling time of the NH_4Cl particles with different diameters in the heating tube. At the experimental conditions, the gas flow was at $V = 2.5m^3/h$. Then, the residence time was about $t = 1.7s$. Through the flowing of the ground particles, the settling time of the big particles ($d_p > 14\mu m$) was shorter than the residence time of flow in the tube. These particles sedimentate on the wall of the heating tube. The sublimation of the sedimentated particles must be taken into account. The particles come from nebulizer collison (Fig.5.7) have a porous structure, the sedimentation is calculated with ε and $k_i = f_i$ (see in Tab.7.2). The calculated settling time of the porous particles is also shown in Fig.7.7. Even the biggest particle among the porous particles has a settling time longer than the residence time in the heating tube. In this case, the sedimentation of the porous particles can be ignored.

The sublimation of sedimentation particles increases the partial pressure in gas phase. Then the sublimation speeds of particles are decreased. The increase of the partial pressure is calculated based on Eq.6.15. The surface area of these big particles are calculated as $A_p = \pi d_p^2$ and used in the Equation.

With the correction of the particle sedimentation (Eq.6.13 $\rho_p^d = \rho_p, k_i = 1$), the simulation results of NH_4Cl particles sublimation are shown in Fig.7.8. The fast sublimation of the sedimentated particles increase the vapor pressure, p_v, in the gas phase, which decrease the sublimation speed of the particles. The particle concentration reduction after heating is lowered. With the correction of the sedimentation factor, the simulation results are roughly in accordance with the experimental results.

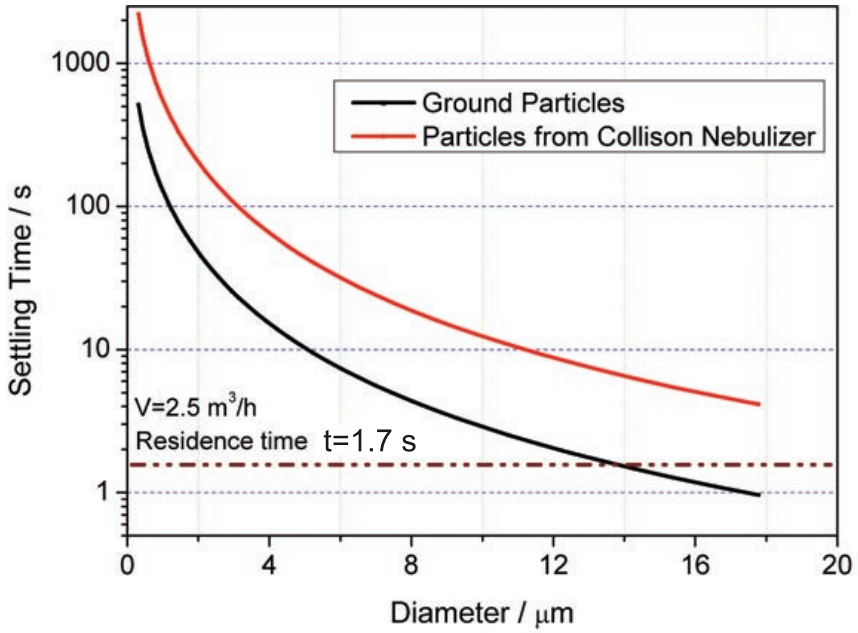

Figure 7.7: Comparison of different particles settling time with residence time in the heating tube

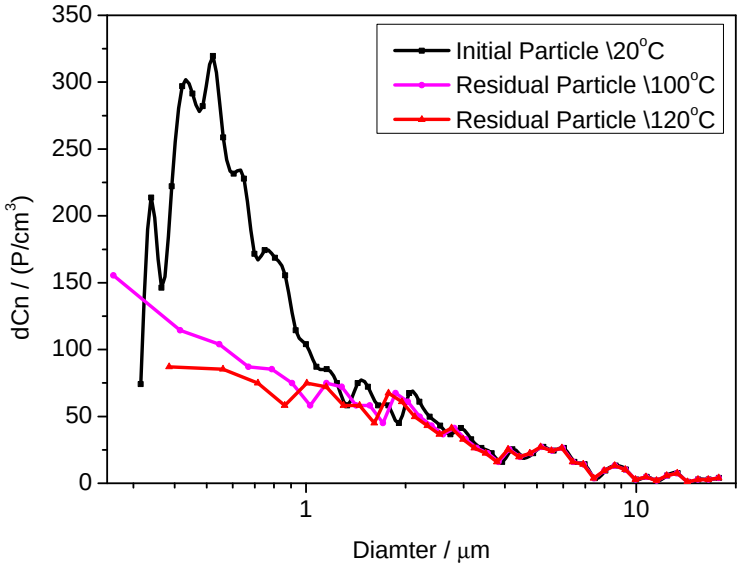

(a) Simulation of NH_4Cl sublimation with sedimentation factor

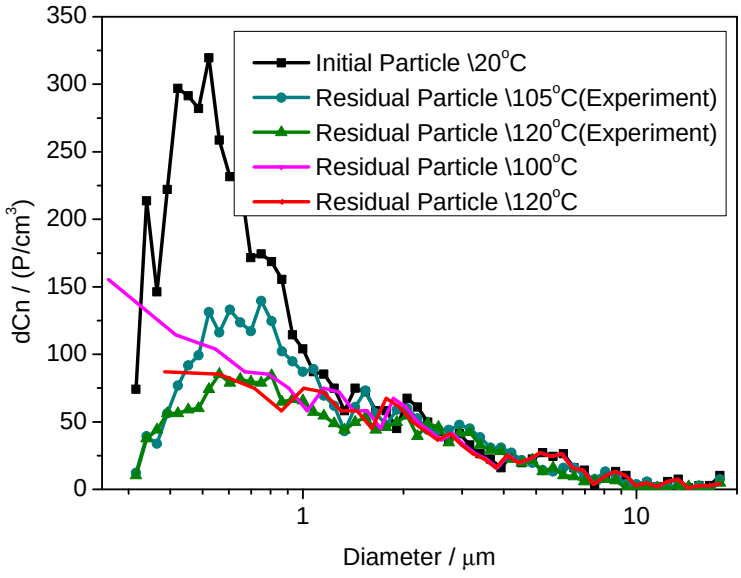

(b) Comparison of simulation and experimental results

Figure 7.8: NH_4Cl sublimation taking sedimentation into consideration

7.3.3 Morphological Effect on Particles Sublimation

Model 2 describes the sublimation behavior of spherical particles. In case of sublimation, aerosol particles have commonly different morphologies. The particles with irregular forms have a high surface ratio and low apparent density. The particles from collison nebulizer in the experiment has a porous structure and a high surface ratio (see Fig.5.7). The different sublimation behaviors have already been tested in the experimental section. In this section, the simulation results of the new model, which has integrated the form factors, are demonstrated.

A model with particle surface ratio factor and porosity (apparent density) is used in this work. Different particle size corresponds to different surface ratios and different particle apparent densities, which leading to different sublimation speed. In the simulation work, aerosol particles are divided into three groups: small, middle and big particles. Three different surface factors (f_i) and porosities (ε_i) are used in the three groups of particles, respectively. They are used in Eq.6.6 to calculate the sublimation behavior of particles with big heat and mass transfer surface.

The decision of different surface factor is based on the BET measurement. The measuring results are shown in Tab.5.3. Due to the properties of NH_4Cl material, it is almost impossible to get the specific surface area of particles accurately. The surface ratio used in this model is shown in Tab.7.2.

Table 7.2: Surface factors for different particles in sublimation simulation

	Big Particle	Middle Particle	Small Particle
Surface area	25 m^2/g	15 m^2/g	5 m^2/g
Surface Factor (f_i)	5	3	1
Porosity (ε_i)	0.5	0.2	0
Diameter (d_{pi})	$> 3\ \mu m$	$1 - 3\ \mu m$	$< 1\ \mu m$

The experimental conditions are used in the theoretical work. The results are shown in Fig.7.9. After sublimation particles concentration decreases. Small particles' concen-

tration decreases and big particles' concentration decreases too. With increased heating temperature from 90 ^oC to 120 ^oC, more particles sublimate into the gas phase.

The comparison between the experimental results and simulation results are shown in Fig.7.10. The new model's results tally with the experimental results with surface area corrector f_i and apparent density $\rho_{pi}^d = \rho_d(1-\varepsilon_i)$ corrector. The high surface ratio (large mass and heat transfer area) leads to a faster sublimation of big particles, which also increases the partial pressure in the gas phase, intensively. The increased partial pressure, however, decreases the sublimation speed of other particles. The whole sublimation behavior of the aerosol particles is correspondingly changed. This change is significantly important in the decrease of the decrease of big particles' concentrations.

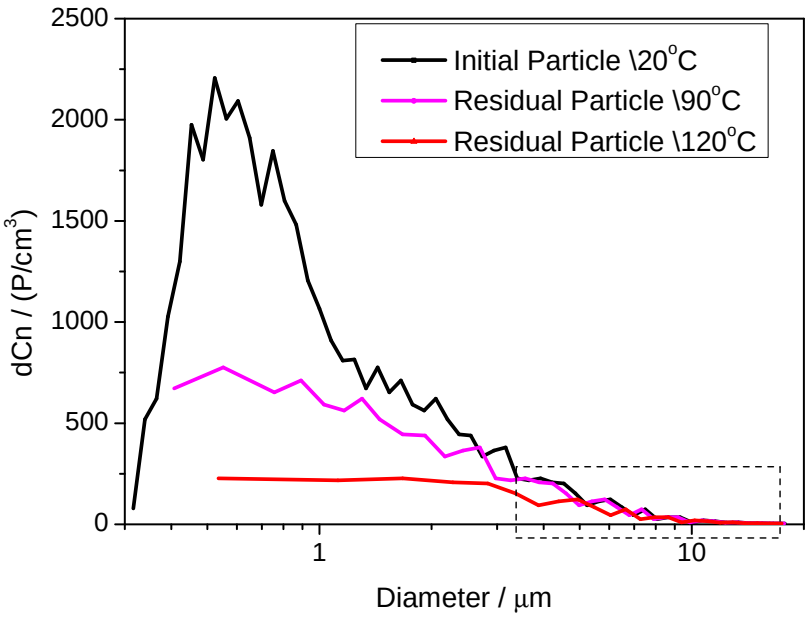

Figure 7.9: Simulated sublimation of NH_4Cl particles from collison nebulizer at 90 ^oC and 120 ^oC $V = 2.5m^3/h$

Due to the porous structure of these particles, the apparent density (Eq.6.7) of NH_4Cl

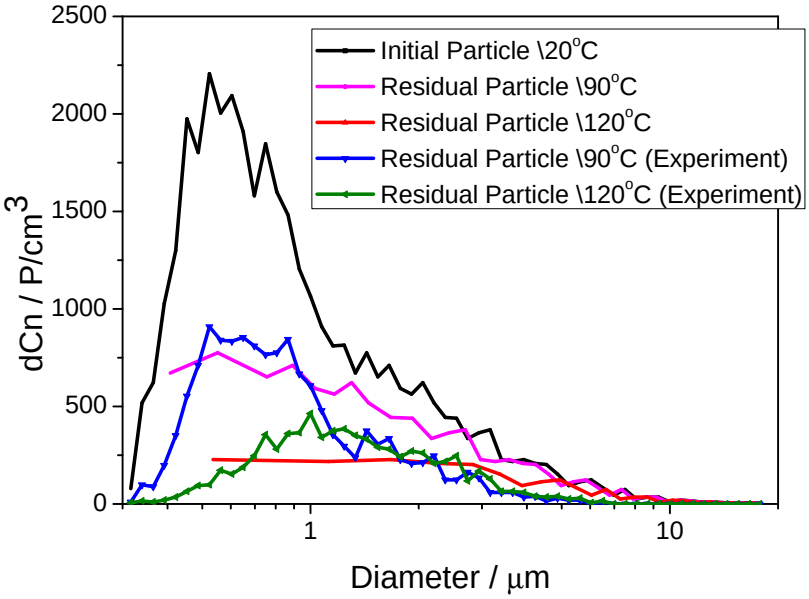

Figure 7.10: Comparison of the experimental results and the simulation results at the same sublimation conditions $V = 2.5m^3/h$

particles is lower than another sample (ground particles). A shape factor (k_i) is introduced to get the settling velocity. The calculation is based on Eq.6.13. With the consideration of shape factor $k_i = f_i$ (in this work) and apparent density $\rho_p^d = \rho_p(1-\varepsilon)$, the settling velocity is largely decreased and the settling time in the heating tube is increased, accordingly. The calculated settling times of different particles are shown in Fig.7.7. As it is already discussed in Section 7.3.2, there are no intensive sedimentation effects in the sublimation of this kind of particles.

7.3.4 Simulation of NH_4Cl Sublimation out of Experimental Conditions

Sublimation experiments are limited by different conditions such as test plants and measurement instruments. Not all of the parameters can be taken into experiments. Subli-

mation work, however, can satisfy this demand and demonstrate the change of aerosol particles under different conditions. In present experimental study, the limitation of the optical particle sensor was up to the concentration of $10^5\ P/cm^3$, therefore the sublimation experiments cannot be carried out under high particle concentration conditions. However, in industrial practices the aerosol in the sublimation process usually has a high particle concentration. The simulation study of particle sublimation under high concentration is carried out in this work. The change of single particle diameter is investigated. The sublimation of solid NH_4Cl particles with high concentration is simulated by the theoretical model. The particle concentration is increased to $4.7 \times 10^6 P/cm^3$.

Under the high particle concentration, the change of PSD in aerosol after heating process is shown in Fig.7.11.a. Increasing particle concentration, less particles are sublimated into the gas phase. The concentration of middle particles decreases while the concentration of small particles increase and that of big particles remains constant. Therefore, there is a broader PSD after heating. The diameter change of single particle in aerosol through the heating process is shown in Fig.7.11.b. The diameter of small particle reduces through the heating process. The change of big particles through the heating process is zoomed in the small figure, where two particles are demonstrated: particle of 0.866 μm and particle of 2.054 μm. At the beginning of the heating process particle with a diameter of 0.866 μm sublimates; the particle diameter decreases. Then the particle diameter begins to increase. The partial pressure p_v in the gas phase is smaller than the vapor pressure at the particle surface $p^*_{v,d}$ at first. There is a driving force for this particle to sublimate. After a while, however, the sublimation of small particles increases the partial pressure p_v in the gas phase, it goes higher than the saturation vapor pressure p^*_v. Then, the molecule concentration in the gas phase is bigger than that on the big particle's surface. The particle does not sublimate any longer. Instead, molecules go from gas phase to the particle surface. The particle can even grow. According to the Kelvin effect (Sec.3.7), the vapor pressure $p^*_{v,d}$ on the particle surface is smaller than that of small particles. Another particle (2.054 μm) has a larger particle diameter. In this case, when $p^*_{v,d} > p_v$, there is not enough driving force for this kind of particles to sublimate. At the beginning of the heating process, the particle stays constant. After a while, the partial pressure p_v in the gas phase increases due to the sublimation of smaller particles. Thus, when $p_v > p^*_{v,d}$ there is a tendency for the molecules from the gas phase to condense on the particle surface, therefore, the

particle grows.

The particle sublimation is not only dependent on the heating temperature and particle size. The particle concentration and the width of particle size distribution are also very important. A high particle concentration increases the partial pressure in the gas phase fast, which reduces the sublimation speed of particles. If there is a broad PSD in aerosol, the small particle sublimates due to the high vapor pressure on particle surface $p^*_{v,d}$. But big particles may grow, since the molecule concentration in the gas phase is higher than that on the particle surface ($c^*_v > c^*_{v,d}$). If there is a narrow size distribution, the difference is not so distinguished any more.

7.4 Simulations of DEHS Droplets Evaporations

Model 2 is used to calculate the change of DEHS droplets through heating process. The DEHS droplets are considered as spheres in the theoretical model. The factors of surface ratio can be ignored and the apparent density is not considered in the evaporation of droplets. The DEHS droplets in the experiments had a narrow size distribution, and the measured size mean diameter was only 0.8 μm. The sedimentation of the DEHS droplets in the heating residence time can be ignored.

The experimental conditions were introduced in the simulation work. The calculated PSD in residual DEHS aerosol is shown in Fig.7.12.a. The simulation results are compared with the experimental results. Due to the limitation of HGS, the measured smallest particle in aerosol is about 0.5 μm. Particles smaller than 0.5 μm cannot be measured by the particle sizer (HGS). In this case, the simulation result has a broader PSD than the experiment. If we look at the same particle range, the simulation and experimental results are in accord with each other. Increasing the heating temperature, less particles are in the residual aerosols.

In Fig.7.12.b, the residual droplets concentrations in aerosol with different heating temperatures are presented and compared with the experimental results. The residual droplet concentration decreases with increased heating temperature. The evaporation

of DEHS aerosol is weak when the heating temperature is below 70 ^oC. There is an intense concentration decrease at the temperature of $90^oC \sim 110^oC$, where the vapor pressure $p^*_{v,d}$ provides a strong driving force for the evaporation of DEHS droplets (see in Fig.5.15). The droplet concentration in the experimental results were lower than the concentration in the simulation results. The difference the simulation results and experimental results comes from the limited measurement range of HGS. A large amount of droplets smaller than 0.7 μm were missed in the experimental measurement, which lowered particle concentrations in the experiment.

One of the important differences between liquid droplets and solid particles is that the droplets are usually uniform, whereas solid particles have different structures. In this work the DEHS droplets have a narrow PSD. The biggest particle is about 2 μm, which is much smaller than that of NH_4Cl particles. NH_4Cl particles, however, have a broader PSD. Due to the great diversity in the NH_4Cl particles' diameter, the sublimation driving forces of NH_4Cl particles are also of great difference. DEHS droplets, however, have almost uniform diameters, which lead to similar evaporation driving forces for all the particles. During the evaporation of DEHS, the concentrations of all droplets (big droplets and small droplets) decrease with increased heating temperature. The phenomenon is presented in both the experimental results and simulation results.

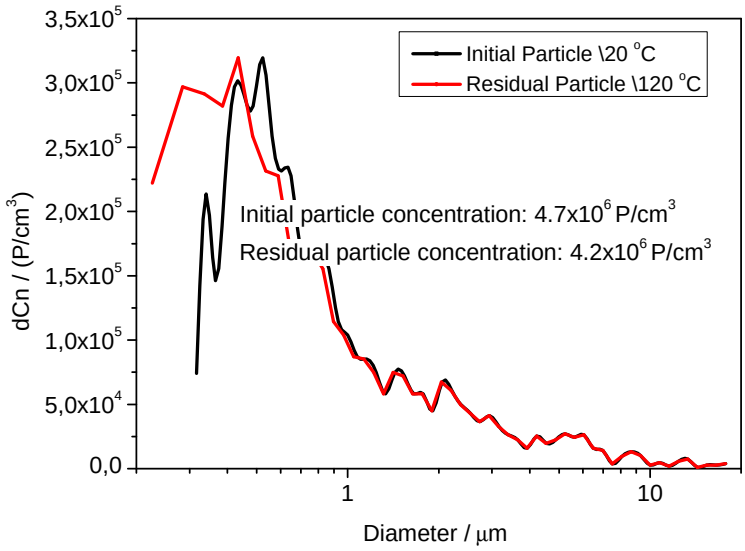

(a) Simulated change of PSD after sublimation.

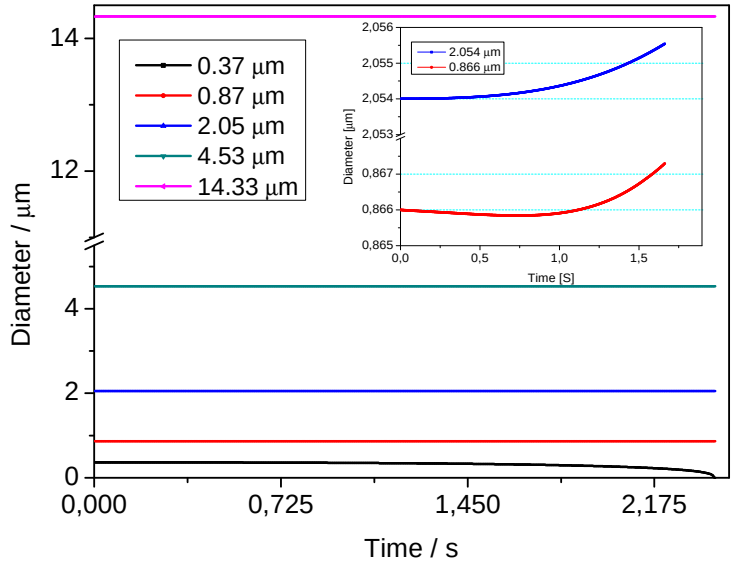

(b) Simulated change of particle diameter through sublimation

Figure 7.11: Simulated sublimation of ground NH_4Cl particles at high concentration $\Sigma Cn = 4.7 \times 10^6 P/cm^3, V = 2.5 m^3/h$.

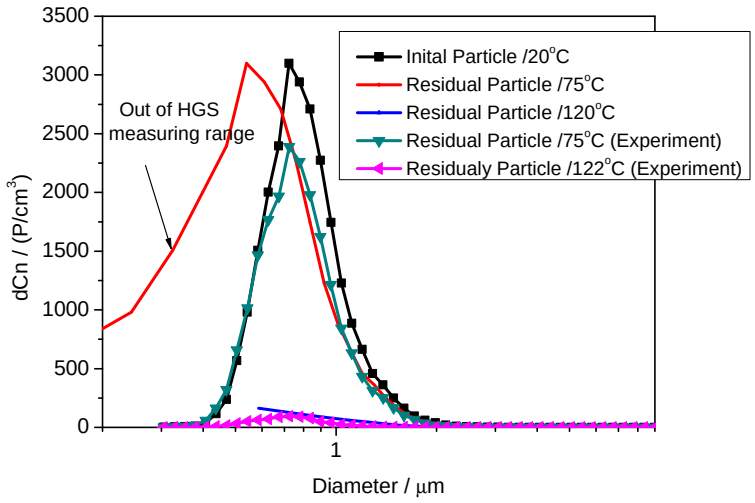

(a) Comparison of simulation and experimental results of the change of PSD after heating

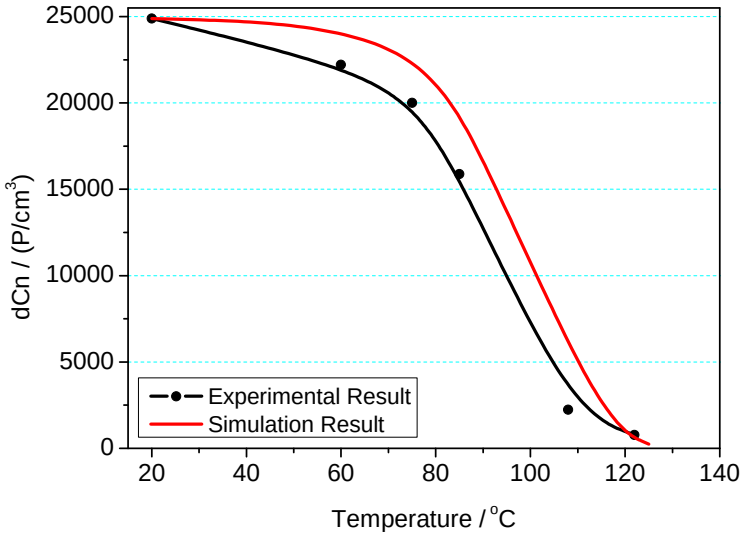

(b) Comparison of the change of particle concentration at different heating temperature

Figure 7.12: Comparison of experimental and simulation results of DEHS evaporation

8 Sublimation Kinetics and Phase Transition Effect

8.1 Sublimation Kinetics

Receiving heat energy, the molecules on the particle surface are activated to be free and go into the gas layer around the particle. The concentration of the activated molecules in the gas layer is dependent on the temperature, the vapor pressure curve of the materials and particle diameter. The activated molecules in the gas layer are, however, in a metastable condition. These molecules can either go back to the particle surface or go into the gas phase mixing with other molecules. When the molecules concentration in the gas phase is lower than that in the gas layer, the molecules go from the gas layer into the gas phase and mixing with other gas molecules. Thus, sublimation happens. On the contrary when the molecule concentration in the gas phase is higher, the molecules in the gas layer go back to the particle surface. Thus, condensation happens. There are two main factors that decide the sublimation kinetics: diffusion coefficient and driving force.

The diffusion coefficient is considered as the motion ability of the free molecules. It is dependent on the total pressure p of the gas phase, temperature T_∞ of the gas phase and the structure of the molecule. Diffusion coefficient D_{AB} (Eq.3.43) is an index of the molecule mobility. Increasing the temperature or decreasing the total pressure can enhance the diffusion coefficient. Small molecules have bigger diffusion coefficient than big molecules at the same condition. The driving force of particle sublimation comes from the difference between molecule concentration in the gas layer (on the particle

surface) $c^*_{v,d}$ and molecule concentration c_v in the gas phase. (Fig.8.1). There is a high driving force with a big molecule concentration's difference between the gas layer and the gas phase. When the difference is small, the driving force is also small. Molecule concentration in the gas layer can be well understood from the vapor pressure on the particle ($p^*_{v,d}$); molecule concentration in the gas phase corresponds the partial pressure in the gas phase (p_v). p_v is based on the amount of sublimated molecules in the gas phase. The two factors: diffusion coefficient and driving force, decide the sublimation kinetics together.

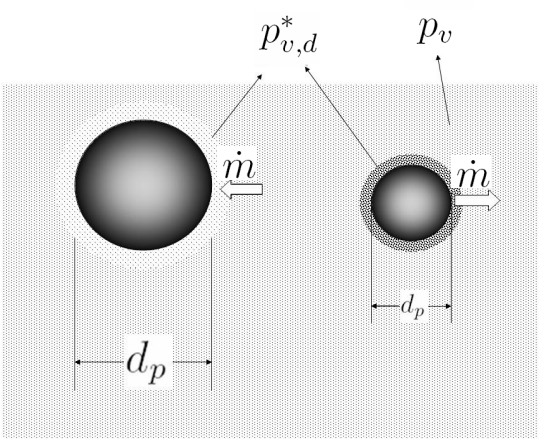

Figure 8.1: Indication of the driving force of particle evaporation.

DEHS is a material with a larger molecule size and molecule weight. So the diffusion coefficient of DEHS molecules is smaller. In this case, the diffusion of the DEHS free molecules from the gas layer into the gas phase is limited. The evaporation kinetics of the DEHS is also limited by the molecule mobility. NH_4Cl, however, has a smaller molecule size and molecule weight. Then the molecule mobility of the NH_4Cl free molecules at the same conditions (temperature, pressure) is "fast". In order to distinguish when the sublimation is controlled by molecule mobility and when is controlled by driving force, a comparison between NH_4Cl sublimation and DEHS evaporation is carried. Saturated molecule concentration c^*_v (according to the vapor pressure) of the two materials at different temperature are shown in Fig.8.3. A simulation was carried out. The two materials are sublimated (evaporated) at 110 ^{o}C, where they have similar saturated molecule concentration in the gas phase. That means the two materials at

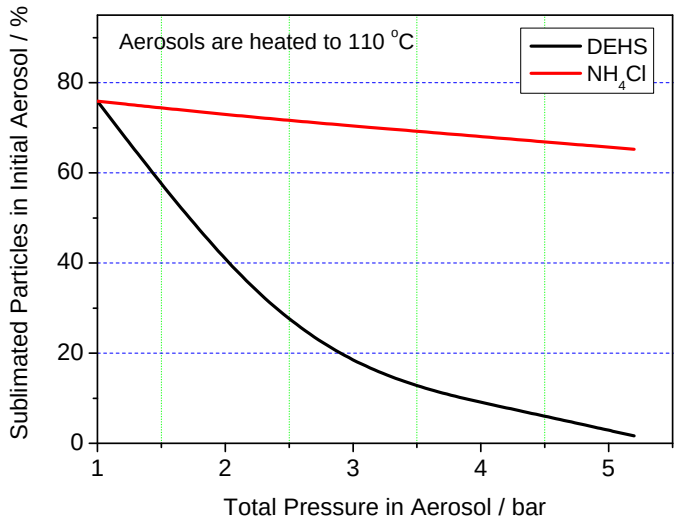

Figure 8.2: Simulated evaporation of DEHS and sublimation of NH_4Cl under different total pressure.

110 ^oC have the similar sublimation (evaporation) driving force. The sublimation (evaporation) was calculated under different total pressures. Increasing the total pressure in the gas phase, the diffusion coefficient of the molecules in the gas phase decreases. That means the molecule mobility decreases. The sublimation (evaporation) driving force is, however, dependent on the partial pressure's difference between in the gas phase and on the particle surface. The results are shown in Fig.8.2, where the two materials have the same percent particle sublimated (evaporated) at ambient pressure. Increasing the pressure, the sublimation (evaporation) of both materials decreases. The evaporation of DEHS droplets decreases intensively, whereas the sublimation of NH_4Cl particles decreases meekly. So it can be deduced that the decrease of diffusion coefficient has a stronger influence on the evaporation kinetics of DEHS droplets. The DEHS evaporation is controlled by the molecule mobility and the decrease of the diffusion coefficient reduces the evaporation kinetics largely. The sublimation kinetics of NH_4Cl particles, however, is controlled by the driving force and the decrease of the diffusion coefficient has less effect on it.

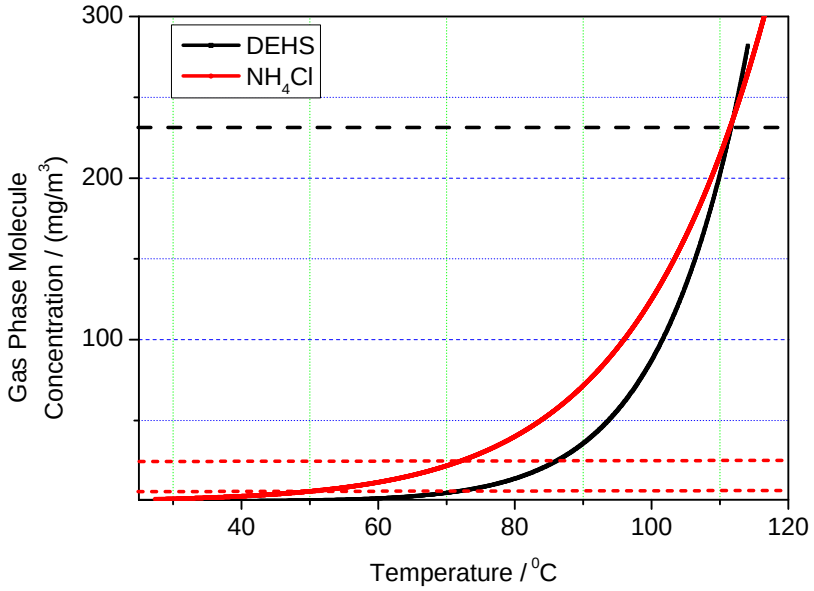

Figure 8.3: Molecule concentration and the corresponding vapor pressure at different temperature

In a short conclusion, when the material has a high vapor pressure or a big molecule size, the diffusion coefficient is relative low in the two factors of sublimation kinetics. The sublimation is controlled by the molecule mobility at first. When the molecule concentration c_v (according to the partial pressure) in the gas phase is near the saturated concentration c_v^*, the situation changes. The driving force decrease intensively. Then, the driving force may control the sublimation kinetics. When the material has a low vapor pressure or small molecule size, the sublimation is controlled by the driving force. In the experimental study of the thesis, the initial molecule concentrations in DEHS droplets and in NH_4Cl particles are shown in Fig.8.3. The initial molecule concentration of DEHS was very low, which wasunder 30 mg/m^3. It cannot get the evaporation to be controlled by the driving force. The initial NH_4Cl particles, however, provided a large amount of molecules, which was higher than 200 mg/m^3 . The driving force is always a key factor in the NH_4Cl sublimation process.

8.2 Phase Transition Effect

In aerosol with single material, the diffusion coefficient is identical for all the particles' molecules. When the diffusion kinetics controls the sublimation, all the particles have almost the same sublimation kinetics. When driving force controls the sublimation kinetics, the effect of particle size on the sublimation kinetics must be taken into account. For monodispersed particles, all of the particles have the same vapor pressure $p^*_{v,d}$ on the particle surface and therefore, the same molecule concentration $c^*_{v,d}$ on the particle surface. Thus, all particles have the same sublimation kinetic at the given temperature. But aerosol particles are always polydispersed. In this work the measured NH_4Cl particle size is from 0.3μ to $20\mu m$. According to the Kelvin effect, the vapor pressures on these particles surfaces $p^*_{v,d}$ are different. Small particles have high vapor pressure $p^*_{v,d}$ and high molecule concentration $c^*_{v,d}$; big particles have low vapor pressure $p^*_{v,d}$ and low molecule concentration $c^*_{v,d}$ on the particle surface. Small particles in aerosols have a higher sublimation driving force than big particles. Thus, small NH_4Cl particles have higher sublimation kinetics than the big particles.

In Fig.8.4, the concept of the Phase Transition effect is put forward. A kind of nonvolatile material is used as an example. Assuming $T_d = T_\infty$, the Δp ($\Delta p = p^*_{v,d} - p_v$) is defined as a sublimation driving force of a given particle. The aerosol has a broad size distribution. According to the Kelvin effect, small particles have higher $p^*_{v,d}$ than big particles. In this case the small particles sublimate faster. With an increased amount of sublimated particles, the partial pressure (p_v) in the gas phase increases. Even when p_v is near or higher than the saturated vapor pressure on flat surface p^*_v, There is still a driving force for the small particle to sublimate. Thus, the partial pressure in the gas phase can be slightly higher than the saturated vapor pressure p^*_v. This partial pressure p_v corresponds to a particle diameter d_0 according to the Kelvin effect. This diameter is in equilibrium with the vapor pressure p_v in the gas phase. The particle neither shrinks nor grows bigger. Particles with $d_p < d_0$ indicate surface vapor pressures higher than the gas phase partial pressures ($p^*_{v,d} > p_v$) and the particles still have driving forces to sublimate. Particles with $d_p > d_0$ have surface vapor pressures lower than the gas phase partial pressure ($p^*_{v,d} < p_v$) and there are no driving forces to sublimate. Condensation can happen on these particles to lower the partial pressure p_v. A molecule transition

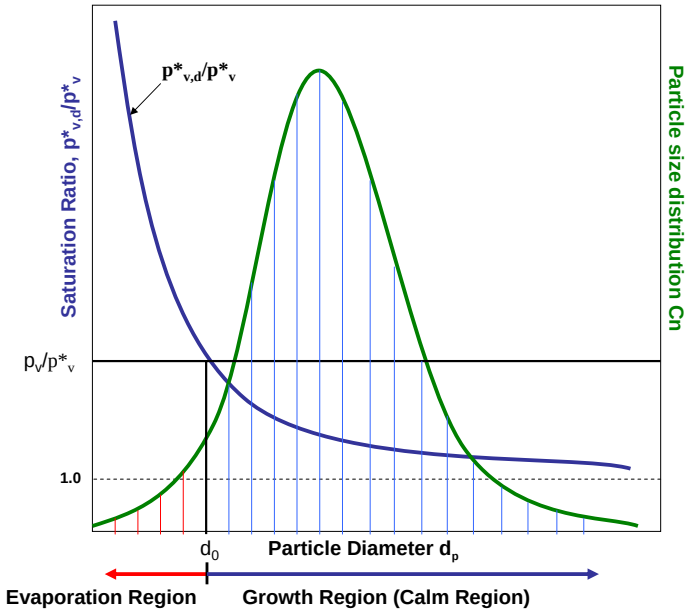

Figure 8.4: Indication of Phase Transition Effect during aerosol evaporation

happens. Molecules go from the gas layer on the particle surface, where $d_p < d_0$, into the gas phase under the working of the driving force on small particles' surfaces. Under the working of the driving force on the surface of big particles, the molecules go from the gas phase into the gas layer on the big particle and condense on the particle surface, where $d_p > d_0$. Thus, small particles sublimate; big particles grow bigger. Sublimation of the small particles increases p_v. Then, big particles grow bigger getting p_v lower. The decreased p_v intensifies the sublimation of small particle further. This effect is called *Phase Transition effect*. (76) (77)

There are several necessary conditions for the *Phase Transition Effect*:

1. Sublimation (evaporation) is controlled by the driving force
2. High partial pressure (molecule concentration) in gas phase.
3. Wide particle size distribution in aerosol. It is distinct for different material with different surface tension. A particle range from nanometer to micrometer is con-

sidered reliable.

4. Sufficient materials from initial particle concentration.

Comparing to the *Phase Transition effect* in the gas phase (between gas-solid or gas-liquid), there is an *Ostwald Ripening effect* in the fluid phase. When the particle phase is present in the form of a distribution with different sizes, the Gibbs-Thomson effect provides a thermodynamic driving force for large particles to grow at the expense of small particles (70) (71) (72). Many scientists (73) (74) have measured the ripening or coarsening of particles/droplets. Usui et.al. (73) detected the growing of mean diameter oil droplets in oil-in-water emulsion systems after hours. Comparing with the *Ostwald Ripening effect* in solution, the *phase Transition Effect* happens in quite a short time and in the gas phase. A similar effect is observed in crystal suspension (called Ostwald ripening) but with another physical background.

9 Summary

This dissertation is focused on the characterization of fine aerosol particles sublimation. The question of particle sublimation in a cluster of particles has been discussed based on experimental and theoretical studies. These studies support the developments of nanoparticles generation through sublimation/condensation, thin films coating through physical vapor deposition, impurities separation according to different vapor pressure, and fuel droplets evaporation through the operating of engines.

9.1 Experiments

The experimental studies were performed in a test plant including on-line control (heating temperature, gas flow, and pressure) and on-line (in-line) particle measurements (Optical particle sensor, APS). The sublimation (evaporation) of polydispersed particles are investigated basing on the relevant parameters such as heating temperature, particle concentration, aerosol residence time.

Inorganic material of NH_4Cl particles and organic material of DEHS droplets were used as test materials. Through the sublimation (evaporation) experiments of the two kinds of materials, it was found that the parameters of temperature, particle size distribution, particle concentration and different volume flow had the following effects:

- The heating process decides the mass transport in the sublimation (evaporation) process.

- Sublimation (evaporation) is dependent on the change of the molecule concentration in the gas phase. The molecule concentration is determined by the particle concentration, particle size distribution, and particle morphology.
- In the sublimation (evaporation) of fine particles (droplet), the increase of the partial pressure on particle surface due to the particle surface curve can not be neglected.
- The properties of the materials such as vapor pressure, surface tension, diffusion coefficient and latent heat of evaporation must be taken into account.

The sublimation of NH_4Cl particles with different particle morphologies (smooth surface or porous structure) was carried out. The sublimation experiments were carried at two steps: heating to 120 ^oC and higher. At first the heating temperature was raised up to 120 ^oC. During the sublimation of the particles with smooth surfaces, significant decreases in the small particle ($< 1\mu m$) concentrations were detected, whereas the concentrations of big particles were almost constant. At the higher heating temperature, both big and small particles concentrations decreased. For the "porous" particles with a high specific surface area, the sublimation speed was higher than that of the particles with smooth surface.

DEHS is an organic liquid which have a relative big molecule size. After the evaporation, an intensive decrease in the particle concentration was detected, even though most of the literatures have described DEHS as a kind of slow evaporated material (75) (78) (79).

9.2 Hot Gas Sensor (HGS)

In the aerosol studies, particle measuring technologies are very important. Among all the particle sensors, optical sensors have the great advantage that the sample can be measured under the same chemical and physical conditions as in the experiments. The present commercial optical particle sensors are strongly limited by the aerosol temperature, limited to 120 ^oC. An important part of this thesis is to develop a Hot

Gas Sensor (HGS), which can meet the demand of aerosol measurement in a high temperature media. The HGS measures the aerosol particles in-line up to 500 ^oC.

9.3 Simulations

Basing on the experiments, different theoretical models were developed to investigate the efficiency of aerosol sublimation. The effects of particle morphology, particle concentration, heating temperature were thoroughly studied. The sublimation kinetics is discussed in detail.

9.4 Results and Discussion

The molecules on the particle surface are activated into the gas layer of particle-gas interface. This layer has been described before by Fuchs (45). The molecule concentration in the gas layer is based on the vapor pressure and particle size. When the molecules in the gas layer transfer to the bulk gas phase, sublimation occurs. There are two main influencing factors in the sublimation kinetics (see in Fig.9.1): diffusion coefficient and driving force. Diffusion coefficient is the dimension of the molecule mobility and is determined by temperature, total pressure, molecule size. Driving force is based on the different molecule concentrations between gas layer on particles and the bulk of the gas phase. DEHS evaporation is controlled by the molecule mobility, which is small due to the big molecule size. In the sublimation of NH_4Cl, which has a small molecule size, the diffusion kinetics is high. NH_4Cl sublimation is, in this case, controlled by the driving force. Increasing the total pressure, the molecule mobility controlled evaporation(sublimation) is attenuated strongly. This property can be used in the separation of materials with similar vapor pressure.

Generally, when a material has a small molecule or low vapor pressure, the sublimation (evaporation) is controlled by driving force. When a material has a big molecule or

high vapor pressure, the sublimation (evaporation) is controlled by molecule mobility at first. With increased partial pressure in the gas phase, however, the diffusion kinetics controlled sublimation (evaporation) may change to be controlled by the driving force.

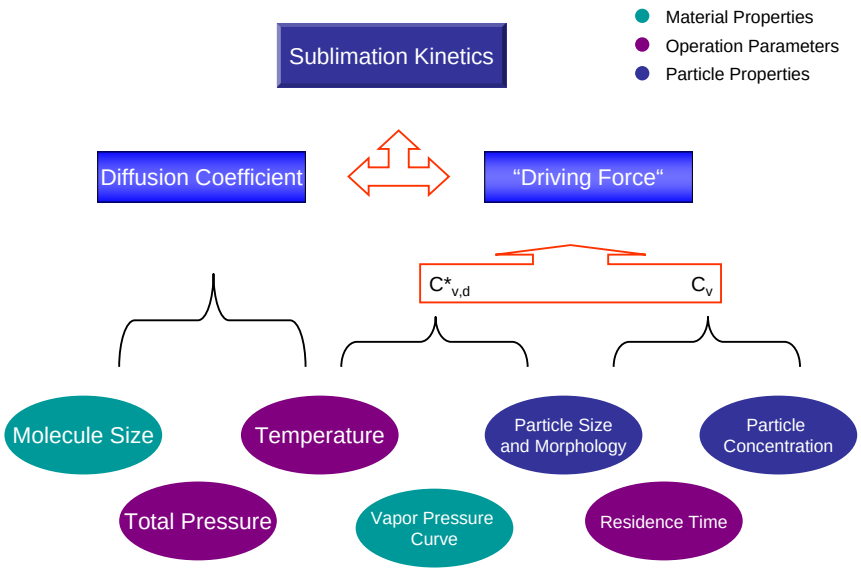

Figure 9.1: Schematic demonstration of sublimation kinetics

Diffusion coefficient is identical to all of the same molecules in sublimation. When the sublimation (evaporation) is controlled by molecule mobility, all the particles/droplets in the aerosol have very close sublimation (evaporation) kinetics.

Driving force is, however, dependent on the different particle size. Smaller particles have higher sublimation driving force due to the higher molecule concentration in the gas layer. When the sublimation is driving force controlled, particles with different diameters have different sublimation speed. Satisfying the following conditions, *Phase Transition Effect* happens between gas phase and particle phase:

1. Sublimation/evaporation is controlled by driving force.
2. Particles/Droplets are polydisperse with wide size distribution.

3. There are sufficient materials to sublimate from the initial aerosol to get the partial pressure p_v saturated.
4. Partial pressure (molecule concentration) in the gas phase is in the range of the saturated pressure p_v^*.

Due to the desire of the system to minimize the free energy associated with the interfaces between the two phases, small particles sublimate faster than big particles. When the partial pressure is near or above the saturated vapor pressure, transfer of the molecules from small particles to big particles happens. Big particles grow up at the expense of small particles. The mean diameter of aerosol particles increases accordingly.

A Determination of Surface Tension

The solid maintains thermodynamic equilibrium through the interface with its vapor.The interface region separates the two homogeneous phases, but the interface itself is not a sharp, well–defined geometrical surface. All physical quantities change more or less gradually from their solid to their vapor values. The interface region is thus a strongly inhomogeneous region in equilibrium with two homogeneous phases, the solid and the vapor. Since the interface layer is a material system with a well–defined volume and material content, most thermodynamic properties are defined as usual. Temperature, free energy, composition, chemical potential per particle etc., all have their usual meaning, as in the neighboring homogeneous phases.(80)

A.1 Application of the Young's Equation

The surface tension of the solid substrate cannot be measured directly. The angle between a liquid in contact with a solid surface is measured. The surface tension of the liquid is already known, in this case the surface tension of the solid can be calculated. Normally a small drop of the liquid is introduced on the flat solid surface (81). Young's equation is harnessed in the calculation.

$$\gamma_{sl} = \gamma_s - \gamma_{lv} \cos\theta \tag{A.1}$$

The measurement indicates if the interface energy is too low (or liquid surface energy is too low), there is nearly complete wetting on the solid surface. Then the contact angle

cannot be measured; if the interface energy is high (or liquid surface energy is high), wetting is limited; in between, it is partial wetting.

When complete wetting takes place on the solid substrate, $\cos\theta = 1$ and $\theta = 0°$; when partial wetting, is $\gamma_s \geq \gamma_l$, the wetting pressure is called P_{sp}, $\gamma_s - (\gamma_{sl} + \gamma_l) \equiv P_{sp} > 0$. When the contact angle $\theta < 30^o$, the solid surface is wettable to the liquid. When $\theta = 180^o$, it means that the surface cannot be wetted by the liquid, which is practically not existed.

Bei the contact of the solid surface and the liquid there is an adhesion ability between the two surfaces (82):

$$W_{ad} = \gamma_s + \gamma_l - \gamma_{sl}. \tag{A.2}$$

A.2 Calculation of the Surface Tension

Surface energy is quantified using a contact angle between a solid substrate and a test liquid. There are different methods used to calculate the surface energy.

A.2.1 Method of Neumann 1

$$\cos\theta = \frac{(0.015\gamma_s - 2)(\sqrt{\gamma_s\gamma_l})}{\gamma_l(0.015\sqrt{\gamma_l\gamma_s} - 1)} \tag{A.3}$$

where θ is the contact angle; γ_s is the surface tension of the solid; γ_l is the surface tension of the liquid.

There is also another equation from Neumann, which offers a better mathematical description.

A.2.2 Method of Neumann 2

$$\cos\theta = -1 + 2\sqrt{\frac{\gamma_s}{\gamma_l}} \cdot e^{-\beta(\gamma_l - \gamma_s)^2} \tag{A.4}$$

where β is constant 0.0001247 [m^2/mJ]^2

A.3 Practical Application

Water, alcohol, and glycerin are used in the measurement as test liquids. Water has the highest surface tension besides mercury. The following table shows the surface tensions of the test liquids (from literature).

Test Liquid	Water	Glycerin	Alcohol
Surface Energy [mN/m]	72.1	62.7	22.1

The contact angle of the test liquids of NH_4Cl and CuPcCl is measured. Then the surface energy is calculated according to the Neumann equation. The results are presented in the following table:

Test Liquid	Water	Glycerin	Alcohol
NH_4Cl	soluble	completely wetting	completely wetting
CuPcCl	87.8^o	95^o	completely wetting

Then, the surface tension of CuPcCl can be calculated:

$$\gamma_{CuPcCl} = 30mN/m \tag{A.5}$$

It can be seen that the calculated surface tension is smaller than that of water and glycerin; bigger than alcohol, while during experiment, alcohol is completely wetting the CuPcCl substrate.

NH_4Cl is completely wettable by glycerin and alcohol. Thus, it may be speculated that the surface tension of the NH_4Cl is large. Because of the high relatively solubility of NH_4Cl in water, the contact angle between the NH_4Cl substrate and water cannot be measured. In this case, an estimation is proposed, as

$$\gamma_{NH_4Cl} = 70mN/m \tag{A.6}$$

which is nearly that of water.

B SEM of NH_4Cl Particles Sublimation

B.1 SEM of Porous NH_4Cl Particles before and after Sublimation

In Fig.B.1 shows the SEM photographs of porous NH_4Cl particles before and after sublimation. After sublimation, the porous structures of the NH_4Cl particles disappears. There are some spherical particles with relative close particles diameters.

B.2 SEM Observation of NH_4Cl Particles Sublimation

The Scanning Electron Microscope (SEM) is a type of electron microscope that images the sample surface by scanning it with a high-energy beam of electrons in a raster scan pattern. The electrons interact with the atoms that make up the sample producing signals that contain information about the sample's surface topography, composition and other properties such as electrical conductivity. In the observation, nonconductive samples tend to charge when scanned by the electron beam, this causes scanning faults and other image artefacts. The samples are therefore coated with a ultrathin coating of electrically-conducting material, such as chromium. In this work the SEM observation was carried out by Raith e-Line (Raith GmbH), which has a max. 1 000 000 times enlarging.

During the observation of NH_4Cl particle size and morphology, some irregular phenom-

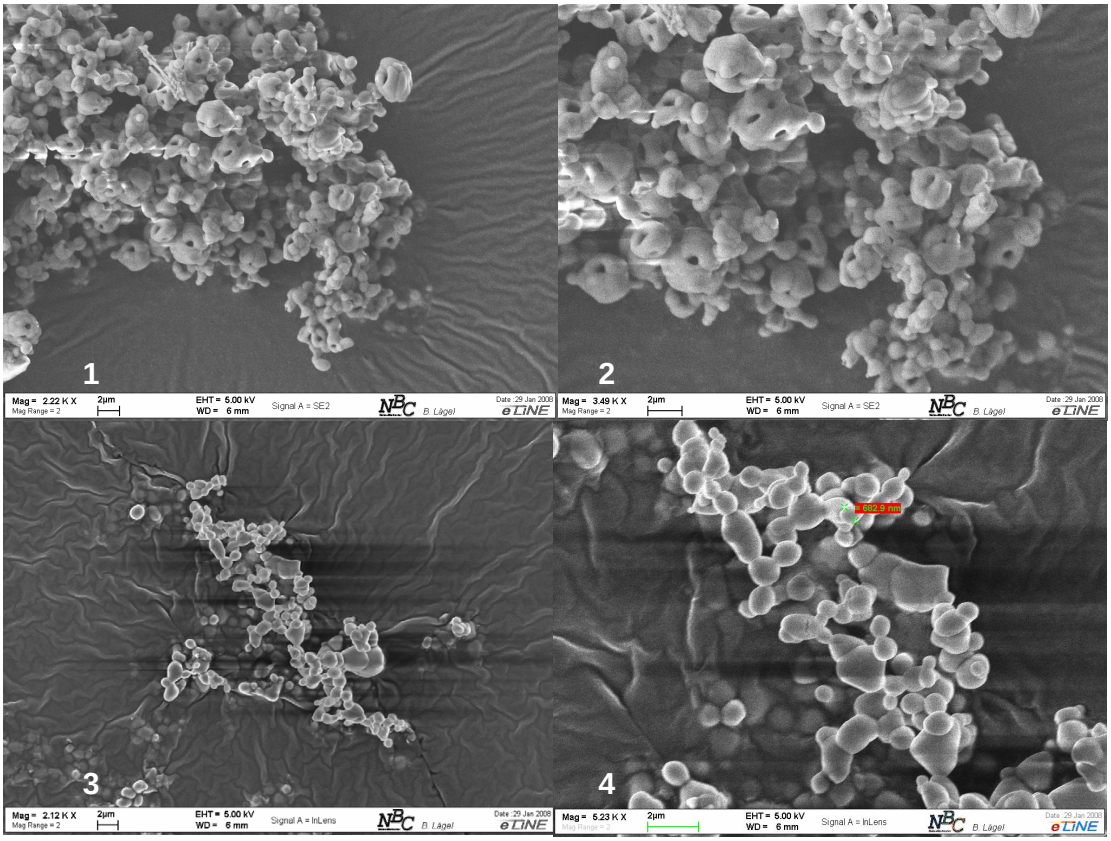

Figure B.1: The SEM photographs of porous NH_4Cl particles before sublimation: (1) and (2); after sublimation: (3) and (4).

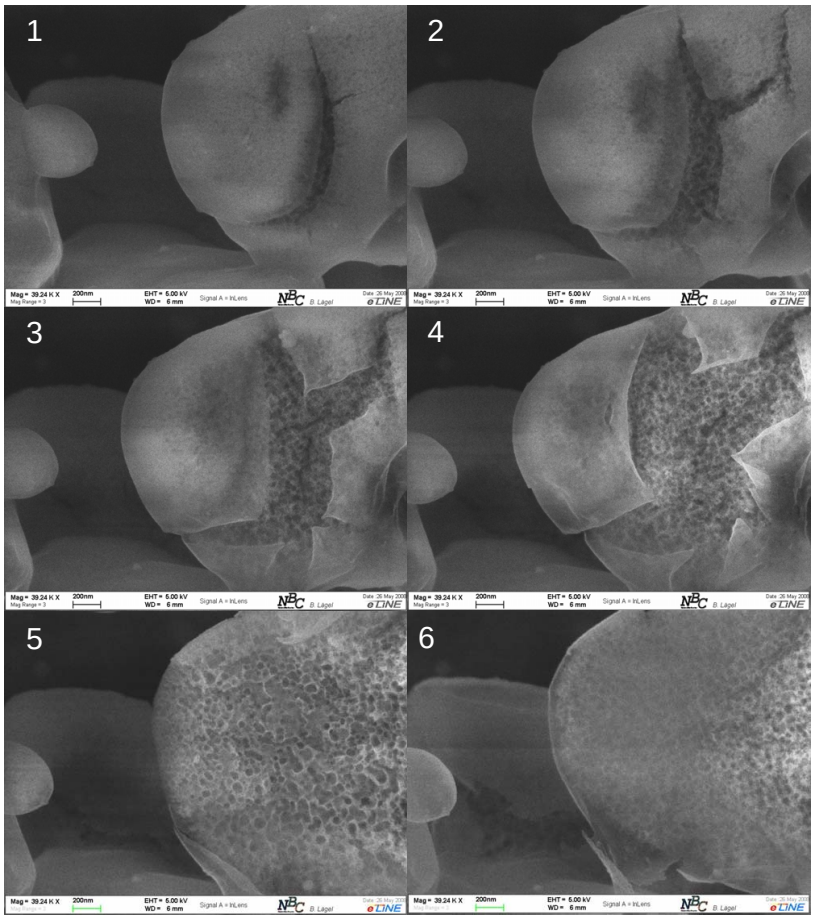

Figure B.2: The observed NH_4Cl particle sublimation in the vacuum chamber of SEM.

ena were observed, which is shown in Fig.B.2. These phenomena are assumed to be the sublimation of NH_4Cl particles in the vacuum chamber under the scanning of high-energy beam.

Bibliography

[1] T.T. Mercer, *Aerosol Technology in Harzard Evaluation, Academic Press, Inc.LTD, 1973.*

[2] H.E. Hesketh, *Fine Particles in Gaseous Media, Lewis Publichers, Inc, 1986.*

[3] W. Mahoney, R.P. Andres, *Aerosol Synthesis of Nanoscale Clusters Using Atmospheric Arc Evaporation, Materials Science and Engineering, A204, 160-164,1995.*

[4] V. Haas, R. Birringer, H. Gleiter, S.E. Pratisinis, *Synthesis of Nanostructured Powders in an Aerosol Flow Condenser, Jouranl of Aerosol Science, 28, 1443-1453, 1997.*

[5] H. Gleiter, *Nanostructured Materials, Advances in Materials, 4,474-481,1992.*

[6] C.G. Granqvist, R.A. Buhrman, *Ultrafine Metal Particles, Journal of Applied Physics, 47, 2200-2219,1976.*

[7] H.G. Scheibel, J. Porstendorfer, *Generation of Monodisperse Ag- and Nacl-aerosols with Particle Diamters between 2 and 300 nm, Journal of Aerosol Science, 14, 113-126, 1983.*

[8] Y. Singh, J. Javier, S. Ehrman, M. Magnusson, K. Deppert, *Approaches to Increasing Yield in Evaporation/Condensation Nanoparticle Generation, Journal of Aerosol Science, 33, 1309-1325, 2002.*

[9] A. Gurav, T. Kodas, T. Pluym, Y. Xiong, *Aerosol Processing of Materials, Aerosol Science and Technology 19, 411-452, 1993.*

[10] A. Gutsch, M. Kraemer, G. Michael, H. Muehlenweg, M. Pridoehl, G. Zimmermann, *Gas-phase-production of Nanoparticles, KONA Powder and Particle 20, 24-37, 2002.*

[11] B. Nakhostenn, *Forschungsschwerpunkte und Forschritt der Duennschichttechnologien Galvanotechnik, 2530-2541, 10/2003.*

[12] V.A. Popkov, G.M. Dugacheva, V. Reshetnyak, N.V. Mashnina, *Purification of Praziquantel by the Method of Directional Sublimation, Pharmaceutical Chemistry Journal, 29(6), 420-421, 1995*

[13] C.A. Holden, H.S. Bryant, *Purification of Sublimation, Separation Science and Technology, 4(1), 1-13, 1969.*

[14] S. Wittig, W. Klausmann, B. Noll, J. Himmelsbach, *Evaporation of Fuel Droplets in Turbulent Combustor Flow, ASME-88-GT-107, 1988.*

[15] M. Hallmann, M. Scheurlen, S. Wittig, *Computation of Turbulent Evaporating Sprays: Eulerian Versus Lagrangian Approach, ASME-93-GT-333, 1993.*

[16] M. Kurreck, M. Willmann, S. Wittig, *Prediction of the Three-dimentional Reacting Two-phase Flow within a Jet-stabilized Combustion, ASME-96-GT-468, 1996.*

[17] T. Shih, C.M. Megaridis, *Suspenden Droplet Evapioration Modeling in a Laminar Convective Environment, Combust. Flame 102, 256-270, 1995.*

[18] J.C. Maxwell, *Diffusion. In Encyclopaedia Britannica*, London Vol. 7 (9th ed.), 214-221, 1878.

[19] M. Abu-Zaid, *Droplet Evaporation on Porous and non-Porous Ceramic Solids heated from top, Heat and Mass Transfer, 38, 203-211, 2002.*

[20] K. Baumeister, F. Simon, *Leidenfrost Temperature-its correlation for liquid metals, crygens, hydrocarbons, and water, J. Heat Transfer, 95, 166-173, 1973.*

[21] P. Halvonson, R. Carson, S. Jeter, S. Abed-khaki, *Critical Heat Flux Limits for a Headed Surface Impacted by a Stream of Liquid Droplets, Int. J Heat Transfer, 116, 679-685, 1994.*

[22] G. Emmerson, *The Effect of Pressure and Surface Material on the Leidenfrost Point of Discrete Drops of Water, Int J Heat Transfer, 18, 381-386, 1975.*

[23] C.N. Davies, *Evaporation of Airborne Droplets, in Fundamentals of Aerosol Science, D.T. Shaw (Ed.)* Wiley, New York, 1978.

[24] K. Prommersberger, J. Stengele, K. Dullenkopf, J. Himmelsbach, S. Wittig *High Intensity Combustors - Steady Isobaric Combustion: Investigations of Droplet Evaporation at Elevated Pressures* Wiley-VCH Verlag GmbH, 2002.

[25] S.El. Golli, J. Bricard, P-Y. Turpin, G. Arnaud, *J. Aerosol Sci.*, 3, 255-274, 1972.

[26] D.C. Kincaid, T.S. Longley, *A Water Droplet Evaporation and Temperature Model, Transactions of the ASAE, 32(2),457-457,1989.*

[28] W.E. Ranz, W.R. Marshall, *Evaporation from droplet Part I, Chem. Eng. Progr.* 48(3), 141-146 1952.

[28] W.E. Ranz, W.R. Marshall, *Evaporation from droplet Part II, Chem. Eng. Progr.* 48(3), 173-179, 1952.

[29] M.A. Silberberg (2006). Chemistry, 4th edition, New York: McGraw-Hill, 431434.

[30] W.C. Hinds, *Aerosol Technology: Properties, Behavior, and Measurement of Airborne Particles, 1982, John Wiley Sons.*.

[31] L.M. Skinner, J.R. Sambles, *J. Aerosol Sci.*, 3, 199-210, 1972.

[32] G. Zebel, *Z. Aerosol-Forsch.*, 5, 263-288, 1956.

[33] F.F. Cinkotai, *The Behavior of Sodium Chloride Particles in Moist Air, J. Aerosol Sci.*, 2, 325-329, 1971.

[34] H. Mori, J. Lee, In Situ Observation of Structural and Morphological Changes in Nanometer-sized Silver Particles on Graphite during Sublimation, *Micros Microanal*, 12, 2006.

[35] H. Schiffter, G. Lee, *Single-Droplet Evaporation Kinetics and Particle Formation in an Acoustic Levitator. Part 1: Evaporation of Water Microdroplets Assessed using Boundary-Layer and Acoustic Levitation Theories, Journal of Pharmaceutical Sciences, 96(9), 2274-2283, 2007.*

[36] J.R. Savage, D.W. Blair, A.J. Levine, R.A. Guyer, A.D. Dinsmore, Imaging the Sublimation Dynamics of Colloidal Crystallites, *Science*, 314, 795, 2006.

[37] P.G. Saffmann, J.S. Turner, *On the Rise of Small air Bubbles in Water, J. Fluid. Mech. 1,16,1956*.

[38] R. Taylor, R. Krishna, *Multicomponent Mass Transfer, John Wiley Sons,1993*.

[39] K.K. Nanda, F.E. Kruis, H. Fissan *Evaporation of Free PbS Nanoparticles: Evidence of the Kelvin Effect, Physical Review Letters, 89(25),2002*

[40] M.J. Lee, Y.W. Kim, J.Y. HA, S.S. Chung, *Effects of Watery Vapor Concentration on Droplet Evaporation in Hot Environment, Internatioal Jouranl of Automotive Technology, 2(3),109-115, 2001.*

[41] J.-G. Lee, J. Lee, T. Tanaka, H. Mori, *In Situ HREM Observation of Crystalline-to-Gas Transition in Nanometer-Sized Ag Particles, Physical Review Letters, 96, 075504, 2006.*

[42] N. Hiromitsu, *The Influence of Stream Turbulence and Vapor Concentration for Evaporation Process of Droplet in Stream* Keio Univ. Ph.D these.

[43] J.J. Hegseth, N. Rashidnia, A. Chai, *Natural Convection in Droplet Evaporation, Physical Review E, 54(2), 1996.*

[44] B.D. Swanson, N.J. Bacon, E. James Davis, M. B. Baker, *Electrodynamic Trapping and Manipulation of Ice Crystals, J.R. Meteorol.Soc. 125, 1039-1058, 1999*.

[45] N.A.Fuchs, *Evaporation and Droplet Growth in Gaseous Media, Pergamon Press, 1959*.

[46] G.M. Hidy, *The Dynamics of Aerocolloidal Systems, Pergamon Press, 1970.*

[47] H.Köhler, *Tansactions of the Faraday Society, 1936,32,1152-1161*.

[48] H.L.Wright, *Proceedings of the Physical Society,1936,48,5,675-688*.

[49] S.K. Friedlander, *Smoke, Dust and Haze: Fundamentals of Aerosol Behavior, John Wiley Sons,1977*.

[50] S.W. Thomsom, *Philosophical Magazine, 1871,4,448-452*.

[51] J. Pich, *Theory of Gravitational Deposition of Particles from Laminar Flows in Channel, J. Aerosol Sci. 3, 1972, 351-361*.

[52] D.B. Taulbee, C.P. Yu, and Heyder, J. D.B. Taulbee, *Aerosol transport in the human lung from analysis of single breaths. J. Appl. Physiol. 44(5), 803812, 1978*.

[53] D.B. Taulbee, C.P. Yu, *A Theory of Aerosol Deposition in the Human Respiratory Tract, J. Appl. Physiol. 38, 77-85, 1975*.

[54] N. Froessling, *Gerlands Beitr Geophys, 52,170,1938.*

[55] W.R. Marshall, *Atomization and Spray Drying, Chemical Engineering Process, Monograph Series No.2 Vol.50, Am. Institute of Chemical Engineers, New York, 1954.*

[56] C.E. Goering, L.E. Bode, M.R. Gebhardt, *Mathematical Modeling of Spray Droplet Deceleration and Evaporation, Transaction, of the ASAE, 15(2),220-220, 1972.*

[57] T.T. Kodas, M. Hampden-Smith, *Aerosol Processing of Materials, Wiley-VCH, 1999*.

[58] J.O. Hirschfelder, C.F. Curtiss, *Molecular Theory of Gases and Liquids, John Wily and Sons Inc, 1954*.

[59] J.C. Barrett, C.F. Clement, *Growth Rates for Liquid Drops, J. Aerosol. Sci, 19(2), 223-242, 1988.*

[60] B.A. Sachweh, *Habilitation: Messen, Konditionieren und Abscheiden feinster Aerosolpartikel, 1996*.

[61] H.C. van de Hulst, *Light Scatterubg by Small Particles, Dover Publications, Inc, 1981*.

[62] P. Ravindran, EJ. Davis, AK. Ray, *Diffusiveties of Low-Volatility Species in Light Gases, AIChE Journal, 25(6), 966-975, 1979*

[63] D.C. Taflin, S.H. Zhang, T. Allen, E. James Davies, *Measurement of Droplet Interfacial Phenomena by Light-Scattering Techniques, AIChE Journal, 34(8), 1988*.

[64] E.R. Whitby, P.H. McMurry, *Modal Aerosol Dynamics Modeling, Aesorol Science and Technology, 27, 673-688, 1997.*

[65] J. Pyykoenen, J. Jokinienmi, *Computational Fluid Dynamics Based Sectional Aerosol Modelling Schemes, J. Aerosol Sci., 31(5), 531-550, 2000.*

[66] R.C. Weast, D.R. Lide, *CRC Handbook of Chemistry and Physics, CRC Press, Inc. 1990*

[67] I. Wichterle, J. Linek, *Antoine Vapor Pressure Constants of Pure Compounds, Academia, Praha, 1971*.

[68] P.A. Small, K.W. Small, P. Cowley, *The Vapor Pressure of Some High Boiling Esters, Trans.Faraday Soc.44, 810, 1948.*

[69] M. Jonasz *Light Scattering by Particles in Water : Theoretical And Experimental Foundations, Academic Pressure, 2007*

[70] M. Petersen, A. Zangwill, C. Ratsch, *Homoepitaxial Ostwald Ripening, Surface Science, 536, 55-60, 2003.*

[71] A. Lo, R.T. Skodje, *Kinetic and Monte Carlo Methods of This Film Coarsening: Cross Over from Diffusion-Coalescence to Ostwald Growth Modes, Journal of Chemical Physics, 112(4),2000.*

[72] W. Adamson, A.P. Gast, *Physical Chemical of Surfaces, Wiley, New York, 1997.*

[73] M. Usui, F. Harusawa, T. Sakai, T. Yamashita, H. Sakai, M. Abe, *Dynamic Light Scattering on Ostwald Ripening and Composition Ripening of Oil Droplets in Oil-in-Water Emulsion Systems, J. Oleo Sci., 53(12), 611-617, 2004.*

[74] J.G. Weers, *Molecular Diffusion in Dmulsions and Emulsion Mixtures in MODERN ASPECTS OF EMULSION SCIENCE, The Royal Society of Chemistry, Cambridge, 1998.*

[75] M. Kerker, A. Chatterjee, D.D. Cooke, *Brownian Coagulation of Aerosols in the Transion Regime, Pure Appl. Chem., 48, 457-462, 1976.*

[76] H. Ding, S. Ripperger, B. Sachweh, *Sublimation Study on NH_4Cl for Production of Tailored Nanoparticles from Vapor-phase transition, Haomin Ding, Siegfried Ripperger, Bernd Sachweh, Chemie Ingenieur Technik, 79(9), 2007.*

[77] H. Ding, S. Ripperger, B. Sachweh, *Sublimation Study on Organic Materials for production of Tailored Nanoparticles, Haomin Ding, Siegfried Ripperger, Bernd Sachweh, Partec2007-International Congress on Particle Technology. 2007.*

[78] Synlubestechnology Data site, Cognis

[79] Topas Data site.

[80] Hans Lueth, *Solid Surfaces, Interfaces and Thin FilmsSpringer-Verlag Berlin Heidelberg 2001*.

[81] Lehrstuhl fuer Kunststofftechnik Universitaet Erlangen Nuernberg, *Oberflaechenspannungen von Kunststoffen Messmethoden am LKT*

[82] S. Wu, *Polymer Interface and Adhesion, Marcel Dekkler, Inc., New York, 1996.*

Nomenclature

$\bar{u}$	Middle speed of the flow, m/s
β	Neumann constant, $(m^2/mJ)^2$
γ	Surface tension, N/m
γ_{lv}	Surface tension between liquid and vapor phase, N/m
γ_{sl}	Surface tension between solid and liquid surface, N/m
λ	Gas mean free path, m
λ	Light wavelength
μ	Gas viscosity, $Pa \cdot s$
ν_g	Kinetic viscosity, m^2/s
ρ_p^d	Deposit density of Particle, kg/m^3
ρ_g	Density of gas, kg/m^3
ρ_p	Density of Particle, kg/m^3
τ_c	Character time of particle coagulation, s
τ_p	Particle relaxation time, s
τ_s	Sedimentation time, s
θ	Contact angle
ε	Energy dissipation rate, m^2/s^3

ε_i Particle porosity

$p_{v,sedim}$ Increased partial pressure in the gas phase due to the sublimation of sedimenting particles, Pa

ΔH Latent heat of evaporation, J/kg

Δt Residence time, s

ΔV Gas volume in the heating tube, m^3

$\dot{m}$ Evaporation rate, mass flux, kg/s

$\dot{m}_c$ Mass flux in continuum case, kg/s

ΣCn Total particle concentration, P/cm^3

θ Scattering angle measured from the back side of the sphere

A_i Particle surface area, m^2

$A_{p,w}$ Area of sedimentated particles at the wall, m^2

A_{si} Spherical particle surface area, m^2

c Mole concentration in the gas phase, mol/m^3

c Mole concentration, mol/m^3

C_c Cunningham correction factor

C_D Drag coefficient of particle

c_d Mole concentration on particle(droplet) surface, mol/m^3

C_{pg} Heat capacity of gas phase, $J/(kg \cdot K)$

C_p Heat capacity, $J/(kg \cdot K)$

$c^*_{v,d}$ vapor concentration at particle surface, mg/m^3

c_v vapor concentration in gas phase, mg/m^3

c^*_v vapor concentration at flat surface, mg/m^3

Cn Condensation number

$Cn(d_{pi})$ Particle concentration, P/cm^3

d^* Critical particle diameter, m

d_0 Particle diameter in equilibrium with partial pressure in the gas phase, m

d_a Aerosol dynamic particle diameter, m

d_m Collision diameter of molecule, m

d_p Particle diameter, m

D_{AB} Diffusion coefficient of two gas molecules, m^2/s

D_{tube} Diameter of heating tube, m

D_{vg} Diffusion coefficient of vapor in the gas phase, m^2/s

F_D Drag force, N

F_G Gravitational force, N

f_i Factor of specific surface ratio

g The acceleration due to gravity, m/s^2

h_m Heat transfer coefficient

h_p Enthalpy of particle material, J/kg

h_v Enthalpy of vapor, J/kg

I Light intensity, W/m^2

I_l The intensity of the scattered light, W/m^2

k Thermal conductivity, $W/m \cdot K$

k_B Boltzmann's constant,$1.3806503 \times 10^{-23} m^2 kgs^{-2} K^{-1}$

k_g Gas conductivity, $W/m \cdot K$

k_i The shape factor used in settling velocity

K_{ij} Coagulation coefficient

Kn Knudsen number $= \frac{2\lambda}{d_p}$

L Length of the heating tube, m

Le Lewis number $= \frac{Sc}{Pr}$

M Molecular weight, kg/mol

m Refractive index

m_p Particle mass, kg

n Number of molecules per unit volume

N_g Gas molar flux, mol/m^2s

N_v Vapor molar flux, mol/m^2s

Nu Nusselt number $= 2.0 + 0.60Pr^{1/3}Re_p^{1/2}$

p Total pressure, Pa

p_i Partial pressure of different component, Pa

p_v Vapor pressure, Pa

p_v^* Vapor pressure at flat surface, Pa

$p_{v,d}^*$ Vapor pressure at particle surface, Pa

Pr Prandtl number $= C_p\mu/k$

Q_c The heat removal rate, W

R Gas constant, $J/mol \cdot K$

r Radium, m

R_{tube} The radium of the heating tube, m

Re	Reynolds number $= \frac{D_{tube}\rho_g u_g}{\mu}$
Re_p	Particle Reynolds number $= \frac{\rho V_{pg} d_p}{\mu}$
S	Saturation ratio
Sc	Schmidt number $= \nu_g / D_{vg}$
Sh	Sherwood number $= 2.0 + 0.60 Sc^{1/3} Re_p^{1/2}$
T	Temperature, K
t	time, s
T_∞	Gas phase temperature, K
T_d	Particle surface temperature, K
T_w	Wall temperature of the heating tube, K
u_g	Gas velocity, m/s
u_p	Particle velocity , m/s
V	Gas volume flow, m^3/s
v_A	Molecule volume
v_i	Particle volume, m^3
v_s	Settling velocity of particles, m/s
V_{pg}	Velocity of particle , m/s
W_{ad}	Adhesion ability, N/m
x	Optical size of particle
x_v	Mole ratio of vapor in mixing gas